A THERMOECONOMIC OPTIMIZATION OF A BINARY GEOTHERMAL POWER PLANT

İKİLİ TİP BİR JEOTERMAL GÜÇ SANTRALİNİN TERMOEKONOMİK OPTİMİZASYONU

ZEKERİYA ÖZCAN

Assoc. Prof. Dr. ÖZGÜR EKİCİ

Supervisor

Submitted to

Graduate School of Science and Engineering of Hacettepe University

as a Partial Fulfilment to the Requirements

for the Award of the Degree of Doctor of Philosophy

in Mechanical Engineering

2021

To my parents…

ABSTRACT

A THERMOECONOMIC OPTIMIZATION OF A BINARY GEOTHERMAL POWER PLANT

Zekeriya ÖZCAN

Doctor of Philosophy, Department of Mechanical Engineering

Supervisor: Assoc. Prof. Dr. Özgür Ekici

July 2021, 132 pages

This research was carried out for the thermodynamic analysis of a binary geothermal power plant and its thermoeconomic optimization based on the results obtained. In this context, initially, data related to the design point and off-design operating points of the plant were collected from a geothermal power plant which is currently operating in the Aydın/Germencik region in southwestern Anatolia. Based on the data obtained, a thermodynamic model of the power plant was constructed as a result of various simulations and this model was verified by using the outputs of the plant (such as net power, first and second law efficiency) and the outputs of similar plants in the literature. By means of this model, an exergy analysis of the power plant was carried out in the first place. Following the exergy analysis, a new method has been proposed, consisting of 4 steps and based on thermodynamic-thermoeconomic criteria, in order to make the selection of working fluid more effective in the existing power plant. As a result of the elimination of 29 candidate fluids from different chemical groups according to the new method, it was evaluated that R113 could be a more suitable alternative to the existing n-pentane fluid. In addition, a waste-heat recovery system was proposed for the re-

utilization of geothermal water, which is re-injected to the soil at the exit of the power plant, and R115 was chosen as the working fluid for this hypothetical system. After this case study, by using 3 different exergoeconomic analysis methods on the power plant, levelized electrical cost (LEC) of the power plant was tried to be estimated through the initial thermodynamic model. Moreover advantages/disadvantages of the methods compared to each other. After this stage, studies were carried out to create a non-design model that can represent the non-design operating points of the plant with sufficient accuracy. At the first stage, the turbine curves in the two cycles were determined and their integration into the thermodynamic model was provided by using off-design plant data. Statistical models for various parameters were also established in the MATLAB environment in order to increase the power and mass flow rate estimation precision of the turbine curves. The results obtained from the turbine curves were compared with various power plant data and empirical correlations. In the last stage, optimum plant configurations have been determined and presented as novel suggestions, both from a retrospective point of view and depending on the changing environment and initial conditions, by using convex and gradient-based optimization algorithms for off-design data points.

Keywords: Binary geothermal power plant, Thermodynamic Modelling, Exergy Analysis, Exergoeconomic Analysis, Statistical Approach, Plant Optimization.

ÖZET

İKİLİ TİP BİR JEOTERMAL GÜÇ SANTRALİNİN TERMOEKONOMİK OPTİMİZASYONU

Zekeriya ÖZCAN

Doktora, Makine Mühendisliği Bölümü

Tez Danışmanı: Doç. Dr. Özgür EKİCİ

Temmuz 2021, 132 sayfa

Bu çalışma ikili (binary) tip bir jeotermal güç santralinin termodinamik açıdan analizi ve elde edilen sonuçlara dayalı olarak termoekonomik yönden optimizasyonu amacıyla gerçekleştirilmiştir. Bu bağlamda ilk olarak güneybatı Anadolu'da Aydın/Germencik bölgesinde halihazırda faaliyette olan bir jeotermal güç santralinden santralin dizayn noktası ve dizayn dışı çalışma noktalarıyla ilgili veriler toplanmıştır. Elde edilen verilere dayalı olarak çeşitli simülasyonlar sonucunda santralin bir termodinamik modeli oluşturulmuş ve bu model santralin kendi çıktıları (net güç, birinci ve ikinci yasa verimi gibi) ile literatürde yer alan benzer santrallerin çıktıları kullanılmak suretiyle doğrulanmıştır. Bu model vasıtasıyla santralin ilk planda bir ekserji analizi gerçekleştirilmiştir. Ekserji analizini takiben mevcut santralde iş akışkanı seçimini daha efektif hale getirmek için 4 adımdan oluşan ve termodinamik-termoekonomik kriterlere dayanan yeni bir yöntem önerisi yapılmıştır. Farklı kimyasal gruplardan 29 adet aday akışkanın yeni yönteme göre eliminasyonu sonucu R113'ün mevcut n-pentan akışkanına göre daha uygun bir alternatif olabileceği değerlendirilmiştir. Ayrıca santral çıkışında toprağa verilen jeotermal suyun yeniden kullanımı için bir geri dönüşüm sistemi önerilerek bu kuramsal sisteme R115 iş akışkanı olarak seçilmiştir. Bu vaka çalışmasından sonra santral üzerinde 3 farklı eksergoekonomik analiz yöntemi

kullanılmak suretiyle ilk termodinamik model vasıtasıyla santralin birim elektrik üretim maliyeti tahmin edilmeye çalışılmış ve yöntemlerin birbirlerine kıyasla avantajları/dezavantajları tartışılmıştır. Bu aşamadan sonra santralin dizayn dışı çalışma noktalarını da yüksek hassasiyette temsil edebilecek bir dizayn dışı model oluşturma çalışmaları gerçekleştirilmiştir. İlk planda iki döngüde yer alan türbin eğrilerinin tespitiyle dizayn dışı data kullanılarak termodinamik modele entegrasyonu sağlanmıştır. Türbin eğrilerinin güç ve akışkan debisi tahmin hassasiyetlerini artırmak amacıyla MATLAB ortamında çeşitli parametreler için istatistiksel modeller de kurulmuştur. Türbin eğrilerinden elde edilen sonuçlar çeşitli santral verileri ve ampirik korelasyonlarla kıyaslanmıştır. Son aşamada ise dizayn dışı veri noktaları için konveks ve gradyan bazlı optimizasyon algoritmaları kullanılarak hem retrospektif bakış açısıyla hem de değişen ortam ve başlangıç koşullarına bağlı olarak optimum santral konfigürasyonları tespit edilmiş ve öneri olarak sunulmuştur.

Anahtar Kelimeler: Jeotermal Güç Santrali, Termodinamik Modelleme, Ekserji Analizi, Eksergoekonomik Analiz, İstatistiksel Yaklaşım, Santral Optimizasyonu.

ACKNOWLEDGEMENTS

Above all, I would like to express my gratefulness to Dr. Özgür Ekici, however I am afraid that the English language may be insufficient for this purpose. Since the very beginning of my graduate studies, his sharp intellect continuously enlightened my path. His deep understanding of the scientific method -which is sort of a holy relic in these days- shaped my vision as a candidate scholar throughout the years. Aside from his scientific qualifications, his friendly and kind nature has always remained the same until the very end. I count myself quite lucky to have such a supervisor and I am sure that our scientific cooperation will continue as long as the circumstances allow us to do so.

Whenever I attended a class of Prof. Murat Köksal, he always impressed us with his ability to express most complex engineering problems in simplest terms, which is an infallible sign of highest proficiency. His remarks and suggestions about my scientific research were constructive without any exception, for which I am very thankful.

Dr. Onur Baş continuously questioned and redirected me with his precise comments on conceptualization and methodology. Thanks to his remarks, I could clarify and eliminate some serious issues, that I think dramatically improved the quality of this research.

Ordinary words can not elucidate the commitment and benevolence of my dear friend Mr. Pietro Ungar, whose contribution was more than vital for this research. He is one of the most ingenious engineers I have ever met, his benefactor and distinguished personality is beyond any question. I would also like to thank Prof. Giampaolo Manfrida very much for his permission that enabled our cooperation with San Pietro. Thanks to Dr. César Torres for his instructions which enabled me to understand the framework of exergy costing.

Many special thanks to plant manager Mehmet Şişman and technical supervisor Aydoğan Oral, whose permission and support enabled this scientific collaboration.

My dear friend Erdem Aktaş yet again provided his mental and material support during this research.

Many sincere thanks to my family, especially to my beloved parents, they would have been proud to see this day. Finally, I would like to quote from W. Churchill -a supreme orator of this language- and whose resilience has always been an admirable example for me: “Success is not final, failure is not fatal. It is the courage to continue that counts.”

TABLE OF CONTENTS

LIST OF FIGURES

LIST OF TABLES

SYMBOLS AND ABBREVIATIONS

Symbols

h	Enthalpy
s	Entropy
$\dot{S}_G$	Entropy generation rate
$\dot{E}x$	Exergy flow rate
η_I	First law efficiency
$\dot{Q}$	Heat flow rate
I	Irreversibility rate
Φ_m	Mass flow rate
C_p^0	Purchased equipment cost
η_{II}	Second law efficiency
ex	Specific exergy
$\dot{W}$	Work flow rate
$\sum \dot{Z}_k$	Levelized sum of initial and maintenance costs
f	Exergoeconomic Factor
Y_D	Stodola Constant
A	Cost attribute of the component

Subscripts

br	Brine
c	Critical
0	Dead state
in	Inlet

m	Mean
out	Outlet
s	Source
wf	Working Fluid
D	Design
off	Off-design
r	Ratio

Abbreviations

KC	Kalina Cycle
ORC	Organic Rankine Cycle
$SPECO$	Specific Exergy Costing
GWP	Global Warming Potential
CEPCI	Chemical Engineering Plant Cost Index
ECT	Exergy Cost Theory
WF	Working Fluid
TLC	Thermal loss coefficient

1. INTRODUCTION

At this section, a general introduction to the subject of this thesis will be presented. A brief overview of worldwide geothermal capacity will be followed by Turkish geothermal capacity, state of art for geothermal power production and research objectives.

1.1 Geothermal Energy – Potentials and Capacities

It is possible to generate power from several different sources, including the fossil resources such as coal and petroleum, or nuclear and renewable resources such as wind, geothermal, and solar energy. Over the past decades, renewable energies were a subject for highly considerable amount of interest because of their advantages. For instance, their environmental impacts are less than conventional resources, they are in fact "renewable" and in some cases they can be quite cost-effective. Among all kinds of renewable sources, geothermal energy can be labeled as one of the most promising ones. Because it is environment-friendly and excellent for meeting the base load energy demand (as opposed to other renewables such as wind and solar) [1], moreover it has a relatively high potential (estimated roughly up to 2 TW worldwide), it is easily adaptable for HVAC applications and available nearly everywhere (only realized whenever it is feasible). Besides, it has a broad range of application possibility according to target temperature range. Examples for application fields of low-temperature geothermal energy are agriculture, greenhouses, refrigeration (absorption chillers) whereas the high temperature applications include HVAC and power production [2].

As the demand for energy increases all over the world, Turkey is not aside from that. However, in our country despite the quite high potential of renewable energies, only around 12% of installed plants capacity is based upon renewable sources, and only 1.4% of the total capacity is directly related to geothermal power plants. Turkey as a geological and geographical place is situated in an active tectonic area and that is why our nation is wealthy in geothermal energy resources. It is estimated that around 1,000 geothermal springs having different temperatures are available throughout Turkey. The installed capacity of geothermal energy as of year 2020 was 14.05 GWe. Despite the low contribution to the total power consumption, Turkey is still placed at top five in the world in terms of geothermal plant capacity with USA, Indonesia, Philippines and New Zealand [3].

1.2 Geothermal Power Production – State of Art

Throughout the years, power generation methodologies from a geothermal source are diversified parallel to the technologic innovations. Depending on the source temperature, dry steam, flash steam and binary steam methods are most common ones for geothermal applications. Dry steam power plants utilize geothermal steam directly extracted from geysers whose temperature can reach up to 300 ºC. Typical application range for flash steam includes the temperatures beyond 180 ºC, where hot brine flows through the well accompanied by a pressure drop that causes vaporization of the geothermal brine. Finally, steam is separated from liquid water and cycled for power generation purposes, where liquid water (and residual condensed steam) is pumped back to the source [4]. On the other hand, binary steam targets low and moderate source temperature ranges (i.e. 100-180 ºC). In this method, enthalpy of extracted brine is transferred in heat exchangers to a second medium with a lower boiling point, which is cycled in closed systems. Based on this principle, state of art demonstrates two common cyclic systems namely- organic Rankine cycle (ORC) and Kalina cycle (KC)-. Kalina cycle operates with ammonia-water mixture as working fluid [5] while ORC systems use *organic* based working fluids as the term implies [6].

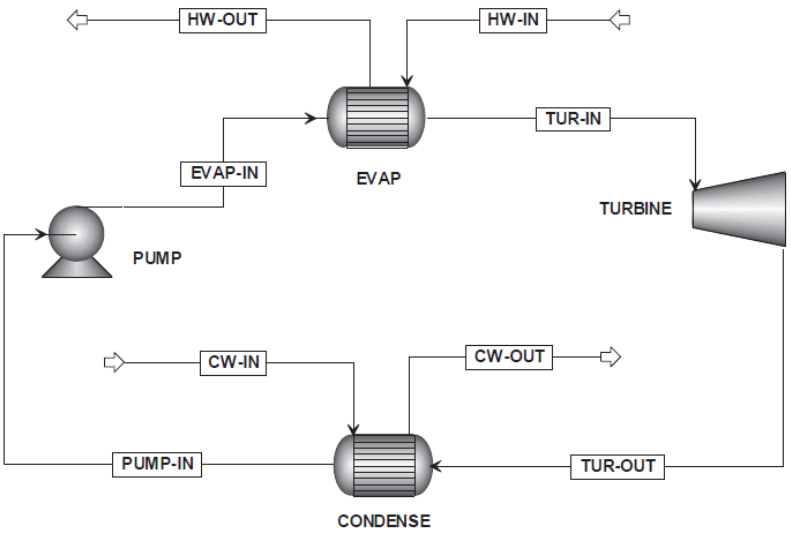

Fig.1: Schematic diagram of an ORC combined with a geothermal source [7]

This working fluid cycles with the same principle as a conventional Rankine cycle as schematized in Figure 1. Working fluid of these systems usually do contain hydrocarbons or they are directly some kinds of the refrigerants.

1.3 Research Objectives & Motivation

It is particularly important to analyze and find optimal working conditions for geothermal power plants due to the fact that the thermal degradation of geothermal source is inevitable due to continuous re-injection of brine water to the underground. This physical constraint dictates that over a plant operation period, extracted brine temperature and accordingly brine enthalpy would decline and plant operation becomes less efficient. Accordingly, main purpose of this research is to analyze and optimize an existing geothermal sourced ORC power plant in Aydın/Germencik from thermodynamic and thermoeconomic points of view respectively.

This thesis will contribute to the literature from different aspects of the geothermal power plant research. Initially, a new thermodynamic analysis with an existing power plant data will be conducted. Afterwards, a novel working fluid selection methodology will be proposed for the ORCs based on existing plant analysis. Combining both thermodynamic and thermo-economic aspects of power production, 29 different single-component working fluid candidates from different chemical branches will be subjected to a four-step elimination methodology. In order to apply this novel approach and investigate a feasible efficiency improvement potential, an option of waste heat recovery from brine re-injection temperature will also be discussed as a separate case study. A comprehensive exergoeconomic analysis comparing different methodologies will follow this section to determine cost relationships in this plant. Another important research topic will be off-design modelling of the plant in order to obtain the turbine (i.e. Stodola) curves. For this purpose, a statistical approach will also be presented. Final part will include the plant optimization from retrospective and dynamic points of view.

2. LITERATURE REVIEW

This study contains five chapters of geothermal sourced binary plant research -namely plant analysis and model validation, working fluid selection, exergoeconomic analysis, turbine curve modelling and plant optimization-. Relevant literature regarding these working fields will be summarized here. Figure 2 provides a general overview for some of the recent research topics in this field:

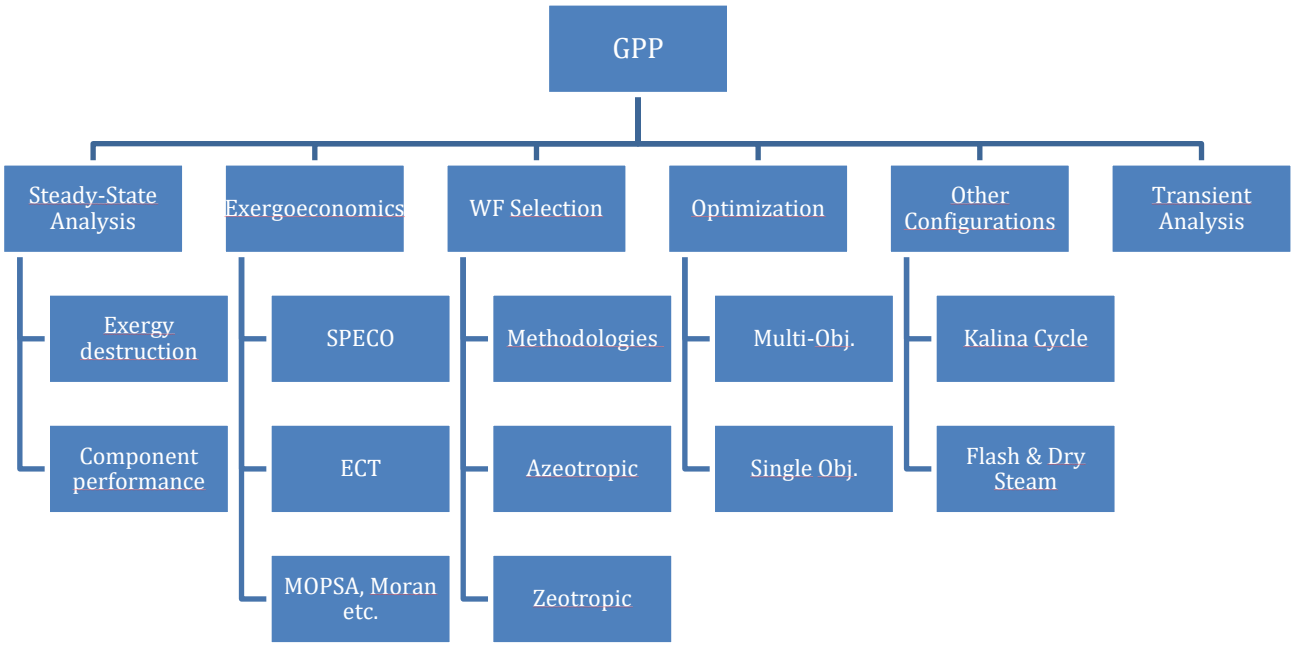

Fig.2: A general overview of the some recent research topics in GPP related fields

In the relevant literature there exist two main approaches for the exergy analysis of binary geothermal power plants: first being the analysis of an existing plant and the second is to analyze a hypothetical plant configuration. Dealing with an existing plant, this research would fall to the first category.

To begin with the examples of existing plant analyses, Kanoğlu [8] conducted a thermodynamic analysis of a two-stage binary power plant with 12.4 MW capacity in Nevada from an exergetic point of view. In that study, brine reinjection was determined as the main reason for exergy losses.

DiPippo [9] examined various binary power plants with low-grade geothermal sources and demonstrated that first law efficiencies of those binary power plants are between 8-12%. Moreover, results also show that it is possible to obtain up to 40% second law efficiencies with geothermal brines having 200 kJ/kg specific exergy or lower.

Özgener et al. [10] conducted a study in order to evaluate binary geothermal power plants Dora I and Dora II; their first law efficiencies were calculated as 5.92% and %5.66, respectively. Additionally, second law efficiencies were found to be around 34.71% and 31.19%, for plants Dora I and Dora II. It is highlighted that the temperature of cooling air, depending on the seasonal effects, plays a major role in the net power output.

In a very recent study, Kahraman et al. [11] analyzed the first and second law efficiencies of Sinem binary geothermal power plant (GPP) in Aydın with 21 MW capacity and investigated the effect of ambient temperature on air cooled condensers (ACC) as well as the overall plant efficiency.

In Yari's study [12], three different geothermal plant types (single-flash, double flash and flash binary) and three different ORC schemes were evaluated against each other in terms of the first and second law efficiencies. Results indicate that brine reinjection is the primary source for exergy losses.

The first and second law efficiency analyzes were conducted at Aydın Germencik Geothermal Power Plant in another research by Unverdi et al [13]. An exergy flow diagram was plotted and sources of exergy destructions were elaborated in detail.

Unverdi [14] evaluated the possibility of waste heat recovery from an existing plant in Aydın/Germencik with a 47.4 MW net power output in his study. R-600 (Isobutane) was pointed out as the best option in terms of the first and second law efficiencies. On the other hand, R-161 was labeled as the least effective refrigerant due to high exergy destruction in heat exchanger.

In a study by Gökgedik et al., another detailed approach regarding an exergy analysis is suggested [15]. An exergetic analysis is conducted in order to determine the potentials of exergy improvement by considering each system component for a certain geothermal plant (Bereket-Denizli). It is shown that the second law efficiency can be enhanced by some improvements in certain components such as evaporator, pre-heater and condenser.

Yılmaz [16] conducted a study from a thermoeconomic point of view and compared different cost evaluation methods against each other for Dora II, a binary power plant in western Anatolia. Specific Exergy Costing (SPECO), Modified Productive Structure Analysis (MOPSA) and Moran methods were used to compare cost flows.

There are also several recent studies regarding ORC analysis with hypothetical approach. Such an example is from Italian Torre Alfina region, which elaborates the energetic and exergetic efficiencies of power production and air conditioning from a geothermal reservoir. The study conducted by Leveni et al. contains a combination of an ORC with water/LiBr absorption chiller. This draft system was validated with reference data. [17].

Li et al. [18] examined the first and second law efficiencies of an ORC for under the influence of different heat sources. Energetic and exergetic efficiencies of an ORC system using different temperature sources (100-90-80-70°C) were evaluated.

Rodriguez et al.'s study comprises a comparison of ORC and Kalina cycle coupled with a projected geothermal system in Brazil. Fifteen distinct operating fluids for ORC and three distinct components of the ammonia-water blend for the Kalina cycle were assessed to obtain superior efficiencies for both cycles [19].

In order to compare sub-and supercritical ORCs for power generation from low-enthalpy heat sources, Vetter et al. [20] conducted another study. Main novelty of study was to elaborate the issue from both the net power output and overall efficiency aspects.

In a recent study of Zare et al. [21] a thermodynamic analysis comparing two different configurations of tri-generation systems (which are fed by a geothermal source) is proposed. The two systems regarded were differentiated by their power generation units, as the ORC is used in one scheme while the other scheme uses the Kalina cycle.

Walraven et al. [22] conducted a comparison of power cycles from a different point of view. Their main objective was to compare a conventional ORC with Kalina cycle. The performance of various kinds of ORCs and the Kalina cycle is explored and optimized for geothermal thermal sources at low temperature (100–150ºC).

Dinçer et al. [23] investigated a hypothetical geothermal sourced organic Rankine cycle for optimization purposes and parametrically studied the system for optimized conditions. Objective criterion for optimization was solely the heat exchanger surface area. Under the optimal conditions, efficiencies were estimated to be 16.37% for energy and 48.8% for exergy.

On the other hand, working fluid selection has been a subject of attention since the very beginning of organic Rankine cycle (ORC) applications, since it is the working fluid that enables heat transfer from different heat sources such as solar, waste heat, geothermal, to the power generation devices, e.g., turbines. Working fluid selection is interconnected to the system design and plant efficiency. Accordingly, various thermophysical properties of different working fluids on system performance were investigated in recent years.

For instance, from a thermodynamic perspective, effect of boiling and critical temperatures and their relationships with source temperature was investigated by Yang et al. [24]. Different source temperature intervals were examined for an ORC in terms of vapor expansion ratio (VER) and maximum net work output ($\boldsymbol{W_{net,max}}$) as key performance indicators. Results show that at low-grade temperatures (between 423.15 K and 473.15 K) there exists a clear correlation between working fluid critical temperature ($\boldsymbol{T_c}$) and $\boldsymbol{W_{net,max}}$. Furthermore, this correlation is independent from boiling temperature ($\boldsymbol{T_b}$) within this interval. However, for a given $\boldsymbol{T_c}$, higher $\boldsymbol{T_b}$ leads to a higher VER, consequently a higher maximum net work output. Therefore, it is safer to use $\boldsymbol{T_b}$ of a working fluid as a second indicator for selection purposes.

Zhai et al. [25] developed a mathematical correlation between the heat source temperature and the critical temperature of single-component working fluid for subcritical ORC's. This correlation applies for a condensation temperature interval 30 ºC to 60 ºC of working fluid. He et al. [26] conducted another study to determine an optimal evaporation temperature and suitable working fluids for subcritical ORC's while aiming the maximization of the net work output. Highlight of this study demonstrates that, higher working fluid (WF) critical temperatures correlate with higher net work outputs. In that study, R114, R245fa, R123, R601a, n-pentane, R141b and R113 were labelled as the most suitable options for subcritical cycles when the net work output, working pressure, heat transfer capacity and expander sizing parameter were taken into the account.

Astolfi et al. [27] studied thermo-economic optimization of power generation from low and medium grade geothermal sources. Results have shown that employing working fluids which have critical temperatures around the source temperature leads minimum electricity costs for the cases in scope of that study. Dinçer et al. [28] presented that higher boiling temperatures reduce irreversibilities for single component and zeotropic working fluids in low-grade sourced ORC's.

In a study by Başaran et al. [29] the comparison of the different working fluids for a certain binary power plant was conducted in terms of the first and second laws as well as thermophysical issues with actual plant data. Highlight of their study implied that the dry refrigerants (such as R600 and R236ea) show better first and second law efficiencies in comparison to wet refrigerants (R134a, R152a etc.).

Thurairaja et al. [30] compared and classified 82 different working fluids based on evaporation temperatures and first law efficiencies by mathematical modelling. Results show that there is a broad range of working fluid options from evaporation temperatures 30 ºC to 320 ºC with different net work outputs and efficiencies.

Power production from a geothermal source with supercritical CO_2 extraction and working fluid selection for ORC of this system was elaborated in a recent study by Wang et al. [31]. In their study, it is demonstrated that performances of working fluids in subcritical and superheated systems are closely dependent on their critical temperature and pressure values.

Zeyghami [32] evaluated 30 different working fluids between a temperature range of 150 ºC and 250 ºC for a combined flash-binary power plant. Overall exergy destruction and vapor expansion ratio in ORC turbine were chosen as primary measures in the evaluation. Findings show that refrigerants lead higher efficiencies for low-grade sources whereas hydrocarbons leading better performance for medium and high-grade sources.

Using zeotropic mixtures as working fluid at an ORC system coupled with a low – grade geothermal resource was the main novelty of the study by Heberle et al. [33]. Working fluids Isobutane, Isopentane, R245fa and R227ea were evaluated separately and as mixtures (Isobutane-Isopentane and R245fa/R227ea) in terms of the second law efficiency. Molar fractions in these mixtures were varied between the geothermal water temperatures 120 - 180 ºC in order to obtain the maximum second law efficiency. The findings indicate that mixtures yield to higher efficiency values in comparison to pure fluids. This is triggered by improved glide matching of the temperature profiles in the heat exchanger. As a consequence, the system's irreversibilities are reduced, particularly in the condenser. A case study demonstrates that significant parameters related to turbine design and cost, such as the outlet to inlet volume flow ratio, are smaller compared to pure working liquids for appropriate fluid mixtures.

Research on working fluids with low global warming potential (GWP) is drawing attention in recent years in frame of efforts to prevent hazardous environmental effects of power conversion systems. Latest research seems to be focused specifically on R245fa, which will be phased out in near future due to its relative high (around 1030) GWP.

Longo et al. [34] experimentally investigated thermodynamic and heat transfer performance of R600a (Isobutane), R1234ze (Z) and R1233zd (E) as alternatives of R245fa. Results indicate that both for heat pump and ORC systems, R1233zd (E) delivers superior efficiency outcomes in comparison to R245a while R1234ze (Z) behaving similarly. R600a is shown to be the least efficient in all cases.

Ye et al. [35] conducted an experimental thermoeconomic and environmental analysis of a similar set of low GWP refrigerants R1234ze (Z), R1233zd (E) and R1366mzz(E) against R245fa. Economic performance evaluation is based on the net power output index to total cost (NPIT). Maximum NPIT value is obtained by R1233zd (E) whereas other working fluids R1234ze (Z), R1366mzz (E) and R245fa are ranked successively.

There exist other examples of experimental comparisons of R245fa alternatives such as study conducted by Yang et al. [36]. In their study, R1234ze (Z) and R1233zd (E) are pointed out as suitable alternatives for R245fa. Utilizing refrigerant mass flow rate and expander rotational speed as control parameters, a comparison of net power outputs and efficiencies are presented. Results indicated that R1233zd (E) and R1234ze (Z) reach similar thermal efficiencies with R245fa in a plus-minus 0.1% margin, 4.7% and 4.5%, respectively.

Working fluid selection process involves several other parameters such as flammability, toxicity or ozone depletion potential (ODP). Papadapoulos et al. [37] proposed a systematic design and selection methodology for ORC systems which includes both economic, environmental and safety aspects such as flammability, toxicity and ODP. Briefly, this methodology suggests an economic objective function to be maximized and at the same time, it draws attention to possible trade-offs between environmental impacts and economic performance.

Zhao et al. [38] classified a set of pure and zeotropic refrigerants based on their environmental impacts and safety issues. Performance characteristics such as refrigeration capacity or coefficient of performance (COP) of these refrigerants are compared at second stage. R513a and R466a are suggested as novel alternatives of R134a (GWP: 1430) and R410a (GWP: 2088). In frame of their study, highly flammable hydrocarbon refrigerants such as R1150 (ethylene), R290 (propane) or R600a (isobutane) and their low GWP alternatives are theoretically and experimentally investigated. Results indicate that phasing out process of pure hydrocarbons would be harder than their halogenated variants -which are highly toxic- in general. Since the working fluid selection is a task, which involves conflicting aims or trade-offs between different aspects, an objective optimization of these targets may play a significant role in decision making processes.

A multi-objective optimization of economic, environmental and safety aspects for ORC's coupled to geothermal sources is employed by Gomez et al. [39]. Aiming to maximize profit from energy and minimize environmental impacts and safety risks, hydrocarbons are pointed out as optimal working fluids under given circumstances.

Bekiloğlu et al. [40] investigated 28 different working fluids from different chemical branches (i.e. hydrocarbons, hydrofluorocarbons and hydrofluoroolefins) in an ORC coupled with three different geothermal source temperatures (-90 ºC, 120 ºC and 150 ºC). A 1-D radial turbine model is accompanied by a genetic algorithm for multi objective optimization purposes. According to the selected decision variables such as pressure ratio or specific speed in turbine and pinch analysis in evaporator; R1234yf, R1234ze (E) and isobutane were determined to be optimal working fluids for the given source temperatures.

Definition of cost from the theory of management perspective is "*the total sum of resources needed to manufacture something or provide a service*". In addition to the managerial approach for calculating the consumption of energy resources, energy cost accounting should provide a reasonable method for determining the cost of production. There exists a common understanding in relevant academic environments which states that *exergy* is an acceptable thermodynamic property, at least for energy systems to be used for cost evaluation. Thermoeconomics incorporates economics and study of the second law relating the principle of economic cost to exergy, which is a definition of the term *exergoeconomics* [41].

Amongst other purposes, an exergoeconomic analysis would provide following outputs; an assessment of reasonable plant production prices in a physical frame, optimization of particular process variables to minimize the system's cost of output, detection of inefficiencies in existing plants and estimation of their economic impacts, i.e. a diagnosis of plant operations, comparison of various design alternatives and maximization of the benefit/cost ratio.

Two mainstream exergoeconomic methodologies are basically proposed in the literature: Functional Analysis and Exergy Cost Theory [42]. Most versatile applications of these approaches were proposed by Moran [43], Tsatsaronis and Lazzaretto (Specific Exergy Costing – SPECO) [44] and Kwak et al. (Modified Productive Structure Analysis - MOPSA) [45]. There are several applications of these methodologies to practical cases in relevant literature.

In a recent study, Pan et al. [46] analysed a hypothetical combined heat pump cycle-organic Rankine cycle(ORC) waste-to-energy (WTE) system from thermodynamic and exergoeconomic perspectives using SPECO method. A multi-objective optimization based on a sensitivity analysis is carried out whilst results indicated ammonia and butane as most suitable working fluids for such a system.

Fiaschi et al. [47] conducted an exergoeconomic comparison of geothermal power plant configurations using Kalina cycle and ORC operating at different geothermal source temperature levels (medium and low grade). Results demonstrate that an ORC operating with R1233zd reaches a 3% lower electricity production cost at medium grade geothermal source whilst a plant operating with Kalina cycle achieves 22-42% more net work output than any other ORC utilizing different working fluids at low grade geothermal source case.

A novel exergoeconomic factor is proposed by Zhao et al. [48] in their study aiming exergoeconomic analysis and optimization of a binary geothermal power plant. Optimization of the system is solely based on minimizing the proposed exergoeconomic factor. Results indicated that it is possible to boost exergoeconomic performance significantly in a slight trade-off against thermodynamic performance.

Abdolalipouradl et al. [49] compared thermodynamic and exergoeconomic performances (based on SPECO) of combined flash-binary cycles for Sabalan geothermal field of Iran. Following a series of parametric studies and optimizations aiming to maximize net work output, results indicate that a single-flash binary plant operating with R123 achieves the best exergoeconomic performance.

Exergoeconomic performance analysis of a new ORC configuration operating with a zeotropic mixture (Isopentane/Isobutane) is conducted by Samadi et al. [50]. Utilizing a multi-objective optimization which incorporates exergy efficiency as thermodynamic indicator and specific investment cost (SIC) as economic indicator, influence of mole fractions in zeotropic mixture is discussed. Results indicate that an increase of Isobutane leads a reduction of return of investment (ROI) factor.

Zare [51] examined three different configurations (simple, regenerative and including internal heat exchanger) of geothermal sourced power plants operating with ORC from an exergoeconomic point of view. Based on total cost minimization as an objective criterion, findings show that simple ORC system holds the best economic indicators whilst an ORC with internal heat exchanger possessing highest efficiency values.

Nasruddin et al. [52] conducted an exergoeconomic and thermodynamic analysis of hypotetical geothermal power plants in Indonesia operating with ORC (Isopentane as working fluid) and Kalina cycle configurations. A multi-objective genetic algorithm optimization demonstrates that the plant configuration operating with ORC has a higher exergy efficiency (88.2%) and lower electricity production cost (0.034 $/kWh) in this potential geothermal field.

Exergoeconomic criteria using SPECO methodology constituted a basis for comparisons and evaluations in study of Shokati et al. [53]. Among the examined configurations, results indicate to a diversion between highest thermodynamic performance (single flash combined ORC cycle) and minimum electric production cost (double flash steam cycle).

Turbine modelling at off-design conditions is another important topic in order to achieve optimal work output from the plant. Ellipse law of Stodola [54] can be considered as the pioneer of in context of modelling off-design multistage turbine pressures. In recent years there also are many studies focusing on that issue.

Gabbrielli [55] proposed a new design approach for a binary geothermal power plant at off-design conditions underlining the thermal degradation effect of geothermal brine re-injection process throughout the years on plant performance. In that study and several other studies [56-58], off-design isentropic turbine efficiencies are calculated with the correlation proposed originally by Keeley [59].

Jüdes et al. [60] implemented another empirical correlation to model the part-load behaviour of a steam turbine in a cogeneration (CHP) plant. In another study, Fiaschi et al. [61] elaborated design of light-duty radial turbines and proposed a 0-D model for design of the ORC turbines. Proposed model is also employed for the prediction of off-design turbine performance by modelling of turbine curves.

Dawo et al. [62] compared different turbine curve modelling approaches in order to validate and simulate part-load performance of an existing Kalina cycle power plant from Unterhaching/Germany.

In engineering related fields, term *optimization* generally contains a design point of view. Over the past decades, thanks to the computer algorithms becoming widespread, single-objective and multi-objective optimization of cyclic systems grew into the main concerns of thermodynamic as well as thermoeconomic research as exemplified in some of the previous review [23,27,38-40, 46,48-50,52].

There are some other studies in the relevant literature dealing specifically with ORC systems sourced by geothermal energy. Yılmaz and Koyuncu [63] utilized an artificial neural network method to optimize Afyon binary geothermal plant. Optimal brine temperature is found to be 110 ºC while optimal mass flow rate is determined to be 150 kg/s. Under that conditions, energetic and exergetic efficiencies are calculated as 10.4% and 29.7% respectively as well as levelized electrical cost is around 0.0176 $/kWh.

Binary geothermal power plant optimization with the help of a gravitational search algorithm aiming to achieve highest exergetic efficiency was the research objective of Özkaraca and Keçebaş [64]. Results indicate that it is possible to improve plant exergetic efficiency from 14% up to 31%.

Clarke and McLeskey [65] employed another methodology on a binary geothermal plant model for optimization purposes. With the help of multi-objective particle swarm optimization, an optimal pareto front is obtained showing the trade-offs between net work output and heat exchanger surface area. It is pointed out that net work maximization may require a working fluid with a lower critical temperature than that required at lower values of net work output.

A transient optimization of an ORC system coupled with a geothermal reservoir model was the novelty of Pollet et al. [66] research among the others that are conducted under steady-state assumptions. Research aims to extract highest possible energy output from the plant over its lifetime. It is claimed that if the plant variables such as mass flow rate ratios between brine and working fluid or evaporator pressure can be continuously manipulated over the plants lifespan, it may be possible to increase energy extraction up to 31%.

3. METHODOLOGY AND RESULTS

In order to achieve the goals presented in Introduction section, following methodology is applied:

i) Design and off-design plant data are collected.

ii) A thermodynamic model of the plant is configurated in simulation environments.

iii) Plant model is validated with similar plant data in the relevant literature.

iv) A novel approach for working fluid selection is proposed by the employment of factorial cost estimation techniques.

v) An exergoeconomic analysis of the plant is conducted.

vi) Turbine curves are modelled with the help of off-design plant data.

vii) A statistical model is proposed in MATLAB environment in order to increase accuracy of the off-design thermodynamic model.

viii) Curve models are validated by empirical correlations proposed in the relevant literature.

ix) Optimization of plant variables according to off-design plant data and validated curve models.

This research can be divided mainly into 5 chapters: Initial thermodynamic analysis, novel WF selection methodology, exergoeconomic analysis, off-design modelling and optimization. For each part, applied methodology and results will be presented subsequently.

3.1. Initial Thermodynamic Modeling of the Kerem GPP

In order to evaluate thermodynamic performance of the plant, an initial thermodynamic model is constructed in UNISIM and Cycle-Tempo softwares based on steady-state plant data and certain assumptions as shown in Fig.3:

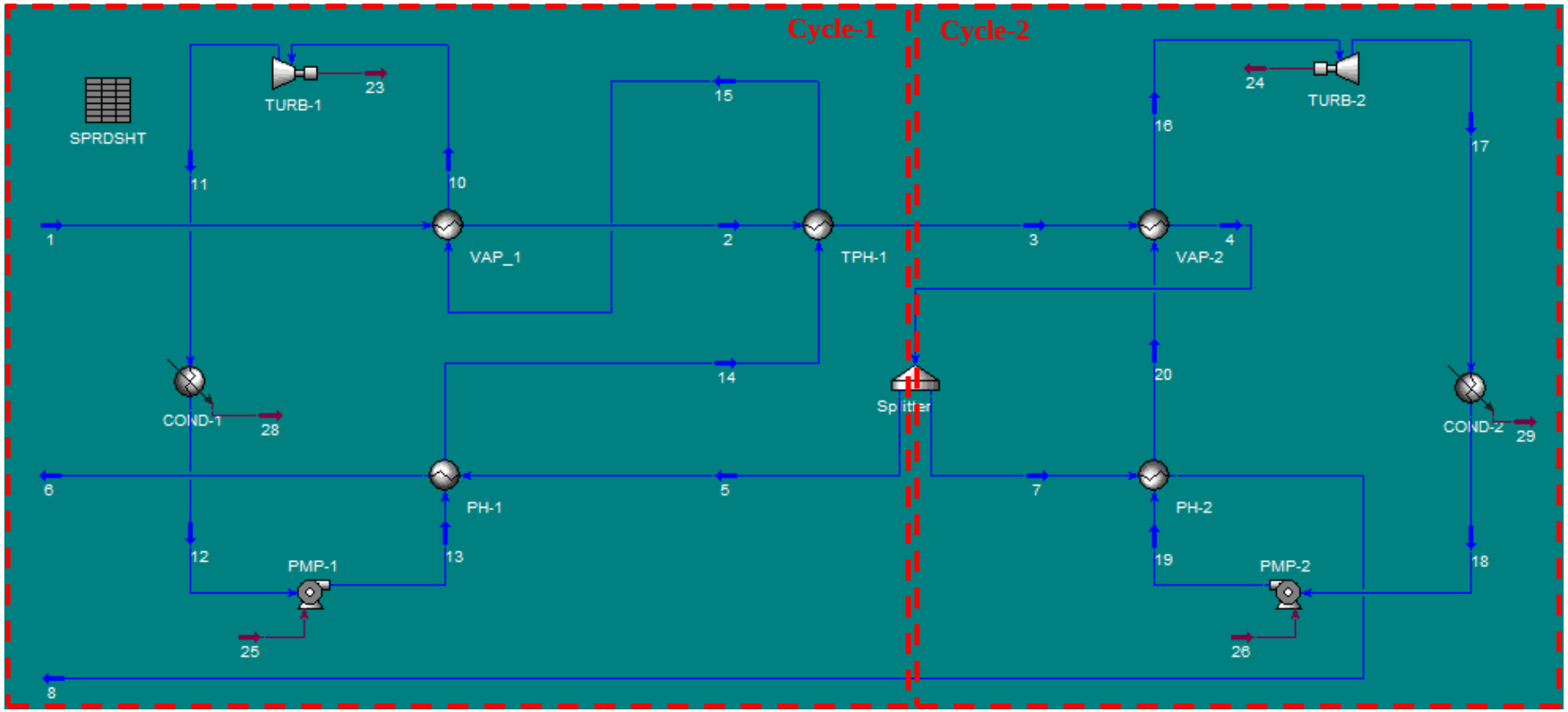

Figure.3: Kerem GPP Model Layout

Nominal plant capacity of Kerem GPP is around 22.5 MW in which geothermal well temperature ranges in between 150 and 175 ºC in this province. Extracted geothermal brine energy is transferred to the n-pentane by successive heat exchangers and re-injected to the soil as depicted in Fig. 1. Being superheated in vaporizers (Vap_1 and Vap_2) and passed through turbines for power conversion purposes, n-pentane is condensed in air cooled condensers and pumped back to the heat exchangers for further heat transfer purposes. Both cycles work under same principle except Cycle-I includes an additional heat exchanger called *Top Preheater* (Tph_1) as an extra internal heat exchanger.

For modelling purposes, a steady-state environment is assumed. Isentropic and mechanical efficiencies of turbines and pumps are utilized as presented in Table-2. Thermal losses, pressure drops and kinetic/potential energy changes are assumed to be negligible. Geothermal brine is modelled as standard water. An ideal gas mixture is employed for ambient air properties. Sample thermodynamic properties of all streams provided in Fig.1 are presented in Table-1. Note that *reference enthalpy of vaporization* ($\Delta_{vap}H$) at 36.05 °C is defined as 25.79 kj/mol. Dead state properties of geothermal brine are denoted by 0 while $0'$ and $0''$ represent n-pentane and ambient air for dead state conditions, respectively:

Table-1: Sample Thermodynamic Properties of Streams in Kerem GPP

State No.	**Description**	**Fluid**	**Phase**	**P(bar)**	**Sp. Enthalpy (kJ/kg)**	**Sp. Exergy (kJ/kg)**	**Mass flow rate (kg/s)**
0	-	Brine	Dead	1.013	62.45	0	-
$0'$	-	N-pentane	Dead	1.013	-395.41	0	-
$0''$	-	Air	Dead	1.013	-98.85	0	-
1	Vaporizer-I Inlet	Brine	Liquid	8.500	732.11	137.01	440.694
2	T. Preheater Inlet	Brine	Liquid	3.528	585.53	88.51	440.694

3	Vaporizer-II Inlet	Brine	Liquid	2.613	541.59	75.60	440.694
4	Vaporizer-II Outlet	Brine	Liquid	1.763	487.97	60.96	440.694
5	Preheater-I Inlet	Brine	Liquid	1.763	487.97	60.96	220.347
6	Preheater-I Outlet	Brine	Liquid	0.5302	346.64	28.87	220.347
7	Preheater-II Inlet	Brine	Liquid	1.763	487.97	60.96	220.347
8	Preheater-II Outlet	Brine	Liquid	0.5944	358.82	31.23	220.347
10	Turbine-I Inlet	N-pentane	Steam	12.80	178.00	132.20	215.584
11	Turbine-I Outlet	N-pentane	Steam	0.8461	94.05	30.81	215.584
12	Condenser-I Outlet	N-pentane	Liquid	0.8461	-358.57	0.97	215.584
13	Pump-I Outlet	N-pentane	Liquid	14.80	-355.93	3.19	215.584
14	T. Preheater Inlet	N-pentane	Liquid	14.05	-211.46	22.66	215.584
15	Vaporizer-I Inlet	N-pentane	Liquid	13.30	-121.65	43.84	215.584
16	Turbine-II Inlet	N-pentane	Steam	4.16	94.61	80.84	113.727
17	Turbine-II	N-pentane	Steam	0.7785	45.56	20.84	113.727

	Outlet						
18	Condenser-II Outlet	N-pentane	Liquid	0.7785	-364.01	0.69	113.727
19	Pump-II Outlet	N-pentane	Liquid	4.54	-363.29	1.29	113.727
20	Vaporizer-II Inlet	N-pentane	Mixture	4.34	-113.13	40.80	113.727
21	Condenser-I Inlet	Air	Gas	1.013	-98.85	0.13	3863.92
28	Condenser-I Outlet	Air	Gas	1.013	-73.60	1.16	3863.92
22	Condenser-II Inlet	Air	Gas	1.013	-98.85	0.13	2305.81
29	Condenser-II Outlet	Air	Gas	1.013	-78.65	0.80	2305.81

Sub- and supercriticality play a decisive role in cycle characteristics of ORC systems. As the term *Subcritical* implies, such systems operate under the critical point of working fluid, which means that it is still possible to condense this fluid with respect to its pressure level. It is possible to extract from Table-1 that maximum pressure within the system occurs at the inlet of Turbine-1, 12.8 bar, which equals around 38% of working fluid's (n-pentane) critical pressure, 33.69 bar [67]. Since the ratio of maximum pressure to critical pressure of working fluid is under 1 in both cycles, it is possible to classify both ORCs as *subcritical*.

Fig.4 shows T-s diagram of subcritical ORC cycles in Kerem GPP:

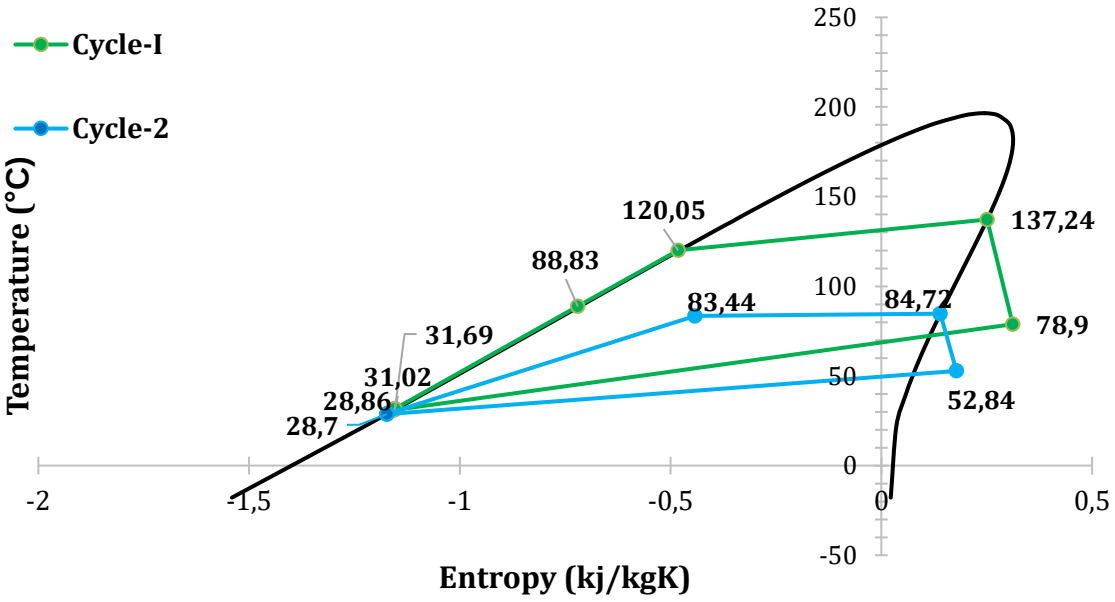

Figure 4: T-s diagram of two cycles working with n-pentane in the plant

Fig.4 contains the T-s datapoints obtained from initial thermodynamical analysis of the plant. It provides that Cycle-1 utilizes the majority of energy and accordingly, exergy provided by the geothermal brine, and produces around 2.24 times more net power than Cycle-2. Note that the plant is operating at 73% (16.4 MW) of its nominal gross capacity (22.5 MW) for analysed conditions due to safety restrictions in ORCs. Collected data shows that plant operates between 60% and 80% of nominal capacity throughout the different seasons of year. Control strategy of the power production is conducted by adjusting mass flow rates of brine and working fluids. Brine pump consumptions are excluded as in similar to different studies for thermodynamic analysis of ORCs [8-16].

Air cooled condenser fan consumptions will be estimated according to correlation between heat removal rate and electric power consumption which is proposed by Pieve and Salvadori [68].

It is possible to write down the mass conservation in the following form for general applications:

$$\sum \Phi_{m,in} - \sum \Phi_{m,out} = 0 \quad (1)$$

Where $\Phi_{m,in}$ stands for inlet mass-flow rate whilst $\Phi_{m,out}$ represents the outlet mass-flow rate. Energy conservation can be written down for every component separately,

however in order to keep long story short, only energy conservation equation for top preheater will be demonstrated as an example according to state numbers shown in Fig.1:

$$\Phi_{m,br}(h_3 - h_2) = \Phi_{m,wf}(h_{15} - h_{14}) \quad (2)$$

General expression for energy conservation is as follows:

$$\dot{Q} - \dot{W} = \sum \Phi_{m,out} h_{out} - \sum \Phi_{m,in} h_{in} \quad (3)$$

General expression of the first law efficiency;

$$\eta_I = \frac{\dot{W}_{net,out}}{\dot{Q}_{in}} \quad (4)$$

For such a geothermal plant depicted in Fig.1, the first law efficiency can be mathematically expressed as in equation (5):

$$\eta_{I,GPP} = \frac{\dot{W}_{gen} - \dot{W}_{pump}}{\Phi_{m,br}\, h_{br,in}} \quad (5)$$

There exist roughly two ways to increase the first law efficiency of this plant: Either to elevate the net power output or to decrease brine re-injection enthalpy, which implies further usage of brine's waste heat.

On the other hand, exergy is defined at dead state conditions. Whilst neglecting all potential and kinetic energy transfers, the specific exergy of geothermal brine can be defined as follows [69]:

$$ex = h - h_0 - T_0(s - s_0) \quad (6)$$

h and *s* are the specific enthalpy and entropy terms in specified state, whereas h_0 and s_0 are the dead state properties at T_0. For a definite mass flow rate $\dot{m}$, physical exergy flow rate can be expressed as in the following form:

$$\dot{E}x = \dot{m}(ex) \quad (7)$$

Accordingly, general exergy or the second law efficiency of a plant can be formulated as:

$$\eta_{II,GPP} = \frac{\dot{W}_{net,out}}{\dot{E}x_{in}} \quad (8)$$

In order to elaborate the second law efficiency of a plant in detail, one should investigate component-based losses and improvement potentials of the system, rather than focusing on general plant efficiency. There exist different approaches in the relevant literature

about definition of the *exergetic efficiency*. First approach could be labelled as *standard exergy efficiency* which is defined as follows:

$$\eta_{II,s} = \frac{\sum Ex_{out}}{\sum Ex_{in}} \tag{9}$$

Since this approach is insensitive to the exergy changes within thermal system, there are other proposals of exergy calculations in several studies [70-71]. For instance, if the top-preheater of plant is taken into account (see Fig.1), standard exergy efficiency is defined as follows:

$$\eta_{II,s,tph} = \frac{Ex_3 + Ex_{15}}{Ex_2 + Ex_{14}} \tag{10}$$

By definition, this approach is an overall approach and it focuses on general balance rather than exergetic conversions within the component. As a result, it does not demonstrate the exergy transfer capability.

To fill this gap, a term called *rational efficiency* was introduced and used by several researchers [72-73]. Rational efficiency can be defined as:

$$\eta_{II,r} = \frac{d(Ex_{medium})}{d(Ex_{source})} \tag{11}$$

Briefly, it is the ratio of exergy change in heat receiving medium and heat source. This approach is more sensible for the evaluation of the second law efficiency of the plant with its particularity on focusing the exergy changes. If we rewrite the second law efficiency of the top-preheater according to definition given above:

$$\eta_{II,r,tph} = \frac{Ex_{15} - Ex_{14}}{Ex_2 - Ex_3} \tag{12}$$

Mathematical definitions of exergy destructions and rational efficiencies of plant components such as turbine, heat exchanger, condenser and pump can be found in relevant literature [41].

From a reverse point of view, it is also possible to obtain lost work rates of plant components with the help of rational second law efficiency definitions. Gouy-Stodola theorem [74] associates level of irreversibility in the system with the lost work rate as follows:

$$\dot{W}_{lost} = T_0 \dot{S}_{G,total} \tag{13}$$

where T_0 is ambient temperature and $\dot{S}_{G,total}$ is the total entropy generation rate of control volume and its surroundings. Once the lost work rate values are obtained for each component, it becomes possible to determine entropy generation rates both at component and plant levels.

Initial model is constructed in Cycle Tempo software and thermodynamic properties of all mediums (water, n-pentane, air etc.) are provided by FluidProp, a database based on REFPROP of NIST [75]. The first law efficiency based on the brine's energy input of plant is calculated around 4.82% and the second law efficiency based on the brine's exergy input is around 25.7% with 16.4 MW of gross power output from the generator, and the auxiliary pump consumption is determined to be around 0.8 MW. Flow of the brine exergy in Kerem GPP is shown in Fig.5:

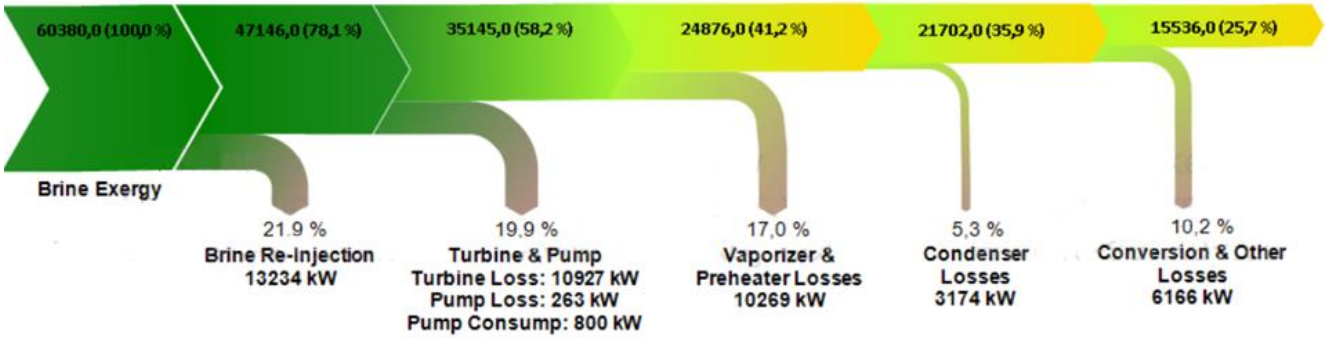

Fig. 5: Exergy flow diagram of Kerem GPP at initial thermodynamic model

Regarding both brine and ORC cycles, majority of the exergy destruction occurs during brine re-injection. This finding is in accordance with previous studies [8-16]. Reason of this loss is the relative narrow gap between brine inlet and re-injection temperatures. Table-2 demonstrates the comparison of results with other GPPs operating in the same geothermal region:

Table-2: Comparison of results with other GPPs in the same region

GPP	**Dora – I [10]**	**Dora – II [10]**	**Bereket [15]**	**Sinem [11]**	**Kerem**
Power Generation (MW)	7.95	9.50	7.50	21.0	16.4
Working Fluid	n-pentane				
Brine Inlet Temp. (°C)	165.0	169.0	145.0	168.2	172.94

Brine Re-inj. Temp. (°C)		82.0	82.0	67.0	78.5	82.8
Cooling Medium Inlet Temp. (°C)		18.3	17.1	16.0	17.5	15.0
Energy Efficiency (%)		5.9	5.7	-	12.9	4.8
Exergy Efficiency (%)		34.7	31.2	9.6	48.2	25.7
Exergy Destruction (%)	Reinjection	22.9	31.7	17.8	22.7	21.9
	Turbine & Pump	15.91	9.5	20.98	9.7	19.9
	Heat Exchangers	13.22	8.0	22.39	11.93	17.0
	Condensers	13.26	19.7	23.61	14.74	5.3

Table-2 presents comparison of analysis outputs in the same region including current study; energy efficiencies are between 5% and 13% whilst exergy efficiencies vary from 9.6% to 48.2%. By means of exergy destruction, turbine losses take a share between 9.5% up to 20.98% of total losses, whilst heat exchanger losses range from 8.0% to 22.39%. Condenser losses seem to be relatively low in Kerem in comparison to other plants with 5.3% of total losses.

Regarding reduction possibility of component sourced losses, pumps and turbines are limited with their fixed isentropic and mechanical efficiencies, thus limiting the exergy destruction of these devices is only possible with parametric alterations -such as turbine inlet temperature & pressure elevations- however it is also constrained with the performance of vaporizers.

Working fluid compatibility is also questionable regarding turbine and pump performances. Heat exchanging losses can also be related with working fluid behaviour. Exergy destruction in condensers is another significant amount with around 5.3%, despite the fact that it seems to be low in comparison to other plants.

Fig. 6 demonstrates the standard and rational exergetic efficiencies of plant components accompanied by the lost work and entropy generation rates. As stated in Guoy-Stodola theorem, work loss rate of components are proportional with the entropy generation rates. Highest and lowest exergy destruction rates correlate with the corresponding entropy generation levels:

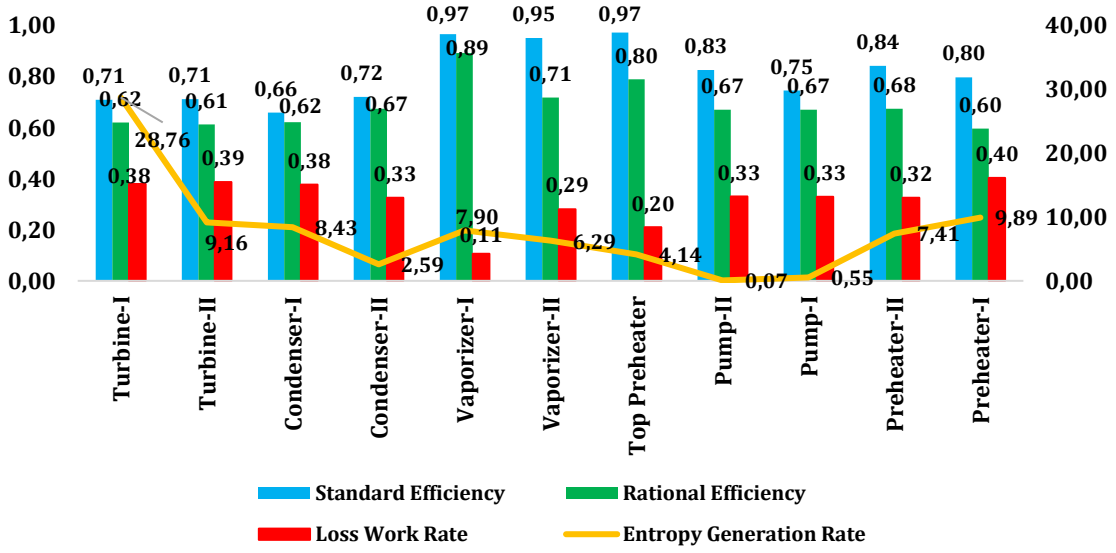

Fig.6: Standard and rational exergetic efficiencies of plant components

As aforementioned in detail, rational efficiencies are more crucial by means of showing the potentials of improvement. Some of the previous studies seemed to be utilizing standard efficiency definition for the exergy evaluation, which could be misleading particularly for vaporizers and preheaters. These devices are operating in quite narrow temperature differences, hence they are expected to have higher efficiencies, however Fig. 3 shows that they still have a room for improvement.

Condensers are operating around 62-67% exergy efficiency due to the relatively low air rejection temperatures. Despite the theoretical improvement potentials (38-33% respectively), options are limited by using air-cooled condensers. At first glance, increasing the air rejection temperature seems to be the ideal solution, however higher air rejection temperatures would contribute further to the greenhouse and air warming effect which is already a problem for Germencik's agricultural fields.

In order to make plant analysis more realistic, condenser fan consumptions will be also taken into the account. Since these values are not available in plant data, theoretical correlations will be utilized. Taking condenser fan consumptions in UNISIM software into the account, Fig. 7 depicts the new exergy flow diagram as follows:

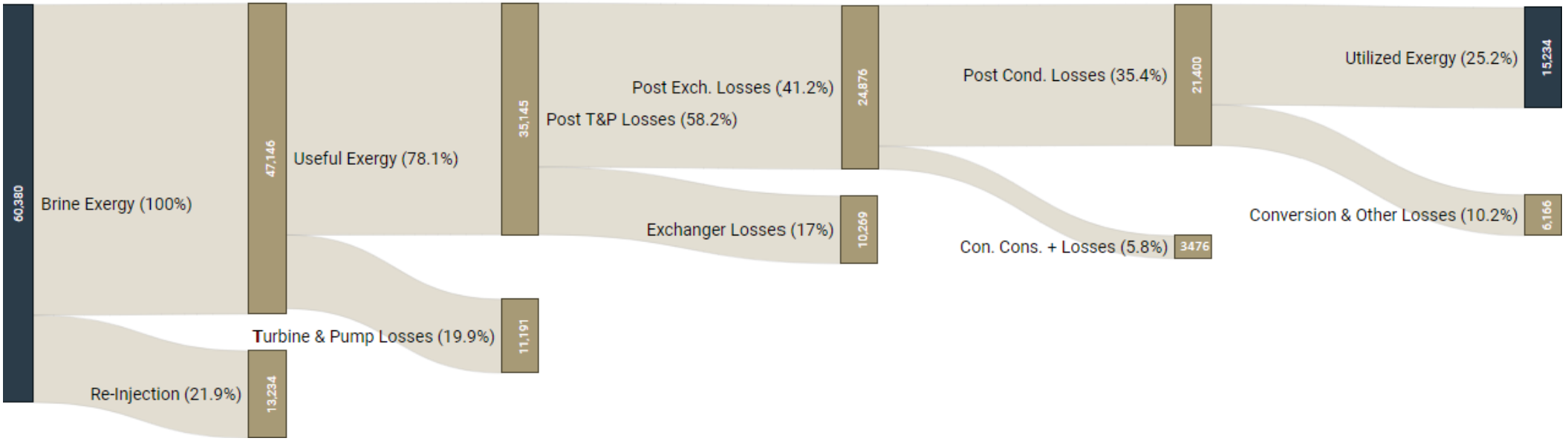

Fig.7: Exergy flows and losses in Kerem GPP

On plant level (including brine re-injection losses) energetic efficiency of the plant is calculated to be 4.73% while the exergetic efficiency is around 25.2%, obtaining 15.23 MW net work output in the updated model.

Turbines and pumps are assumed to be operating under fixed isentropic efficiency at part load as discussed before, by definition, general component efficiency is also limited with mechanical efficiency of these devices. It can be stated that re-injection and expansion processes are the two main sources of exergy destruction in such systems. Heat exchanging behaviours are also validated under different part-load input conditions. Results obtained from plant thermodynamic model indicate that inlet/outlet temperatures and exchanged heat values do not diverge more than 0.8% in comparison to off-design data. Heat exchanging processes including air cooled condenser takes 22.8% of the share in exergy destruction, which can directly be related to working fluids compatibility with heat source. Auxiliary power consumption of condenser fans are estimated around 5 kW and 1.3 kW per unit fan respectively for Condenser-I and Condenser-II according to correlation proposed for 15 ºC ambient temperature by Pieve and Salvadori [68]. Condensers had both 48 active fans under considered part load conditions, which equals 302 kW power consumption.

3.2. A Novel Working Fluid Selection Methodology for Kerem GPP

To achieve this goal, a novel working fluid selection methodology is proposed for the ORC system using a geothermal source for power production, based on the existing plant data of *Kerem* GPP. Combining both thermodynamic and thermo-economic aspects of power production, 29 different single-component working fluid candidates from different chemical branches are subjected to a four-step elimination methodology. Briefly, this methodology includes a preliminary elimination of working fluids based on their critical and boiling temperatures followed by evaluation of their T-s curves for thermodynamic classification purposes.

Suitable candidates are applied to existing plant model at third stage of this methodology and then the final evaluation of remaining candidates is made according to a thermoeconomic criteria which is related to levelized electrical cost (LEC) of plant. Initial thermodynamic analysis results of the power plant, which operates originally with n-pentane, will be presented as a basis for comparison of different candidates. In order to apply this novel approach and investigate a feasible efficiency improvement potential, an option of waste heat recovery from brine re-injection temperature (82.78 ºC) will also be discussed as a separate case study.

Table-3 provides pre-defined design constraints for working fluid candidate applications in the Kerem GPP to apply novel methodology:

Table-3: Design Constraints for Novel Working Fluid Selection Methodology

Parameter	Cycle-I	Cycle-II
Maximum ORC Pressure	0.38 P_c	0.12 P_c
Cooling Air Temperature	15 ºC	
Cooling Air Rejection Temp.	40 ºC	35 ºC
Condenser Outlet Temperature	31.02 ºC	28.70 ºC
Turbine Isentropic Efficiency	0.8	
Pump Isentropic Efficiency	0.83	
Turbine Mechanical Efficiency	0.75	
Pump Mechanical Efficiency	0.80	
Generator Electrical Efficiency	0.92	
p_{out}/p_{in} **(Vaporizer-I)**	0.96	-
p_{out}/p_{in} **(Vaporizer-II)**	-	0.96
p_{out}/p_{in} **(Top-preheater)**	0.95	-
p_{out}/p_{in} **(Preheater-I)**	0.95	-
p_{out}/p_{in} **(Preheater-II)**	-	0.96
p_{out}/p_{in} **(Condenser-I)**	1	-
p_{out}/p_{in} **(Condenser-II)**	-	1
Theoretical Max. for ORC's	24.1 bar	15.8 bar

Brine Inlet Temperature	172.94 ºC	116.28 ºC
Brine Mass Flow Rate	440.694 kg/s	

Since it is the *criticality level* of working fluid -subcritical or super/transcritical- that defines characteristics of ORC systems, first design constraint for different working fluid applications is selected to be the ratio of maximum working fluid pressure (which practically occurs at turbine inlets) to working fluid critical pressure. In order to ensure same level of *subcriticality* for all working fluid applications, this ratio is assumed to be fixed for Cycle-1 and Cycle-2 at 0.38 and 0.12 respectively, which do represent design conditions for n-pentane.

Theoretical maximum values define the upper design pressure limits for different working fluids at Vaporizer-I and II. Cooling air is assumed to be entering the condenser at 15 ºC, the value is based on the data published by Turkish State Meteorological Service (abb. MGM) [76]. Condenser outlet temperature for all fluids is fixed in order to ensure identical ΔT_{low} and ΔT_{high} at condensers as a second criterion.

Third criterion is to apply the same outlet to inlet pressure ratios in heat exchangers as of n-pentane for all working fluids to avoid the rapid pressure elevations within the cycle.

Four-stage novel assessment systematic is schematized in Fig. 8:

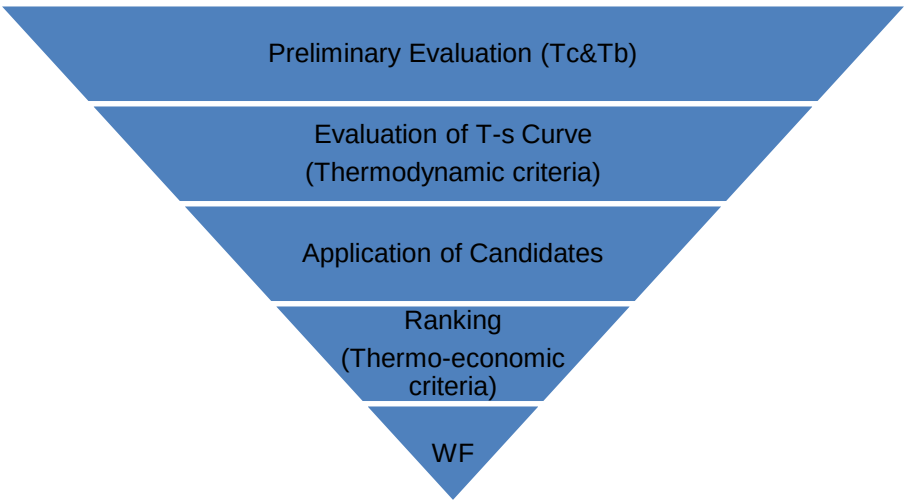

Figure 8: A WF assessment systematic for single-component working fluids in Kerem GPP

Suggested preliminary evaluation criterion is based upon the relationship between geothermal source temperature and candidate working fluid's critical and boiling temperatures. As mentioned before, different studies [24-28] show that, there is a clear relationship between working fluid's critical temperature and source temperature. Critical temperatures that are slightly less than or around the source temperature yield higher efficiencies while critical temperatures which are lower than the half of source temperature indicate the incapability of candidate working fluid. Accordingly, following criterion is suggested for a preliminary evaluation based on WF critical temperature:

$$1.3 > {}^{Tc,wf}/_{Ts} > 0.5 \tag{14}$$

Such a range covers most of the viable working fluids from different chemical groups for a subcritical geothermal cycle. On the other hand, boiling temperature stands out as useful secondary criteria owing to the fact that at a given critical temperature point, higher boiling temperatures lead to lower irreversibilities [24,29].

Moreover, physical constrains dictate that at a given pressure, boiling point of working fluid must be lower than the source temperature so that evaporation occurs. There is also a relationship defined between Tc and Tb which is labelled as $Tbr = Tb/Tc$ (reduced boiling temperature) [24]. Very low boiling points correlate with a ${}^{Tc}/_{Ts}$ ratio lower than 0.5, which should also be prevented. Consequently, boiling point should be "low" enough to facilitate the vaporization and concurrently it should be "high" enough to ensure the lowest possible exergy destruction during phase change. A range of WF boiling temperature to source temperature ratio is proposed as a secondary evaluation criterion:

$$0.9 > {}^{Tb,wf}/_{Ts} > 0.3 \tag{15}$$

29 possible working fluid candidates from 12 different chemical groups were subjected to preliminary evaluation according to the eqns. (14) and (15) as tabulated in Table-4:

Table-4: Preliminary evaluation of working fluids according to critical and boiling temperatures

CANDIDATE WORKING FLUID GROUPS		**Tc/Ts (1.3>x>0.5)**	**Tb/Ts (0.9>y>0.3)**	**Suitability**
Linear Alkanes	**n-Pentane***	0.88	0.79	**OK**
	n-Butane	0.88	0.56	**OK**
	Ethane	0.42	-0.06	**NOK**
	Methane	0.42	-0.64	**NOK**
	n-Hexane	1.36	1.00	**NOK**
Branched Alkanes	**Isopentane**	1.08	0.74	**OK**
	Isobutane	0.78	0.76	**OK**
Cyclic Alkanes	**Cyclohexane**	1.36	1.20	**NOK**
Hydrofluorocarbons (HFC)	**R245fa**	0.89	0.60	**OK**
	R134a	0.59	0.32	**OK**
	R32	0.45	0.20	**NOK**
	R125	0.38	0.14	**NOK**
Chlorofluorocarbons (CFC)	**R11**	0.80	0.79	**OK**
	R12	0.65	0.35	**OK**
	R113	1.24	0.88	**OK**
	R114	0.84	0.54	**OK**
	R115	0.46	0.20	**NOK**
	R13	0.16	-0.07	**NOK**
Perfluorocarbons (PFC)	**R218**	0.42	0.18	**NOK**

	R14	-0.27	-0.44	**NOK**
Inorganics	**Ammonia**	0.77	0.47	**OK**
	Carbondioxide	0.77	-0.05	**NOK**
	Hydrogenesulfide	0.77	0.28	**NOK**
Alcohols	**Methanol**	1.39	1.08	**NOK**
Aromatics	**Toluene**	1.39	1.41	**NOK**
Hydrochloroflorocarbons (HCFC)	**R142b**	0.79	0.47	**OK**
	R22	0.56	0.28	**NOK**
Ethers	**Dimethylether**	0.74	0.44	**OK**
Hydroflouroethers (HFE)	**HFE-245mc**	0.77	0.49	**OK**

Initial source temperature of 172.94 ºC is taken into the account for all calculations. Results show that 15 of 29 working fluid candidates are failed to be selected for further evaluation. In some cases, it is physically impossible to evaporate those working fluids (like toluene, methanol, cyclohexane or n-hexane) at the vaporizers, and in some other cases, low boiling and critical temperatures (R13, R115, R125 or R218) lead negative turbine work outputs at given cycle conditions.

At the second stage, the remaining 14 working fluid candidates are subjected to a *thermodynamic criterion* based on their T-s diagrams. It is a known fact that any working fluid can be classified as *dry, isentropic or wet* depending on slope of saturated vapor side of its T-s curve [77-78]. If slope of this curve is positive, WF can be considered as dry, if this slope is around zero (in a range between 0.5>x>-0.5) considered as isentropic. Working fluids that have saturated vapor T-s slope value below -0.5 can be labelled as wet working fluids. Working fluid classification is another subject of attention, therefore recent studies elaborate classification process in more detail [79].

Thermodynamic criteria will be explained on the T-s curve of n-pentane visually in Fig. 9:

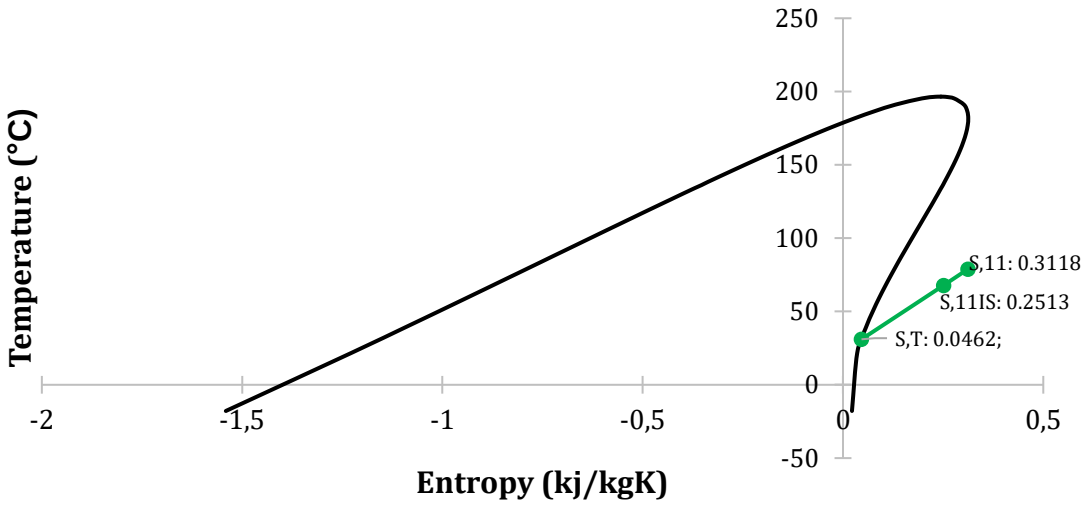

Fig. 9: T-s curve of n-pentane with turbine outlet entropy values

As shown in Fig. 9, S_{11} indicates the WF entropy at turbine outlet (78.9 ºC) with isentropic efficiency of 80% $S_{11,IS}$ shows the WF entropy at isentropic outlet conditions (67.9 ºC) with 100% isentropic efficiency of turbine and S_T represents the saturated vapor entropy at condenser outlet temperature (31.02 ºC). It is obvious that as far as $S_{11,IS}$ converges to S_T, slope of this line would be flatter (~ 0) and working fluid would behave isentropic. Wet fluids have a different T-s curves that demonstrate a reverse trend of this entropy line, which indicates a negative slope. Mathematical expression by assuming a linear variation is as follows:

$$m = \frac{s_{11,IS} - s_T}{s_{11} - s_{11,IS}} \tag{16}$$

14 WF candidates are subjected to T-s criteria and it is found out that 4 of those candidates demonstrate a wet-fluid behaviour. Classification of these working fluids are tabulated in Table-5:

Table-5: Working fluid classification according to thermodynamic criterion

Working Fluid	**Saturated Vapor Entropy [kj/kgK]**	**Isentropic Proc. Entropy Turbine Outlet [kj/kgK]**	**Entropy at Turbine Outlet [kj/kgK]**	**T-S Slope Calculation**	**Classification**
n-Pentane*	0.0462	0.2513	0.3118	3.39	Dry

n-Butane	-0.1394	-0.0631	-0.0216	1.84	Dry
Isopentane	0.0113	0.2013	0.2547	3.56	Dry
Isobutane	-0.1968	-0.1401	-0.1100	1.88	Dry
R245fa	-0.0275	0.0170	0.0403	1.91	Dry
R134a	-0.1786	-0.1857	-0.1766	-0.78	Wet
R11	-0.0084	-0.0105	0.0201	-0.07	Isentropic
R12	-0.1483	-0.1569	-0.1487	-1.05	Wet
R113	0.0364	0.1083	0.1358	2.61	Dry
R114	-0.0399	-0.0022	0.0115	2.75	Dry
Ammonia	-1.2645	-1.7418	-1.6369	-4.55	Wet
R142b	-0.1178	-0.1195	-0.1005	-0.09	Isentropic
Dimethylether	-0.3633	-0.4103	-0.3768	-1.40	Wet
HFE-245mc	-0.0432	0.0023	0.0169	3.12	Dry

Results show that Ammonia, Dimethylether, R12 and R134a demonstrate a wet behaviour while R11 and R142b behaves isentropical. Other candidates are classified as dry working fluids. Wet fluids are incompatible with subcritical cycles, due to the fact that they require a superheating process to prevent the risk of liquid drop formation during the turbine expansion process. On the other hand, dry and isentropic fluids are desirable for their 100% vapor quality at the turbine expansion, so that the fluids in this category will be utilized in succeeding cycle analyses.

Last criterion includes a thermoeconomic indicator to evaluate economic performance of the remaining working fluid candidates. This indicator will be the *levelized electrical cost* (LEC) based on second law plant efficiency proposed by Moran [43]. Different studies were conducted using

this methodology for estimation of unit electricity production cost and results show that it is a useful tool for performance evaluation [16]. Moran's LEC based on second law efficiency can be expressed as follows for a geothermal power plant [16,43]:

$$c_{electricity} = \frac{c_{geo}}{\eta_{II,GPP}}\left(1 + \frac{\sum \dot{Z}_k}{c_{geo}\, \dot{Ex}_{in}}\right) \quad (17)$$

c_{geo} is levelized geothermal brine extraction cost per kg, $\eta_{II,GPP}$ is the second law efficiency, $\sum Z_k$ is levelized sum of initial capital investment and maintenance costs and Ex_{in} stands for brine exergy input rate.

Levelized geothermal brine extraction cost can be defined as [16]:

$$c_{geo} = \frac{C_{ext}\, CRF}{t_{op}\, \dot{m}_{brine}} \quad (18)$$

Durmuş [80] determined a geothermal brine extraction cost (C_{ext}) for Salavatlı region of Aydın in his study.

Owing to the fact that Germencik shares similar resources with Salavatlı, this cost statement can be adapted for this study by using 2019 Chemical Engineering Plant Cost Index (CEPCI) [81] for actual price adjustment.

CRF is the capital recovery factor which is defined as:

$$CRF = \frac{i(1+i)^n}{(1+i)^n - 1} \quad (19)$$

i is the interest rate and n represents economic lifetime of the GPP. In the scope of this study, interest rate is assumed to be 10% and plant lifetime is taken as 20 years. t_{op} represents operating time of the plant. In order to determine $\sum \dot{Z}_k$, levelized equipment cost rate defined by Bejan et al. [82], one should define cost parameters that constitute Annual Capital Investment (C_k , \$/year) [83]:

$$C_k = PW_k * CRF \quad (20)$$

Present worth or amortizing worth of different plant components are defined as follows [84]:

$$PW_k = PEC - SV\ (PWF) \quad (21)$$

PEC is the purchased equipment cost, SV is salvage value or scrap value of the component which can be assumed as 20% of PEC [85], and PWF is the present worth factor of the component which is defined as:

$$PWF = \frac{1}{(1+i)^n} \tag{22}$$

Purchased equipment costs (PEC) are considered as confidential information, therefore it is necessary to make some estimations by applying cost engineering methods. Lemmens [86] summarized the cost engineering method applications for ORC's in her study, stating that accuracy range is diverging between 10% to 30% for these methods.

Best estimations are seemed to be obtained by factorial estimation techniques, accordingly, initial equipment purchasing cost estimations are determined by using different correlations suggested [87-89] for different plant components in this study.

Turton et al. [87] suggested following correlation for cost estimations of heat exchangers, turbines and pumps:

$$\log_{10} C_p^0 = K_1 + K_2 \log_{10}(A) + K_3 [\log_{10}(A)]^2 \tag{23}$$

C_p^0 represents purchased equipment cost and K_1, K_2 and K_3 are the equipment-specific coefficients. A is the cost attribute of component (i.e. surface area for heat exchangers or capacity for turbines and pumps). Smith [88] and Toffolo et al. [89] suggested different correlations for air cooled condensers and generators. For air cooled condensers [88]:

$$C_p^0 = 12300 * \left(\frac{Q}{50}\right)^{0.76} \quad (Q \ in \ kW) \tag{24}$$

Q is the transmitted heat flow in condenser.

Generator cost estimation correlation is as follows [89]:

$$C_p^0 = 1850000 * \left(\frac{P}{11800}\right)^{0.94} \quad (P \ in \ kW) \tag{25}$$

in where, P is the generator power output.

Coefficients for different components are tabulated in Table-6:

Table-6: Coefficients for cost estimation of different plant components

Component	Coefficients		
	K1	**K2**	**K3**
Heat Exchanger	4.6656	-0.1557	0.1547
Turbine	2.2476	1.4965	-0.1618
Pump	3.3892	0.0536	0.1538

Estimations of Turton et al. [87] are based on the value of USD_{2001}. Smith [88] used USD_{2000} values and Toffolo et al. made estimations [89] by employing value of USD_{1993}. Calculations performed with these correlations are adjusted to 2019 USD value with CEPCI 2019 Index (607.5) as follows [86-87]:

$$C_{p\,2019}^{0} = C_{p\,2013}^{0} * (\frac{CEPCI_{2019}}{CEPCI_{1993}}). \quad (26)$$

After the purchased cost estimation of components, it is possible to calculate annual capital investment C_k according to Eq. (20). To improve the accuracy of predictions for this value, it is necessary to take maintenance costs into account as well. Several studies show that it is acceptable to assume Φ_k maintenance factor around 1.06 [90-91]. Levelized cost rate for each component can be calculated as follows:

$$\sum \dot{Z}_k = \frac{C_k * \Phi_k}{N * 3600} \quad (27)$$

N is annual operation time of the plant and it is multiplied with a factor of 3600 to convert it from hours to seconds. Plant operation time is around 290 days a year and accepted as 7000h.

Respective LEC's for different working fluids will be calculated according to equation proposed by Moran [43]. Eq. (17) with inputs expressed between Eq. (18-27) and a final ranking of potential working fluids will be demonstrated as an output of novel WF selection methodology in Results section.

Before presenting the results, it is worth noting that, a drawback of this four – step elimination methodology can be expressed as follows; this method is proposed under part-load conditions with definite environmental circumstances. However, in a renewable energy conversion system, environmental conditions do always have an effect on the conversion performance. Kahraman et al. [11] demonstrated that fluctuations in ambient temperature at different seasons of the year (from 5 ºC to 35 ºC) may reduce the energy efficiencies of geothermal power plants around 4.5% and exergy efficiencies around 18.2% at the same region. On the other hand, Dawo et al. [62] conducted a study which discusses part load behaviour data modelling in a Kalina Cycle power plant. Results indicate that a more comprehensive modelling of turbine isentropic efficiency -i.e. Stodola's law for multistage turbines- is required to estimate gross power output more accurately under different loading circumstances. Despite this fact, it is also pointed out that if the loading behaviour of turbine does not fluctuate in a broad range, it may be feasible to use constant efficiency approach either.

Proposed novel methodology promises a better match between heat source and working fluid, which will be discussed in this section. Figure-10 shows exergy efficiencies and destructions of various plant components operating with n-pentane:

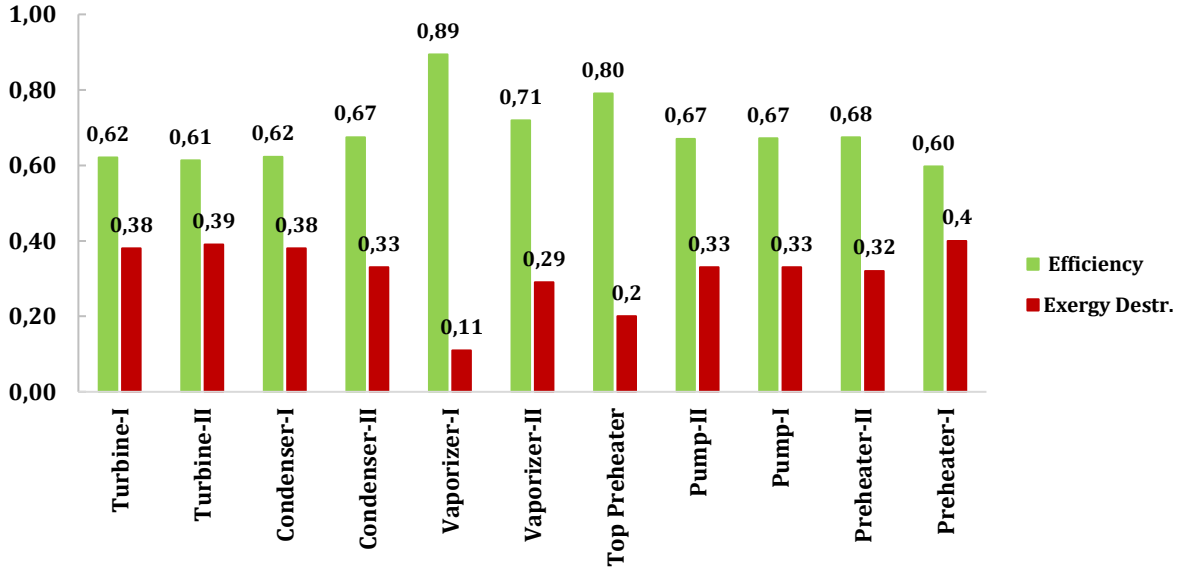

Figure 10: Component second law efficiencies and exergy destructions with n-pentane

In order to reduce the exergy destruction in components (see Fig. 10) and improve the overall second law efficiency of the plant, selecting a more compatible WF is questioned in detail

according to the methodology which was explained in the previous part. Estimations of purchased equipment costs (PEC) for the plant configurations with different working fluid candidates are tabulated in Table-7:

Table-7: PEC Estimations and Levelized Cost Rates for Kerem GPP

	PEC ($)	**Levelized Cost Rate ($/s)**
Vaporizer-I	1,290,877	0.00619
Vaporizer-II	1,467,759	0.00704
Top-Preheater	674,973	0.00324
Preheater-I	2,333,060	0.01119
Preheater-II	658,363	0.00316
Condenser-I	6,000,831	0.02878
Condenser-II	3,424,221	0.01642
Turbine-I	719,069	0.00345
Turbine-II	541,048	0.00259
Pump-I	95,913	0.00046
Pump-II	18,277	0.00009
Generator	4,250,225	0.02038
TOTAL	21,474,616	0.10298

According to 2017 Report of IRENA [92] (International Renewable Energy Agency), worldwide plant investment costs per kW capacity for flash steam and binary power plants were between 1870-5050 $/kW in 2016. Calculations provided in Table-7 show that with this approach, plant investment cost per kW capacity for Kerem GPP is around $1382. But one should not forget that all the plant equipment and their costs (installation, piping, valves, etc.) are not included in these calculations unlike the data provided in IRENA Report. Table-7 only provides an estimation for the main components two ORC cycles in the plant. Additionally, according to the same report, plant installation costs are in a decreasing trend year by year.

Moreover, it is necessary to underline that there is a divergence possibility from real market prices up to 30% with this cost engineering methods [86]. Nevertheless, results are in accordance with recent studies conducted with economic module of Aspen HSYS [11] in the similar geothermal area.

Second law efficiency of Kerem GPP is 25.23% based on brine exergy input. LEC of Kerem GPP with levelized capital costs from Table-7 and levelized brine extraction cost c_{geo} ($/kg) is calculated as 0.0232 $/kWh. According to Eq. (17), in order to minimize the levelized electrical cost, one should either maximize the second law efficiency or brine exergy input, or minimize the levelized equipment cost rates, hence the initial capital investment.

Increasing the second law efficiency (parallel to the first law efficiency) of the plant is either possible by increasing the gap between inlet and outlet temperatures of geothermal brine or reducing the exergy destructions within the system. By this means, a higher amount of exergy would be transferred to turbines and will be converted to more useful work output. Reduction of exergy destruction within the ORC is possible by using more thermally *compatible* working fluids as stated previously.

Consequently, all working fluid candidates are subjected to LEC calculation based on Moran method at this stage of working fluid selection process. Using the same levelized brine extraction costs and brine exergy inputs, change of LEC for different working fluids is only sensitive to second law efficiencies of different working fluids and levelized equipment cost rates. Heat exchanger surface areas are assumed to be the same for all working fluids in order to observe the effect of pump, turbine, condenser and generator sizing for different working fluids. Heat exchanger surface area optimization for different working fluids requires another study which is not included in the scope of this study. However, it is necessary to emphasize that heat exchanger costs are roughly 30% of total capital investment, meaning an optimization of heat exchanger surface areas may have an important impact on total capital investments. Ranking of working fluids based on thermo-economic criteria (LEC) is given in Table-8:

Table-8: Ranking of working fluids based on LEC

Working Fluid	**I. Law Eff.**	**II.Law Eff.**	**LEC ($/kWh)**	**Classification**
R113	0.0532	0.2841	0.0206	**Dry**
R11	0.0496	0.2648	0.0221	**Isentropic**
n-Pentane*	0.0473	0.2523	0.0232	**Dry**
Isopentane	0.0447	0.2331	0.0251	**Dry**
R245fa	0.0347	0.1866	0.0314	**Dry**
n-Butane	0.0304	0.1625	0.0361	**Dry**
R114	0.0283	0.1509	0.0388	**Dry**
HFE-245mc	0.0247	0.1319	0.0444	**Dry**
R142b	0.0234	0.1248	0.0470	**Isentropic**
Isobutane	0.0219	0.1169	0.0501	**Dry**

Result show that LEC of candidate working fluids are more sensitive to the second law efficiency rather than the initial capital investment. Reason of this phenomenon is that; cost estimations for all plant configurations with different working fluids vary in a narrow gap. For instance, isobutane has the lowest second law efficiency with levelized equipment cost rate of 0.0934 $/s while R113's equipment cost rate is around 0.1027 $/s with the highest second law efficiency. That result also reveals that there is not much difference between transmitted heat amount at condensers or auxiliary pump consumptions of candidate working fluids. On the other hand, note that there is nearly a ratio of 2.5 between second law efficiencies of those working fluids. A future work of heat exchanger surface area optimization may be complementary of this study by showing the effect of surface area on levelized electrical costs.

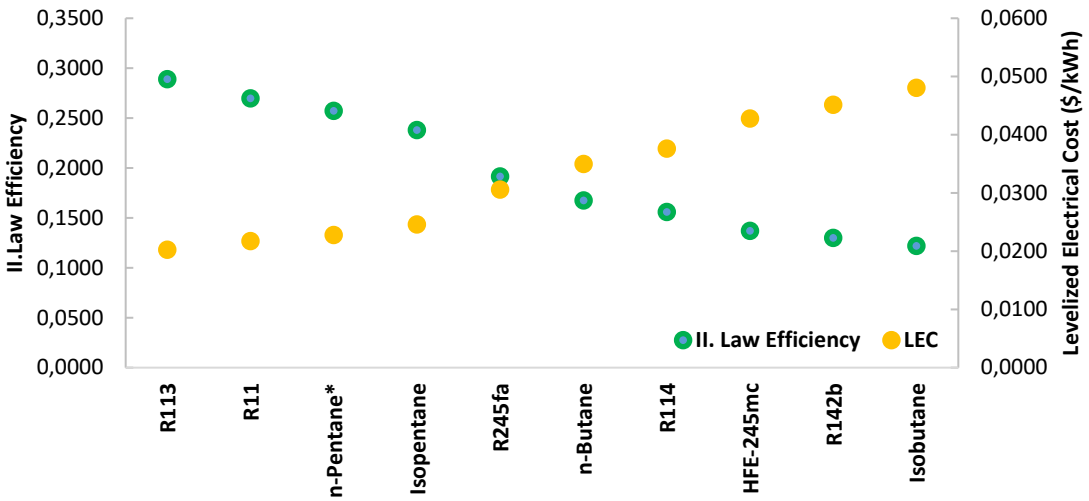

Fig. 11: Relationship between second law efficiency and LEC

Fig.11 demonstrates the relationship between second law efficiencies and levelized electrical costs of the cycle. R113 and R11 are possible candidates for replacing n-pentane at this stage of the evaluation. Higher second law efficiencies of these candidates are caused by higher net work output from turbines. Net work outputs from turbines are closely related to vapor expansion ratio (VER) of the fluid. It can be basically defined as the ratio of vapor pressures before and after the expansion in turbine. Relationship between vapor expansion ratio and net work output are given in Fig.12:

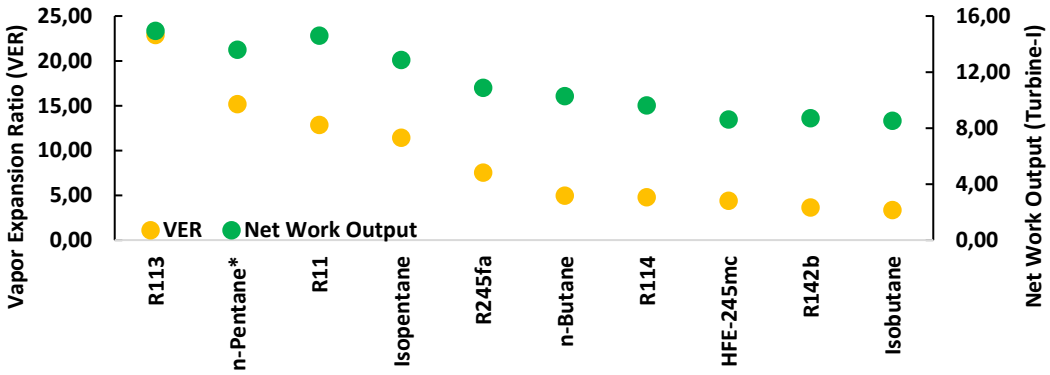

Fig.12: Relationship between VER and net work output

Results show that there is a visible correlation between VER and net work output for dry working fluids. However isentropic fluids (R11 and R142b) behave differently. Even with lower VER, for

instance R11, can lead to a more net work output than n-pentane. Nevertheless R113 shows a better performance in comparison to R11 according to Figs 11 and 12.

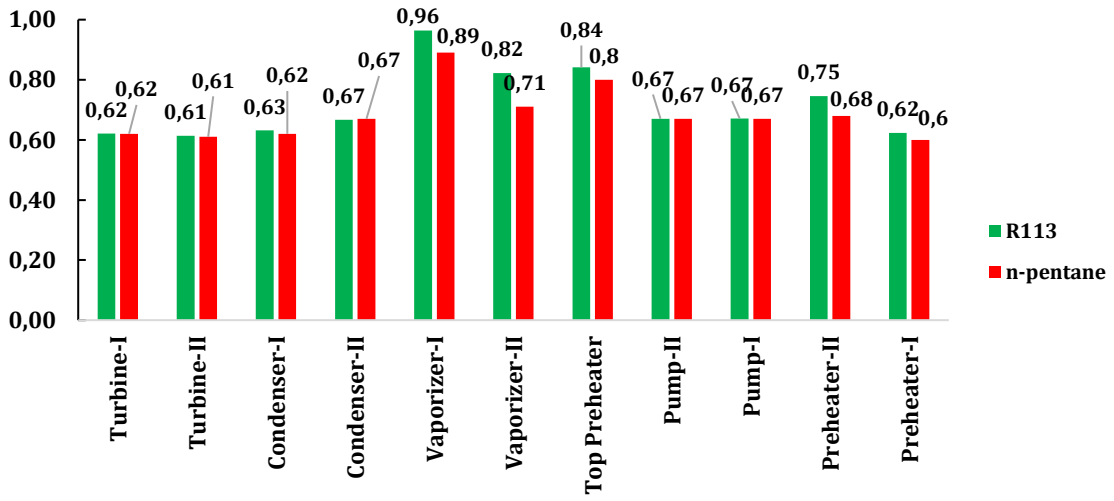

Fig.13: Exergetic efficiencies of plant components with R113 and N-pentane as WF

Fig.13 demonstrates a comparison of R113 and n-pentane for component based exergetic efficiencies under given circumstances. R113 obviously causes less exergy destruction in heat exchangers, consequently, yields to a more useful energy in turbines. Combining with expanding capability (VER) of this refrigerant, simulations yield to a higher plant efficiency and lower levelized electrical cost.

Based on this four-step elimination systematic, R113 seems to be the most suitable candidate for replacing n-pentane. This result is in accordance with [26] where n-pentane and R113 were nominated as candidate working fluids in a subcritical cycle, with turbine sizing and net work output were objective criteria. The methodology presented here is solely based on thermodynamic and economic indicators. And it is worth noting that environmental indicators such as GWP (Global Warming Potential) and ODP (Ozone Depletion Potential) are not taken into the account for WF selection in this study.

3.2.1 Waste Heat Recovery From Re-Injection By Employment of New WF Selection Method

As the majority of exergy destruction occurs during the brine re-injection, an option of waste heat recovery cycle application to brine re-injection process will be the final subject of this part of the study. In order to examine its further applicability, working fluid selection for this WHR cycle will be carried out according to methodology proposed in previous section.

Brine input temperature is limited to current value due to the capacity of geothermal wells in the region, but it is always theoretically possible to utilize re-injected brine and increase the gap between inlet an outlet temperatures of brine cycle. ORC will be the recovery tool for waste heat. A simple 1-cycle system is analyzed with the following process parameters:

Table-9: Process parameters of ORC cycle for waste heat recovery

Parameter	**Cycle-I**
Maximum ORC Pressure	0.38 P_c
$\boldsymbol{\Delta T}$ **of Cooling Air**	25 ºC
Condenser Outlet Temperature	31.02 ºC
Turbine Isentropic Efficiency	0.8
Pump Isentropic Efficiency	0.83
Turbine Mechanical Efficiency	0.75
Pump Mechanical Efficiency	0.80
Generator Electrical Efficiency	0.92
$\boldsymbol{p_{out}/p_{in}}$ **(Vaporizer)**	0.96
Theoretical Max. for ORC's	24.1 bar

Brine Inlet Temp.	82.78 ºC
Brine Final Re-Inj. Temp.	54.00 ºC
Brine Mass Flow Rate	440.694 kg/s

Fig. 14 shows the configuration of WHR cycle:

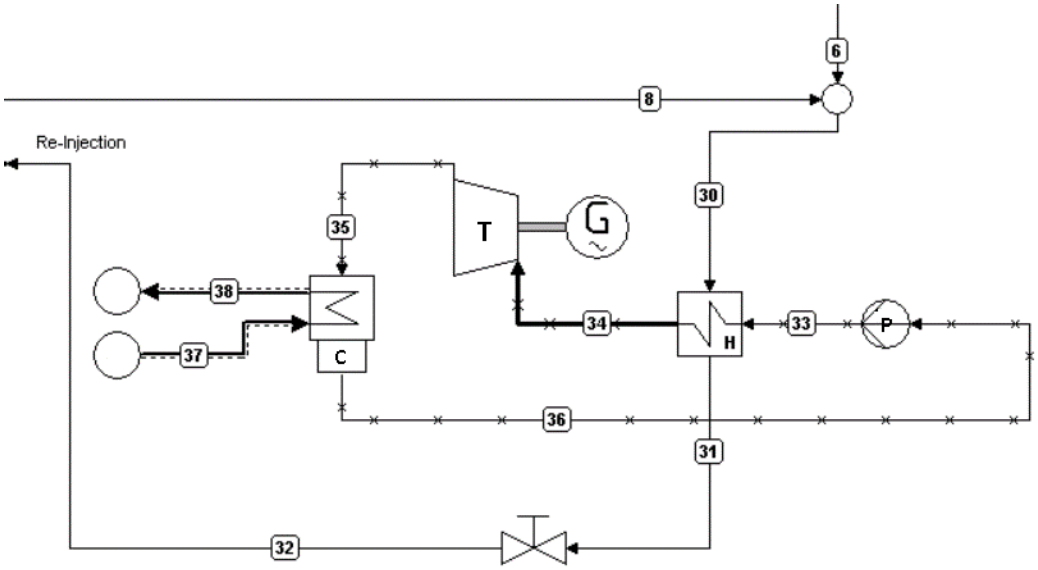

Figure 14: Configuration of WHR cycle

WHR cycle consists of a vaporizer, pump, turbine, condenser, generator and exhaust valve as shown in Fig. 14. Condenser outlet temperature is fixed to the value of 31.02 °C as it is in the main power cycle. Working fluid selection results, LEC values and efficiency improvements achieved with the help of this hypothetical WHR cycle will be demonstrated.

To begin with, WF candidates for WHR cycle according to preliminary evaluation are tabulated in Table-10:

Table-10: Working fluid candidates for WHR according to preliminary criterion

CANDIDATE WORKING FLUIDS	Tc/Ts (1.3>x>0.5)	Tb/Ts (0.9>y>0.3)	Suitability
R134a	0.82	0.68	**OK**
R12	1.28	0.74	**OK**
R32	0.95	0.42	**OK**
R22	1.16	0.59	**OK**
R115	0.97	0.42	**OK**

Applying the thermodynamic criteria (T-s slope) results yield to:

Table-11: Working fluid classification for WHR

Working Fluid	Saturated Vapor Entropy [kj/kgK]	Isentropic Proc. Entropy Turbine Outlet [kj/kgK]	Entropy at Turbine Outlet [kj/kgK]	T-S Slope Calculation	Classification
R134a	-0.1786	-0.1857	-0.1768	-0.80	**Wet**
R12	-0.1483	-0.1569	-0.1489	-1.08	**Wet**
R32	-0.5448	-0.5581	-0.5557	-5.54	**Wet**
R22	-0.2648	-0.2861	-0.2797	-3.33	**Wet**
R115	-0.1410	-0.1398	-0.1389	1.33	**Dry**

Since this cycle will also be a subcritical cycle, wet fluids should be eliminated for further assessment. As a consequence, R115 is the only working fluid option among the working fluids considered in scope of this study. Table-12 provides sample thermodynamic properties of fluids (i.e. R115, air and brine water) in WHR cycle are tabulated according to state numbers at Fig.14:

Table-12: WHR cycle thermodynamic properties according to state numbers

State No.	Description	Fluid	Phase	T(°C)	P(bar)	Sp. Enthalpy (Kj/Kg)	Sp. Entropy (Kj/Kg* K)	Sp. Exergy (Kj/Kg)	Mass flow rate (kg/s)
0	-	Brine	Dead	15	1.013	62.45	0.2207	0	-
0′	-	R115	Dead	15	1.013	-7.98	-0.0268	0	-
0′′′	-	Air	Dead	15	1.013	-98.85	6.8652	0	-
30	Vaporizer Inlet	Brine	Liquid	82.78	0.53	352.73	1.1255	30.03	440.694
32	Valve Outlet	Brine	Liquid	54.00	0.15	226.05	0.7552	10.04	440.694
33	Vaporizer Inlet	R115	Liquid	36.78	12.39	-90.52	-0.4141	29.06	660.605
34	Turbine Inlet	R115	Steam	35.11	11.89	-6.01	-0.1398	34.53	660.605
35	Turbine Outlet	R115	Steam	31.80	10.73	-7.03	-0.1389	33.27	660.605
36	Condenser Outlet	R115	Liquid	31.02	10.73	-96.47	-0.4330	28.56	660.605
37	Condenser Inlet	Air	Gas	15	1.013	-98.85	6.8652	0.13	2190.14
38	Condenser Outlet	Air	Gas	40	1.013	-73.60	6.9493	1.16	2190.14

Note that WF of the main cycle was replaced with R113 (instead of n-pentane). An additional WHR recovery to this cycle -with a system utilizing R115- under these circumstances bring around 160

kW additional net power excluding standard auxiliary pump and air cooled condenser consumptions which are estimated around 303 kW. Summarized improvements of WF re-selection and WHR application to existing plant are tabulated in Table-13:

Table-13: Change of performance outputs according to plant configurations

	Existing Plant	**WF Re-Selection**	**WHR Application**
I.Law	4.73%	5.32%	5.41%
II. Law	25.23%	28.41%	28.67%
LEC ($/kWh)	0.0232	0.0206	0.0204

Levelized cost rate of new system will be as follows:

Table-14: PEC Estimations and Levelized Cost Rates for new system

	PEC ($)	**Levelized Cost Rate ($/s)**
Vaporizer-I	1,290,877	0.00619
Vaporizer-II	1,467,759	0.00704
Top-Preheater	674,973	0.00324
Preheater-I	2,333,060	0.01119
Preheater-II	658,363	0.00316
Condenser-I	5,921,410	0.02840
Condenser-II	3,371,355	0.01617
Turbine-I	729,607	0.00350
Turbine-II	568,297	0.00273
Pump-I	92,923	0.00045
Pump-II	18,289	0.00009
Generator	4,293,568	0.02059
Vaporizer-III	1,176,546	0.00564

Turbine-III	180,586	0.00087
Condenser-III	3,896,653	0.01869
Pump-III	7,862	0.00004
Generator-II	127,721	0.00061
TOTAL	26,809,849	0.12857

Surface area of new Vaporizer-III is estimated from transmitted heat flow/surface area (kW/m^2) ratios of the main system. New LEC of the system is calculated to be 0.0204 $/kWh. This again, proves that the sensitivity of LEC expression against the second law efficiency term. Levelized capital investment increased from 0.1030 $/s to 0.1286 $/s while the second law efficiency rose from 28.41% to 28.67%. Therefore, even with a low-performance working fluid such as R115, waste heat recovery seems to be as another option for reducing the unit electrical costs and increasing the efficiency according to LEC formulation used in the scope of this study.

In the following part, results obtained according to different exergoeconomic methodologies will be provided. Three different methodologies were applied on the plant data -namely Moran, SPECO and ECT- to estimate LEC and cost flows within the plant.

3.3 Exergoeconomic Analysis

In frame of this study, three different exergoeconomic evaluation methodologies are employed for comparison and validation purposes. These methodologies are Moran [43], SPECO [44] and Exergy Cost Theory (ECT) [42] respectively. Moran's method is explained in detail previously, SPECO and ECT are worth of elaborating in detail either.

3.3.1 Specific Exergy Costing (SPECO)

Proposed by Tsatsaronis and Lazzaretto [44], SPECO constitutes its foundations on allocation of costs to the exergy streams within the system following an exergy analysis. At first stage, all exergy streams are identified. Following this identification, streams are decomposed as fuels and products (i.e. F-P table) of all system components. Last stage consists of cost associations with stream exergy values, which compose together exergy costs of the system. Fuel and investment-maintenance costs

of the system are calculated according to principles and equations explained in previous section between eq. (17-27).

A cost balance for a steady-state system can be defined as follows [82]:

$$\sum_{j=1}^{n} \dot{C}_{j,k,out} = \sum_{j=1}^{m} \dot{C}_{j,k,in} + \dot{Z}_k \quad (28)$$

$\dot{C}_{j,k}$ denotes cost rate of j'th stream at k'th component.

Exergy related specific cost can be defined as:

$$c = \frac{\dot{C}}{\dot{\Phi}} \quad (29)$$

$\dot{C}$ denotes stream cost whilst $\dot{\Phi}$ is the exergy rate.

There are two valid principles that should be complied with whilst producing F-P table of a system. F-Principle dictates that exergy extracted from previous component equals the sum of inlet exergy of supplied component(s) as mentioned before and P-Principle says that each exergy unit shall be supplied at the same average cost to any stream associated with the product.

After the application of F-P principles and association of the costs with exergy streams, different indicators can be defined for the interpretation of results. For instance, exergy destruction rate can be extracted from exergy balance within the kth component [93]:

$$\dot{I}_{D,k} = \dot{\Phi}_{F,k} - \dot{\Phi}_{P,k} - \dot{\Phi}_{L,k} \quad (30)$$

where $\dot{\Phi}_{F,k}$, $\dot{\Phi}_{P,k}$ and $\dot{\Phi}_{L,k}$ demonstrate exergy rates of fuel, product and residues/losses respectively. From that term, another important indicator can be identified as *exergy destruction ratio* as follows [94]:

$$y_k = \frac{\dot{I_{D,k}}}{\dot{\Phi_{Fuel}}} \quad (31)$$

Definition of *exergy destruction ratio* is the proportionality between exergy destruction rate at kth component and exergy rate of fuel input to the system. By adapting exergy related specific cost equation (29) to the F-P concept, it is possible to generate specific cost of fuel and product at kth component as follows:

$$c_{F,k} = \frac{\dot{C_{F,k}}}{\dot{\Phi_{F,k}}} \quad (32)$$

$$c_{P,k} = \frac{\dot{C_{P,k}}}{\dot{\Phi_{P,k}}} \tag{33}$$

Cost rate of exergy destruction:

$$C_{D,k} = c_{F,k}\, \dot{I_{D,k}} \tag{34}$$

Hereafter, cost balance equation (28) can be specified for kth component:

$$\sum c_{P,k}\, \Phi_{P,k} \quad = \sum c_{F,k}\, \Phi_{F,k} + \dot{Z}_k \tag{35}$$

Maybe the most important indicator for exergoeconomic performance is the *exergoeconomic factor* which is defined as follows [94]:

$$f = \left(\frac{\dot{Z}_k}{c_{F,k}\, \dot{I_{D,k}} + \dot{Z}_k}\right) \tag{36}$$

Interpretation of exergoeconomic factor is crucial to understand the cost effectiveness of kth component. By mathematical expression, it is obvious that this factor varies between 0 and 1. If this term converges to zero, this implies that cost rate of exergy destruction is dominant in this device rather than initial capital investments. Consequently, more money can be invested in this component to reduce irreversibilities and improve overall cost efficiency of the plant. In contrast, if this value reaches to 1. it explains that initial investments overwhelm the irreversibility related costs, accordingly there is less room for investment. In general, a balanced device with f value around 0.5 is desired for power plants [94].

3.3.2 Exergy Cost Theory (ECT)

Exergy costing problem was introduced by Valero et al. [42] as follows; under the light of a system whose boundaries and degree of aggregation for its constituting subsystems have been specified, the problem is about *obtaining the cost of flows which are interrelated*. In order to solve such a problem, four prerequisites should be fulfilled [42,95]:

(i) Identification of the boundary conditions. All resources used within the system shall be specified: Energy inputs, raw materials, economic resources, labour resources etc.

(ii) Aggregation level of the system: System shall be decomposed properly into its subsystems (flows and processes) until viable information can be obtained.

(iii) Exergetic efficiency, as an indicator of irreversibility level of a process, shall be utilized as a physical measure for allocating all costs. Exergetic cost of the sources (i.e. fuels) utilized in the process shall be allocated to their outputs (i.e. products) in proportion to their exergetic content.

(iv) Origins of the wastes: Waste formation processes shall also be analyzed aiming to find roots of waste production within the system sub-components. It may be possible to refine cost-allocation with re-distribution of wastes to their main responsible within the system [95].

In order to establish an exergoeconomic analysis of the energy system based on Exergy Cost Theory, a collection of information is needed, which forms the exergoeconomic model of the energy system. This includes physical structure, thermodynamic model, economic model (not always) and efficient structure.

Physical structure simply defines system components and their interactions including turbines, generators, exchangers, pumps etc. An effective data structure representation of the physical structure of an energy system for a particular level of aggregation is rendered by means of a directed graph which includes:

$$\zeta = \{v_0, v_1, v_2 \dots v_n\} \tag{37}$$

Equation (37) defines a collection of graph nodes for system sub-components. Index 0 denotes the environment. Any v_i element includes features such as title, process etc.

$$E = \{e_1, e_2, e_3 \dots e_n\} \tag{38}$$

$$e = (u, v) \tag{39}$$

As equation (26) shows, e_i terms are ordered pairs of different nodes which are related to components they are connected. They constitute a set of graph lines (Eq.38). Aside from mathematical definition, they do represent the *flows* and different flow types can be applied in this concept such as heat, mass, waste etc.

Incidence matrix ($A_{i,j}$) reveals the interrelation between flows and components.

$$A_{i,j} = \begin{cases} +1 \; if \; e_j = (v_k, v_i) \\ -1 \; if \; e_j = (v_i, v_k) \\ \quad 0 \; otherwise \end{cases} \tag{40}$$

As explained in Eq. (40), if e_j flow enters to v_i component, all elements of incidence matrix become +1. -1 will be the value of all elements at leaving conditions. If there is not any relation between a flow and component, matrix turns to zeros. Physical structure of the system is expressed with the help of incidence matrix, therefore it is possible to label it as an auxiliary matrix for the formation of aforementioned F-P tables.

Thermodynamic model includes a thermodynamic analysis of the plant by the help of mass-heat-work sets of equations. With the help of thermodynamic model, exergy rates of all streams identified in physical structure can be associated.

All parameters that may affect costing should be provided in an *economic model* such as; purchased equipment costs, present worth factors, operation times, maintenance costs, interest rates etc. Economic model of the existing power plant is presented in previous sections.

Physical structure of a system (where all physical flows appear) needs to be transformed into a *productive structure* defined by the F-P table, which explains how the production processes are interrelated among each other. Efficiency of kth component can be expressed in F-P concept as follows:

$$\varepsilon_K = {}^{\Phi_P}/_{\Phi_F} \tag{41}$$

Unit Exergy Consumption (K) is another indicator in ECT which is defined as an inverse of this statement. In order to define the *productive structure* mathematically, one should recognize for each part, one or more fuel and product streams from the entire set of flows that constitute them. That can be performed through the utilization of proper incidence matrices.

Incidence matrix of the fuel:

$$A_F(i,j) = \begin{cases} A(i,j)\ if\ e_j \in F_i \\ 0\ otherwise \end{cases} \tag{42}$$

Where F_i defines a set of fuel streams to the v_i component.

Incidence matrix of the product:

$$A_P(i,j) = \begin{cases} -A(i,j)\ if\ e_j \in P_i \\ 0\ otherwise \end{cases} \tag{43}$$

Where P_i defines a set of fuel streams from the v_i component.

Multiplication of incidence matrices with exergy flow vector provides *fuels* and *products* of the F-P table:

$$A_F * E = F \tag{44}$$

$$A_P * E = P \tag{45}$$

Although the name of this structure is *productive*, cyclic systems always include *dissipative* units for the sake of consistency. To distinguish between them, dissipative and productive devices are labeled separately at the very beginning of analysis.

3.3.2.1 Calculation of F-P Table

An Exergy Cost Theory based analysis primarily constitutes on F-P table of the plant. With the help of this table, it becomes possible extracting further conclusions and extending the depth of analysis to the different points of view. To begin with the F-P concept, one should understand the input-output economic analysis of Leontief [97].

Taking a system which consists n-processes into the account, let say P_i is the amount of total exergy of ith process and E_{ij} represents the exergy pair (j denotes utilized resource to produce i), P_i or a row of an input-output matrix can be expressed as follows:

$$P_i = E_{i0} + \sum_{j=1}^{n} E_{ij} \quad i = 1 \dots n \tag{46}$$

where 0 denotes the system environment, accordingly E_{i0} represents the production of ith component which leaves the system as a final product or a waste/residue.

Table-15: Fuel-Product Table Structure

		Final Product	**Process Resources**					**Total**
			1	**…**	**j**	**…**	**n**	
External Resources			E_{01}	…	E_{0j}	…	E_{0n}	P_0
	1	E_{10}	E_{11}	…	E_{1j}	…	E_{1n}	P_1
	.	.	.		.		.	.

Process **Products**	. .	. .	. .		. .		. .	. .
	i	E_{i0}	E_{i1}	…	E_{ij}	…	E_{in}	P_i
	. . .	. . .	. . .		. . .		. . .	. . .
	n	E_{n0}	E_{n1}	…	E_{nj}	…	E_{nn}	P_n
Total		F_0	F_1	…	F_j	…	F_n	

In this matrix, sum of the external exergy values equals to *production* of the environment which can be interpreted as *fuel input* to the whole system in other words.

Mathematical description of the fuel input:

$$F_T = P_0 = \sum_{j=1}^{n} E_{0j} \tag{47}$$

From the environmental point of view, system also does a work against the environment and it can inversely be interpreted as the *fuel input to the environment* or product of the system which is:

$$P_T = F_0 = \sum_{j=1}^{n} E_{j0} \tag{48}$$

Each process utilizes a part of the total external resource and resources left from other processes, therefore fuels of processes within the system can be expressed as follows:

$$F_i = E_{0i} + \sum_{j=1}^{n} E_{ji} \qquad i = 1 \ldots n \tag{49}$$

In this concept, it is straightforward to interpret irreversibility as an output of the second law again: it equals to difference between fuels and products of a process and has always a positive value (except the isentropic case).

So far F-P table is nothing more than the distribution of exergy inputs and outputs to the components. Essence of the *exergy costing* is now vital to transfer the system from exergy balance to the exergy cost balance. Exergy cost is defined as follows: *Given a system whose limits, level*

of aggregation and production purpose of its components have been defined, exergy cost $\dot{E}_i$ *of the physical flow* E_i *is the amount of exergy needed to produce this flow* [42]*:*

$$c_i = \dot{E}_i / E_i \tag{50}$$

Long story short, by conducting an exergoeconomic analysis based on ECT, one should take lost exergies into the account due to the irreversibilities during the formation of new flows:

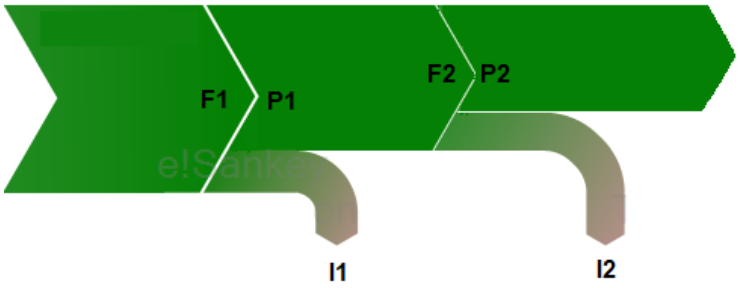

Fig.15: Exergy Diagram of a Sequential Flow

By definition of exergy costing [42], Figure-15 demonstrates that one can state exergy cost of a product equals the exergy of the product plus all exergy losses due to irreversibilities on the way:

$$\dot{P}_i = P_i + \sum_{j=1}^{i} I_j \tag{51}$$

It is possible to extract another conclusion from this definition. Recalling the definition of *exergy unit consumption* of i'th component or process ($\Phi_{F,i}/\Phi_{P,i}$), it is possible to argue that exergy cost of a product equals to multiplication of previous unit exergy consumptions of processes which play role in the production of final flow of product:

$$\dot{k}_{p,i} = \prod_{j=1}^{i} K_j \; where \; K_j \geq 1 \tag{52}$$

Under the light of this explanation, transition from exergy balance to exergy cost balance for equations 46 and 49 are straightforward:

$$\dot{P}_i = \dot{E}_{i0} + \sum_{j=1}^{n} \dot{E}_{ij} \quad i = 1 \dots n \tag{53}$$

$$\dot{F}_i = \dot{E}_{0i} + \sum_{j=1}^{n} \dot{E}_{ji} \qquad i = 1 \dots n \tag{54}$$

$\dot{E}_{ij}$ stands for cost of exergy flow whilst $\dot{F}_i$ and $\dot{P}_i$ are exergy costs of fuel and product.

Based on these principles, ECT postulates three assumptions in order to draw a framework:

A1: External/Internal Assessment Assumption: Briefly, this assumption dictates the vitality of system boundaries selected. If anyhow irreversibilities are not taken into the account, then the assessment turns to an internal assessment in which *exergy* of a flow equals to its *exergy cost.*

$$\dot{E}_{0i} = E_{0i} \tag{55}$$

A2: Conservation of the exergy cost: Anywhere in the system, exergy cost of a fuel equals to exergy cost of a product.

$$\dot{F}_i = \dot{P}_i \tag{56}$$

A3: Proportionality of the costs: Exergetic efficiency of a process is the proportionality factor for cost allocation to different flows originating from the process:

$$\dot{E}_{ij} = \dot{k}_{p,i} E_{ij} \tag{57}$$

Rearranging eqn. (53) according to equations (54-55) yields:

$$\dot{P}_i = \dot{E}_{0i} + \sum_{j=1}^{n} \dot{k}_{p,i} E_{ji} \quad i = 1 \dots n \tag{58}$$

A further arrangement of this equation with the term unit exergy cost (eqn. 50) provides:

$$\dot{P}_i - \sum_{j=1}^{n} E_{ji} \frac{\dot{P}_j}{P_j} = \dot{E}_{0i} \qquad i = 1 \dots n \tag{59}$$

Exergy costs of all products in the system can be determined according to the solution of this linear equations set. A specific term called *distribution coefficient (y)* is also coined for proportion of product of ith process utilized in j-th process:

$$y_{ij} = \frac{E_{ij}}{P_i} \tag{60}$$

Exergy costs of all products originate from a component or process are distributed to other components and environment in compliance with distribution coefficient. Described in exergy terms, exergy costing theory produces outputs without units. However, it is very straightforward to apply monetary inputs, all cost allocations are executed with same exergy cost distribution principles according to the initial costs of external resources.

3.3.2.2 An Application of Exergy Cost Theory to Kerem GPP

Figure-16 illustrates all main components and streams (i.e heat and work) in Kerem GPP at given operating conditions.

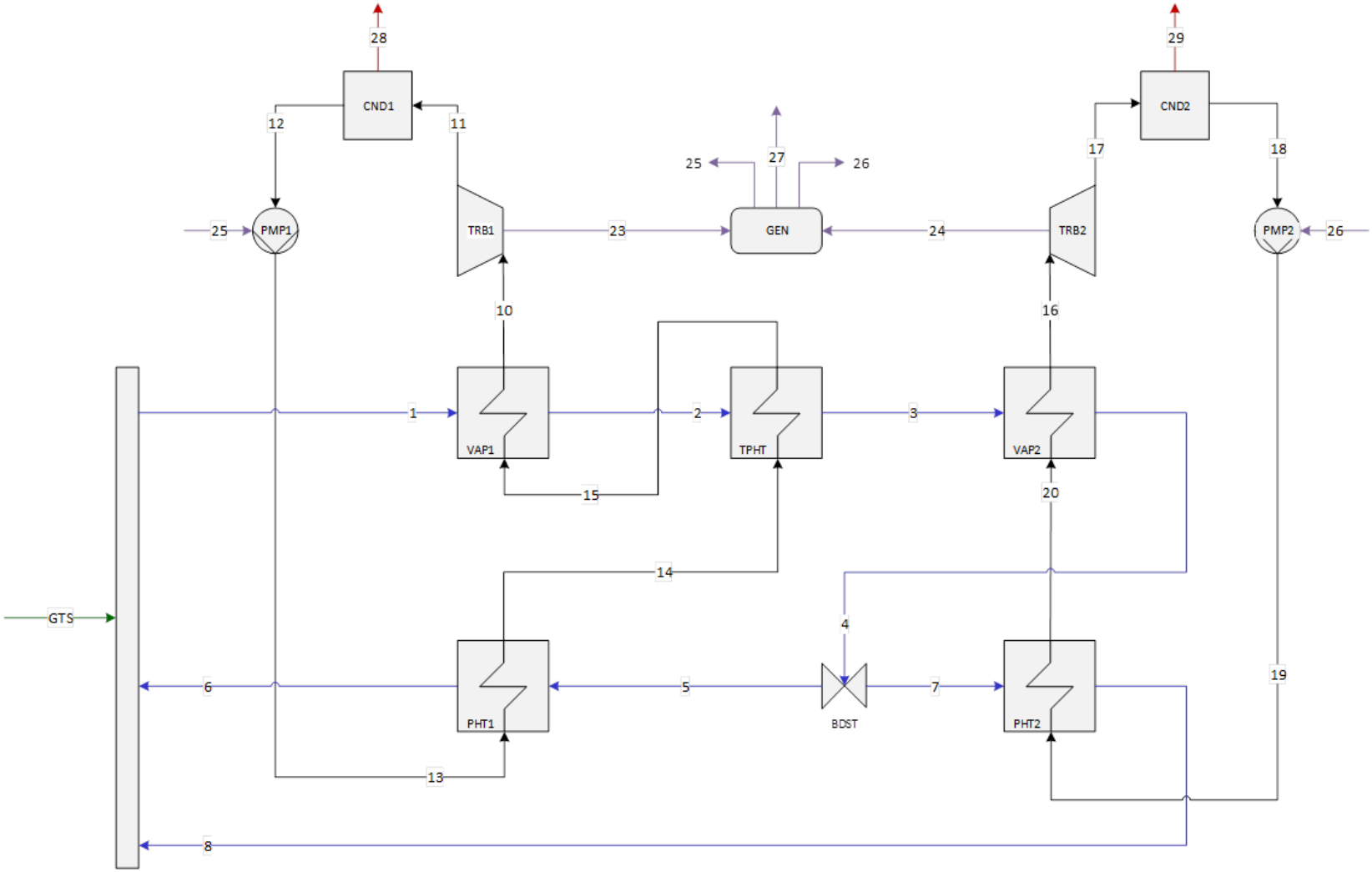

Fig. 16: Main Components and Streams in Kerem GPP

Working principle and a comprehensive thermodynamic analysis of Kerem GPP was already provided in previous sections, therefore they will not be mentioned here again. To begin with, it is necessary to define fuels and products of every process in this geothermal system. Table-16 classifies streams as fuels and products and components as productive and dissipative:

Table-16: Classification of Components and Streams

	NR	PROCESS	FUEL	PRODUCT
PROD	0	Environment	$E_{27}+E_{28}+E_{29}$	E_{21}
	1	Vaporizer 1	E_1-E_2	$E_{10}-E_{15}$
	2	Organic Turbine 1	$E_{10}-E_{11}$	E_{23}
	3	Cycle Pump 1	E_{25}	$E_{13}-E_{12}$
	4	Preheater 1	E_5-E_6	$E_{14}-E_{13}$
	5	Top Preheater	E_2-E_3	$E_{15}-E_{14}$
	6	Vaporizer 2	$E_9+(E_3-E_4)$	$E_{16}-E_{20}$
	7	Organic Turbine 2	$E_{16}-E_{17}$	E_{24}
	8	Cycle Pump 2	E_{26}	$E_{19}-E_{18}$
	9	Preheater 2	E_7-E_8	$E_{20}-E_{19}$
	10	Brine Distributor	E_4	E_5+E_7
	11	Geotermal Source	E_{21}	$E_1-E_6-E_8$
	12	Generator	$E_{23}+E_{24}$	$E_{25}+E_{26}+E_{27}$
DIS	13	ACC- 1	$E_{11}-E_{12}$	E_{28}
	14	ACC- 2	$E_{17}-E_{18}$	E_{29}

There are twelve productive units -including environment- and two dissipative units in this plant. Since there are mainly four different flows within the system, namely **B**rine, Organic **V**apor, **W**ork and heat (**Q**), these symbols can be utilized for the characterization of different flows in different components.

By this means it is possible to convert Table-16 to Table-17:

Table-17: Symbolic Transformation of Flow Types

Abb.	Component	Fuel	Product	Type
GTS	Geothermal Source	GTS	B1-B6-B8	PRODUCTIVE
VAP1	Vaporizer 1	B1-B2	V10-V15	PRODUCTIVE
PHT1	Preheater 1	B5-B6	V14-V13	PRODUCTIVE
TPHT	Top Preheater	B2-B3	V15-V14	PRODUCTIVE
VAP2	Vaporizer 2	B3-B5-B7	V16-V20	PRODUCTIVE
PHT2	Preheater 2	B7-B8	V20-V19	PRODUCTIVE
TRB1	Organic Turbine 1	V10-V11	W23	PRODUCTIVE
PMP1	Cycle Pump 1	W25	V13-V12	PRODUCTIVE
TRB2	Organic Turbine 2	V16-V17	W24	PRODUCTIVE
PMP2	Cycle Pump 2	W26	V19-V18	PRODUCTIVE
GEN	Generator	W23+W24	W25+W26+W27	PRODUCTIVE
CND1	ACC-1	V11-V12	Q28	DISSIPATIVE
CND2	ACC-2	V17-V18	Q29	DISSIPATIVE

In order to obtain the F-P table of the plant, it is necessary to conduct sort of a *prosecution* -which device feeds and fed by which one- within the plant to understand the interrelations between the components. Despite they seem to be a sequential process at the first glance, heat and work flows

in power plants are usually much more complex. From Figure-15 and Tables 16-17, it is straightforward to say that geothermal source feeds all heat exchangers in the system and constantly fed by the environment. In other words, brine line provides all the exergy to the heat exchangers. It is certainly known that pumps are fed by electricity created by the generator. Generator is fed by turbines with relevant work flows. Taking Cycle-I into the account, starting from Pump-I, Preheater-I, Top-Preheater and Vaporizer-I do increase the exergy of organic vapor for power production in Turbine-I and rejection of the waste exergy in ACC-I. Cycle-II works according to the same principle except there is no top preheater. Figure-17 visualizes these relationships on graphical description:

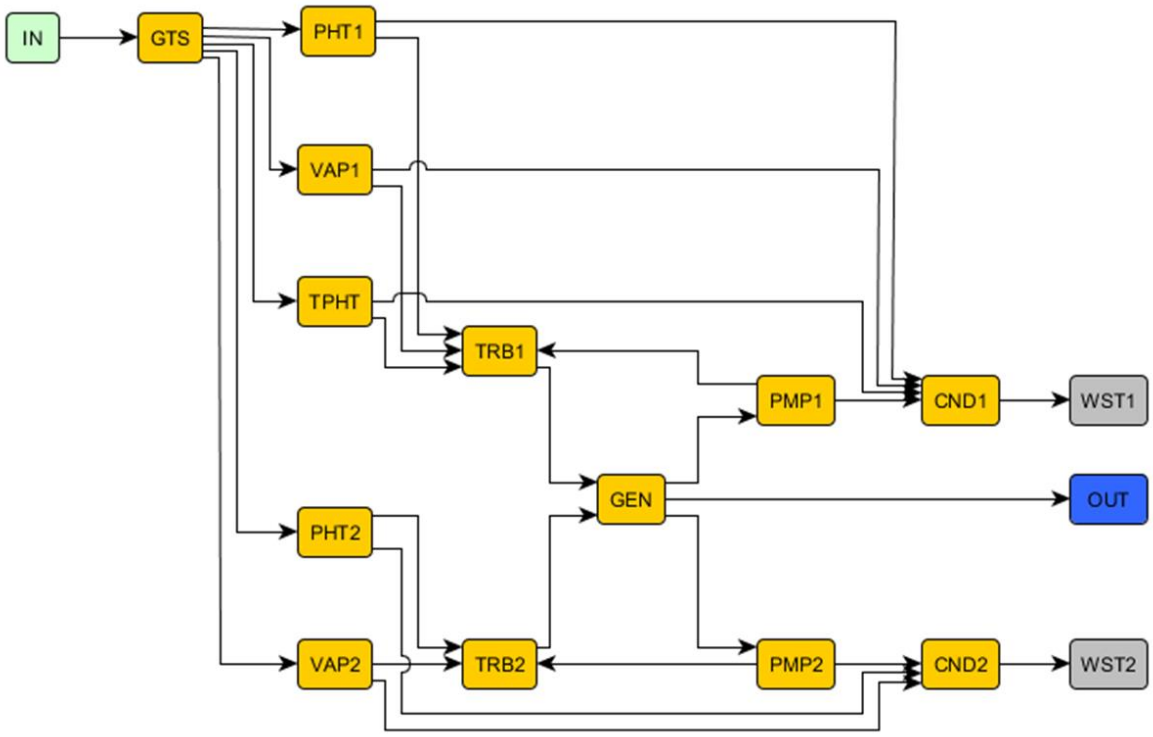

Fig.17: Exergy Transfers Between Kerem GPP Components and Environment

Relation between geothermal source and heat exchangers is one-to-one, so there is no proportionality and *distribution coefficient* is not necessary. However for example CND-1 and TRB-1 are fed by same devices, therefore a distribution coefficient of exergy cost should be defined. If one simply sums all products of the devices which feed CND1. without any distribution the value should equal to fuel input of CND1. It will not due to the fact that a proportion of this exergy is also transferred to TRB-1.

Figure-18 explains the problem further:

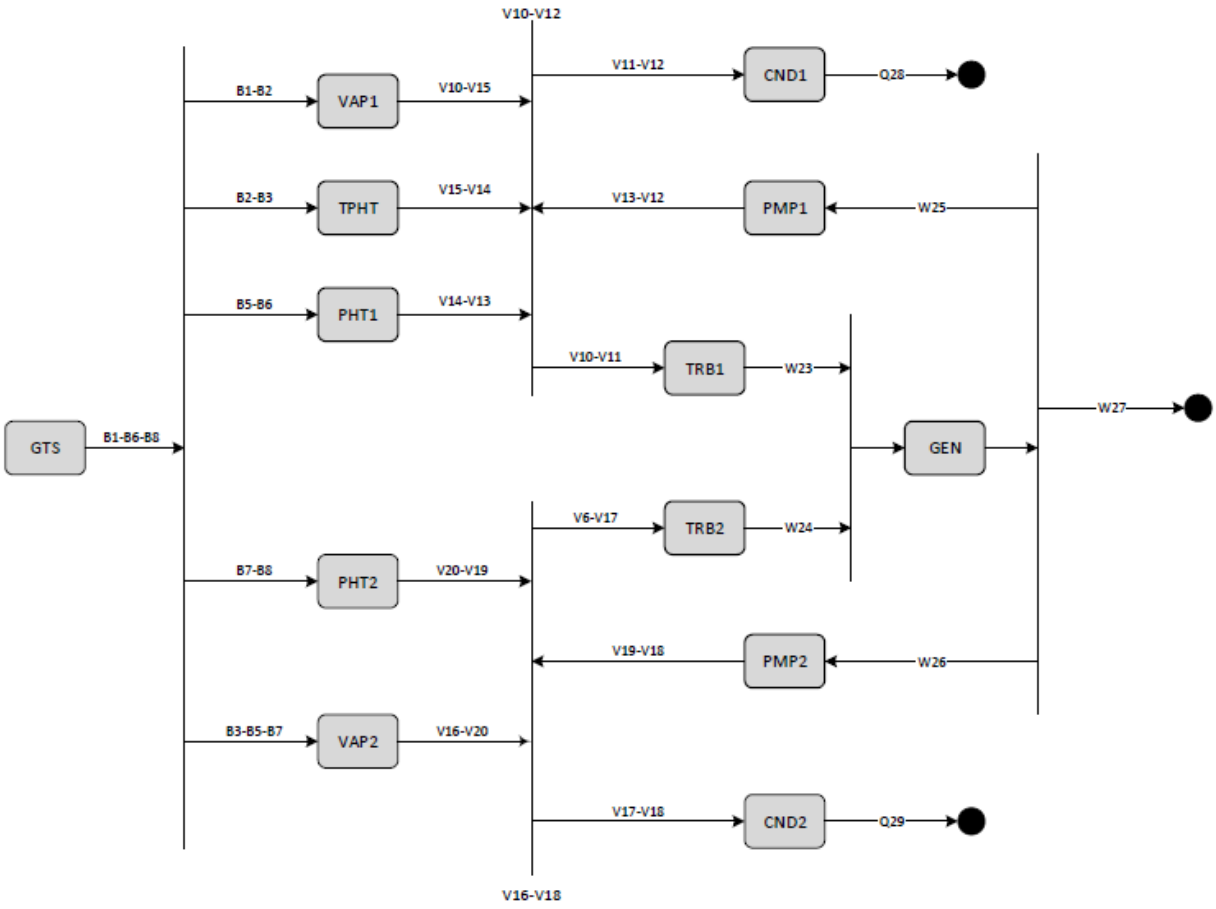

Fig. 18: Productive Structure of Kerem GPP

Productive structure of the plant enables the algebraic definitions of distribution coefficients in this plant:

$$y_{TRB,1} = \frac{V_{10} - V_{11}}{V_{10} - V_{12}} \tag{61}$$

$$y_{TRB,2} = \frac{V_{16} - V_{17}}{V_{16} - V_{18}} \tag{62}$$

$$y_{CND,1} = \frac{V_{11} - V_{12}}{V_{10} - V_{12}} \tag{63}$$

$$y_{CND,2} = \frac{V_{17} - V_{18}}{V_{16} - V_{18}} \tag{64}$$

Since all exergy streams and distribution rules are defined, it is now possible to construct a F-P table. Table-18 shows the F-P table of Kerem GPP in analytic format:

	GTS	VAP1	PHT1	TPHT	VAP2	PHT2	TRB1	PMP1	TRB2	PMP2	GEN	CND1	CND2	ENV	Total
GTS	0	B_1-B_2	B_5-B_6	B_2-B_3	B_3-B_5-B_7	B_7-B_8	0	0	0	0	0	0	0	0	B_1-B_6-B_8
VAP1	0	0	0	0	0	0	$y_1(V_{10}$-$V_{15})$	0	0	0	0	$y_2(V_{10}$-$V_{15})$	0	0	V_{10}-V_{15}
PHT1	0	0	0	0	0	0	$y_1(V_{14}$-$V_{13})$	0	0	0	0	$y_2(V_{14}$-$V_{13})$	0	0	V_{14}-V_{13}
TPHT	0	0	0	0	0	0	$y_1(V_{15}$-$V_{14})$	0	0	0	0	$y_2(V_{15}$-$V_{14})$	0	0	V_{15}-V_{14}
VAP2	0	0	0	0	0	0	0	0	$y_3(V_{16}$-$V_{20})$	0	0	0	$y_4(V_{16}$-$V_{20})$	0	V_{16}-V_{20}
PHT2	0	0	0	0	0	0	0	0	$y_3(V_{20}$-$V_{19})$	0	0	0	$y_4(V_{20}$-$V_{19})$	0	V_{20}-V_{19}
TRB1	0	0	0	0	0	0	0	0	0	0	W_{23}	0	0	0	W_{23}
PMP1	0	0	0	0	0	0	$y_1(V_{13}$-$V_{12})$	0	0	0	0	$y_2(V_{13}$-$V_{12})$	0	0	V_{13}-V_{12}
TRB2	0	0	0	0	0	0	0	0	0	0	W_{24}	0	0	0	W_{24}
PMP2	0	0	0	0	0	0	0	0	$y_3(V_{19}$-$V_{18})$	0	0	0	$y_4(V_{19}$-$V_{18})$	0	V_{19}-V_{18}
GEN	0	0	0	0	0	0	0	W_{25}	0	W_{26}	0	0	0	W_{27}	W_{25}+W_{26}+W_{27}
CND1	0	0	0	0	0	0	0	0	0	0	0	0	0	Q_{28}	Q_{28}
CND2	0	0	0	0	0	0	0	0	0	0	0	0	0	Q_{29}	Q_{29}
ENV	GTS	0	0	0	0	0	0	0	0	0	0	0	0	0	GTS
Total	GTS	B_1-B_2	B_5-B_6	B_2-B_3	B_3-B_5-B_7	B_7-B_8	V_{10}-V_{11}	W_{25}	V_{16}-V_{17}	W_{26}	W_{23}+W_{24}	V_{11}-V_{12}	V_{17}-V_{18}	W_{27}+ Q_{28}+ Q_{29}	

Table-18: F-P Table of Kerem GPP in Analytic Format

There are also other complementary tables and concepts for interpretation of the exergy flows and irreversibilities according to Exergy Cost Theory. Most important contribution of Torres et al. [95-96] to the ECT is the Flow-Process approach. This new approach is a modification of cost allocation assumptions postulated before:

FP-1: Remains pretty much the same as A1. Flows cycling within the system is assumed to be reversible. Selected system boundaries are decisive to define irreversibilities.

$$\dot{E}_i = E_i \tag{65}$$

FP-2: Conservation of the exergy cost is modified. Product cost of an exergy flow shall equal the fuel cost and *exergy cost of residues* produced.

$$\dot{P}_i = \dot{F}_i + \dot{R}_i \tag{66}$$

FP-3: Proportionality of irreversibilities: The costs of the process irreversibility must be allocated to their products and distributed in proportion to their exergies.

$$\dot{P}_i = \dot{k}_{p,i} P_i \tag{67}$$

FP-4: Re-distribution of waste exergy costs. A new rule which postulates that all waste exergycosts shall be distributed to their generators.

$$\dot{R}_i = \sum_i^j \dot{k}_{p,i} r_{ij} \tag{68}$$

Based upon these rules, it is possible to generate a F-P-R direct cost table. This extension enables the mathematical balance within the F-P exergy cost table. By this means, sums of all rows equals to sums of all columns and cost calculations become rational because without this balance, a basic assumption which dictates that exergy cost conservation is not valid. Total exergy costs of products must equal the total exergy costs of the fuels within the system boundaries. It is also possible to distinguish between *recoverable (irreversibilities)* and *unrecoverable (residues)* losses by the help of this table. Economic model can easily be adjusted to exergetic costing model by simply associating and distributing all investment, maintenance and fuel costs to the exergy cost streams as in SPECO [44].

Exergy streams of Kerem GPP according to Figure-16 is presented below according to SPECO principles:

Table-19: Exergy streams within the Kerem GPP

Flow	From Process	To Process	Reference Exergy [kW]
1	11	1	60379.48
2	1	5	39005.83
3	5	6	33316.47
4	6	10	26864.71
5	10	4	13432.35
6	4	11	6361.418
7	10	9	13432.35
8	9	11	6881.437
10	1	2	28500.2
11	2	13	6642.143
12	13	3	209.1165
13	3	4	687.713
14	4	5	4906.692
15	5	1	9403.774
16	6	7	9193.691
17	7	14	2370.071
18	14	8	78.47163
19	8	9	137.6097
20	9	6	4553.629
21	0	11	47136.63

23	2	12	13572.9
24	7	12	4183.65
25	12	3	712.77
26	12	8	87.66
27	12	0	15535.6
28	13	0	6433.027
29	14	0	2291.599

In order to obtain the cost flows, it is necessary to calculate purchased equipment costs and accordingly, levelized investment/maintenance costs as explained in previous sections according to cost correlations provided by Lemmens et al. [86]. Table-20 provides levelized investment/maintenance costs for plant components as well as levelized extraction cost of geothermal brine:

Table-20: Levelized costs of plant components and extraction cost of brine

Name	**Component Type**	**Cost Input *[$/s]***
Pump-I	Pump	4.60E-04
Preheater-I	Heat Exchanger	1.12E-02
Top-Preheater	Heat Exchanger	3.24E-03
Vaporizer-I	Heat Exchanger	6.19E-03
Turbine-I	Expander	3.45E-03
Air Cooled Condenser-I	Condenser	2.88E-02
Pump-II	Pump	8.76E-05
Preheater-II	Heat Exchanger	3.16E-03
Vaporizer-II	Heat Exchanger	7.04E-03

Turbine-II	Expander	2.59E-03
Air Cooled Condenser-II	Condenser	1.64E-02
Generator	Alternator	2.04E-02
*Geothermal Brine **($/kj)***	Fuel Input	1.19E-08

Table-21 provides specific and total exergy costs of streams according to cost allocation rules of SPECO method:

Table-21: Specific and total costs of exergy in Kerem GPP (SPECO)

Stream	**Specific Cost ($/kJ)**	**Total Cost ($/s)**
1	1.18794E-08	0.000717274
2	1.18794E-08	0.000463367
3	1.18794E-08	0.000395781
4	1.18794E-08	0.000319138
5	1.18794E-08	0.000159569
6	0	0
7	1.18794E-08	0.000159569
8	0	0
10	2.52042E-06	0.071832375
11	2.52042E-06	0.016740964
12	0.000217669	0.045518113
13	7.37746E-05	0.050735773
14	1.26528E-05	0.062083595
15	6.95338E-06	0.065388032
16	4.0339E-06	0.037086438

17	4.0339E-06	0.00956063
18	0.000331095	0.025981576
19	0.000193695	0.02665435
20	6.58181E-06	0.029971116
23	4.31299E-06	0.058539726
24	7.19955E-06	0.030120418
25	6.67495E-06	0.004757707
26	6.67495E-06	0.000585126
27	0	0
28	0	0
29	6.67495E-06	0.103699381

Different expressions of levelized cost of electricity based on exergy is calculated as follows in SPECO method:

Table-22: Unit cost of electricity according to SPECO in Kerem GPP

$c_{electricity}(\$/kJ)$	$c_{electricity}(\$/kWh)$
6.67495E-06	0.0240

SPECO provides a general overview of cost associations of fuel input and equipment investment & maintenance costs with exergy streams of the system. In terms of electricity production cost, outputs of SPECO varies 5.5% from Moran which predicts $c_{electricity}$ around 0.0228 according to eq. (17) at 25.7% second law plant efficiency (see initial analysis without fan consumptions). This result is in consistence with a similar study where there is a 3.7% gap between electricity cost predictions of these two methods [16]. A more comprehensive analysis will be conducted by the help of ECT.

Utilizing same exergy input values and levelized costs provided in Tables 19 and 20, a deeper analysis is conducted with cost allocations according to ECT rules. To begin with, it is necessary to decompose all flows to fuels/products and irreversibilities. Table-23 shows this decomposition according to relevant component/process:

Table-23: Fuels, Products, Irreversibilities and Unit Exergy Consumptions of Processes

	F(MW)	**P(MW)**	**I(MW)**	**k(J/J)**
GTS	47.1366	47.1366	0.0000	1.0000
VAP1	21.3737	19.0964	2.2772	1.1192
PHT1	7.0709	4.2190	2.8520	1.6760
TPHT	5.6894	4.4971	1.1923	1.2651
VAP2	6.4518	4.6401	1.8117	1.3904
PHT2	6.5509	4.4160	2.1349	1.4834
TRB1	21.8581	13.5729	8.2852	1.6104
PMP1	0.7128	0.4786	0.2342	1.4893
TRB2	6.8236	4.1837	2.6400	1.6310
PMP2	0.0877	0.0591	0.0285	1.4823
GEN	17.7566	16.3360	1.4205	1.0870
CND1	6.4330	6.4330	0.0000	1.0000
CND2	2.2916	2.2916	0.0000	1.0000

Recalling that unit exergy consumption factor k is the inverse of component efficiency, it is straightforward to say that Preheater-I and both turbines are the less efficient components, which is a confirmation of previous analyses. It is assumed that geothermal source (GTS) transfers its exergy without any loss to the cycles and condensers transfer all exergy to the environment as waste heat, therefore their exergy consumption factors equal 1. That is a controversial issue, efficiency of heat dissipation can theoretically be 100% since it is dependent to rejection

temperature. In real conditions rejection temperatures are fixed due to environmental constraints, therefore exergetic efficiency of these devices were presented around 62%-67% in exergy analysis, however for economic evaluation they are considered to be rejected at ideal temperature values. Since there is no efficiency of ACC fan included in analyses, rejection temperature at condensers would not affect plant overall efficiency and economic variables.

As explained in previous section, it is possible to now to visualize relationships between components in terms of fuels and products in a F-P table according to schemes provided in Figures 16 and 17 in Table-24:

Table-24: F-P Table of Kerem GPP

	GTS	VAP1	PHT1	TPHT	VAP2	PHT2	TRB1	PMP1	TRB2	PMP2	GEN	CND1	CND2	ENV	Total
GTS	0.00	21.37	7.07	5.69	6.45	6.55	0.00	0.00	0.00	0.00	0.00	0.00	0.00	0.00	47.14
VAP1	0.00	0.00	0.00	0.00	0.00	0.00	14.75	0.00	0.00	0.00	0.00	4.34	0.00	0.00	19.10
PHT1	0.00	0.00	0.00	0.00	0.00	0.00	3.26	0.00	0.00	0.00	0.00	0.96	0.00	0.00	4.22
TPHT	0.00	0.00	0.00	0.00	0.00	0.00	3.47	0.00	0.00	0.00	0.00	1.02	0.00	0.00	4.50
VAP2	0.00	0.00	0.00	0.00	0.00	0.00	0.00	0.00	3.47	0.00	0.00	0.00	1.17	0.00	4.64
PHT2	0.00	0.00	0.00	0.00	0.00	0.00	0.00	0.00	3.31	0.00	0.00	0.00	1.11	0.00	4.42
TRB1	0.00	0.00	0.00	0.00	0.00	0.00	0.00	0.00	0.00	0.00	13.57	0.00	0.00	0.00	13.57
PMP1	0.00	0.00	0.00	0.00	0.00	0.00	0.37	0.00	0.00	0.00	0.00	0.11	0.00	0.00	0.48
TRB2	0.00	0.00	0.00	0.00	0.00	0.00	0.00	0.00	0.00	0.00	4.18	0.00	0.00	0.00	4.18
PMP2	0.00	0.00	0.00	0.00	0.00	0.00	0.00	0.00	0.04	0.00	0.00	0.00	0.01	0.00	0.06
GEN	0.00	0.00	0.00	0.00	0.00	0.00	0.00	0.71	0.00	0.09	0.00	0.00	0.00	15.54	16.34
CND1	0.00	0.00	0.00	0.00	0.00	0.00	0.00	0.00	0.00	0.00	0.00	0.00	0.00	6.43	6.43
CND2	0.00	0.00	0.00	0.00	0.00	0.00	0.00	0.00	0.00	0.00	0.00	0.00	0.00	2.29	2.29
ENV	47.14	0.00	0.00	0.00	0.00	0.00	0.00	0.00	0.00	0.00	0.00	0.00	0.00	0.00	47.14
Total	47.14	21.37	7.07	5.69	6.45	6.55	21.86	0.71	6.82	0.09	17.76	6.43	2.29	24.26	MW

In general, F-P table is nothing but a decomposition of Table-23 according to exergy transfers between the plant components. Rows indicate fuels provided from the relevant component or process to subsequent components/processes. On the other hand, sum of rows in columnal direction demonstrates the products of these processes/components. It is obvious that ratio between sum of fuels and sum of products for a component will provide second law efficiency of this device since it is the table which is composed from exergy distributions within the plant.

Exergy costing is introduced with fuel-residue-product cost table. This table is constructed upon F-P table and main idea is the re-distribution of wastes/residues to their responsible as explained before. Aiming the conservation of exergy costs as provided in eqn. (66), a series of matrix operations are executed in order to equal sums of fuels and products by distributing exergy costs due to wastes / residues Theoretical basis of this matrix operations are explained in detail by Torres et al. [95]:

Table-25: Exergy Cost Table of Kerem GPP Based on Residue Cost Re-Distribution

	GTS	VAP1	PHT1	TPHT	VAP2	PHT2	TRB1	PMP1	TRB2	PMP2	GEN	CND1	CND2	ENV	Total
GTS	0.00	21.37	7.07	5.69	6.45	6.55	0.00	0.00	0.00	0.00	0.00	0.00	0.00	0.00	47.14
VAP1	0.00	0.00	0.00	0.00	0.00	0.00	22.21	0.00	0.00	0.00	0.00	6.54	0.00	0.00	28.74
PHT1	0.00	0.00	0.00	0.00	0.00	0.00	6.70	0.00	0.00	0.00	0.00	1.97	0.00	0.00	8.67
TPHT	0.00	0.00	0.00	0.00	0.00	0.00	5.72	0.00	0.00	0.00	0.00	1.68	0.00	0.00	7.40
VAP2	0.00	0.00	0.00	0.00	0.00	0.00	0.00	0.00	6.53	0.00	0.00	0.00	2.19	0.00	8.72
PHT2	0.00	0.00	0.00	0.00	0.00	0.00	0.00	0.00	6.54	0.00	0.00	0.00	2.20	0.00	8.73
TRB1	0.00	0.00	0.00	0.00	0.00	0.00	0.00	0.00	0.00	0.00	36.30	0.00	0.00	0.00	36.30
PMP1	0.00	0.00	0.00	0.00	0.00	0.00	1.67	0.00	0.00	0.00	0.00	0.49	0.00	0.00	2.16
TRB2	0.00	0.00	0.00	0.00	0.00	0.00	0.00	0.00	0.00	0.00	13.27	0.00	0.00	0.00	13.27
PMP2	0.00	0.00	0.00	0.00	0.00	0.00	0.00	0.00	0.20	0.00	0.00	0.00	0.07	0.00	0.27
GEN	0.00	0.00	0.00	0.00	0.00	0.00	0.00	2.16	0.00	0.27	0.00	0.00	0.00	47.14	49.57
CND1	0.00	7.37	1.60	1.71	0.00	0.00	0.00	0.00	0.00	0.00	0.00	0.00	0.00	0.00	10.68
CND2	0.00	0.00	0.00	0.00	2.27	2.18	0.00	0.00	0.00	0.00	0.00	0.00	0.00	0.00	4.46
ENV	47.14	0.00	0.00	0.00	0.00	0.00	0.00	0.00	0.00	0.00	0.00	0.00	0.00	0.00	47.14
Total	47.14	28.74	8.67	7.40	8.72	8.73	36.30	2.16	13.27	0.27	49.57	10.68	4.46	47.14	MW

At first glance, it can be easily ascertained that sums of rows and products are equalized, therefore conservation of the exergy cost is satisfied. It is possible to derive further conclusions from this table, for instance rows of CND1 and CND2 represent the residual exergy costs of relevant responsible devices, which are unrecoverable part of cost formation. Table-26 shows the decomposition of direct exergy costs for ORC components in tabulated form:

Table-26: Direct Exergy Costs Within ORC Components

	P*(MW)	**Pe*(MW)**	**Pr*(MW)**	**F*(MW)**	**R*(MW)**
VAP1	28.7445	21.3737	7.3709	21.3737	7.3709
PHT1	8.6733	7.0709	1.6024	7.0709	1.6024
TPHT	7.3985	5.6894	1.7092	5.6894	1.7092
VAP2	8.7243	6.4518	2.2726	6.4518	2.2726
PHT2	8.7344	6.5509	2.1835	6.5509	2.1835
TRB1	36.2966	27.6372	8.6594	36.2966	0.0000
PMP1	2.1626	1.6371	0.5255	2.1626	0.0000
TRB2	13.2686	9.8845	3.3842	13.2686	0.0000
PMP2	0.2660	0.2013	0.0646	0.2660	0.0000
GEN	49.5652	37.5217	12.0435	49.5652	0.0000
CND1	10.6824	8.1339	2.5485	10.6824	0.0000
CND2	4.4561	3.3195	1.1365	4.4561	0.0000

Results show a pretty much balanced distribution of waste exergy costs to the components, which is an expected outcome. Main purpose of this table is to show the formation of additional exergy costs on processes due to formation of waste heat at condensers. Only heat exchanging devices include a part of residue cost (R^*) owing to the fact that they are responsible for waste heat formation. $P_R{}^*$ shows the propagation of these costs within the plant components. An unitary form of this table is presented in Table-27. which explains proportions between residual and other exergy costs in unitary (levelized- exergy costs of fuels and products by exergies of fuels and products) terms:

Table-27: Unit Exergy Costs Within ORC Components

	kP*	**kPe***	**kPr***	**kF***	**kR***	**k**
VAP1	1.5052	1.1192	0.3860	1.0000	0.3860	1.1192
PHT1	2.0558	1.6760	0.3798	1.0000	0.3798	1.6760
TPHT	1.6452	1.2651	0.3801	1.0000	0.3801	1.2651
VAP2	1.8802	1.3904	0.4898	1.0000	0.4898	1.3904
PHT2	1.9779	1.4834	0.4944	1.0000	0.4944	1.4834
TRB1	2.6742	2.0362	0.6380	1.6606	0.0000	1.6104
PMP1	4.5187	3.4207	1.0980	3.0341	0.0000	1.4893
TRB2	3.1715	2.3626	0.8089	1.9445	0.0000	1.6310
PMP2	4.4974	3.4046	1.0928	3.0341	0.0000	1.4823
GEN	3.0341	2.2969	0.7372	2.7914	0.0000	1.0870
CND1	1.6606	1.2644	0.3962	1.6606	0.0000	1.0000
CND2	1.9445	1.4486	0.4959	1.9445	0.0000	1.0000

This table presents nothing but the levelized forms of Table-29 values with F and P exergy values. As far as all streams within the plant concerned, Table-31 illustrates all exergetic costs occur at brine, vapor, work and heat streams:

Table-28: Exergetic Costs of All Streams in Kerem GPP

	B(MW)	**B*(MW)**	**Be*(MW)**	**Br*(MW)**	**k***	**ke***	**kr***
GTS	47.1366	47.1366	47.1366	0.0000	1.0000	1.0000	0.0000
B1	60.3795	60.3795	60.3795	0.0000	1.0000	1.0000	0.0000
B2	39.0058	39.0058	39.0058	0.0000	1.0000	1.0000	0.0000
B3	33.3165	33.3165	33.3165	0.0000	1.0000	1.0000	0.0000
B5	13.4324	13.4324	13.4324	0.0000	1.0000	1.0000	0.0000
B6	6.3614	6.3614	6.3614	0.0000	1.0000	1.0000	0.0000
B7	13.4324	13.4324	13.4324	0.0000	1.0000	1.0000	0.0000
B8	6.8814	6.8814	6.8814	0.0000	1.0000	1.0000	0.0000
V10	28.5002	47.3262	36.0355	11.2907	1.6606	1.2644	0.3962
V11	6.6421	11.0297	8.3983	2.6314	1.6606	1.2644	0.3962
V12	0.2091	0.3472	0.2644	0.0828	1.6606	1.2644	0.3962
V13	0.6877	2.5099	1.9015	0.6083	3.6496	2.7650	0.8846
V14	4.9067	11.1832	8.9725	2.2107	2.2792	1.8286	0.4505
V15	9.4038	18.5817	14.6618	3.9199	1.9760	1.5591	0.4168
V16	9.1937	17.8773	13.3177	4.5596	1.9445	1.4486	0.4959
V17	2.3701	4.6086	3.4332	1.1754	1.9445	1.4486	0.4959
V18	0.0785	0.1526	0.1137	0.0389	1.9445	1.4486	0.4959
V19	0.1376	0.4186	0.3150	0.1035	3.0416	2.2892	0.7524
V20	4.5536	9.1529	6.8659	2.2870	2.0100	1.5078	0.5022
W23	13.5729	36.2966	27.6372	8.6594	2.6742	2.0362	0.6380
W24	4.1837	13.2686	9.8845	3.3842	3.1715	2.3626	0.8089

W25	0.7128	2.1626	1.6371	0.5255	3.0341	2.2969	0.7372
W26	0.0877	0.2660	0.2013	0.0646	3.0341	2.2969	0.7372
W27	15.5356	47.1366	35.6832	11.4534	3.0341	2.2969	0.7372
Q28	6.4330	0.0000	8.1339	2.5485	1.6606	1.2644	0.3962
Q29	2.2916	0.0000	3.3195	1.1365	1.9445	1.4486	0.4959

Since the exergetic cost is proportional with exergy content of a stream, highest exergetic costs occur at the streams with highest exergetic content such as W27 and V10 which are electricity production and vapor flow to the Turbine-1 respectively. Monetary equivalent of W27 will provide levelized cost of electricity according to ECT in forthcoming calculations. Final non-monetary values that will be presented are the irreversibility matrices. Contribution of irreversibilities to the unit exergy cost formation is formulated by Torres et al. [96]:

Table-29: Irreversibility- Unit Exergetic Cost Table

	GTS	VAP1	PHT1	TPHT	VAP2	PHT2	TRB1	PMP1	TRB2	PMP2	GEN	CND1	CND2
GTS	**0.0000**	0.0000	0.0000	0.0000	0.0000	0.0000	0.0000	0.0000	0.0000	0.0000	0.0000	0.0000	0.0000
VAP1	0.0000	**0.1192**	0.0000	0.0000	0.0000	0.0000	0.1342	0.1667	0.0018	0.1659	0.1119	0.0833	0.0011
PHT1	0.0000	0.0000	**0.6760**	0.0000	0.0000	0.0000	0.1680	0.2088	0.0022	0.2078	0.1402	0.1043	0.0013
TPHT	0.0000	0.0000	0.0000	**0.2651**	0.0000	0.0000	0.0702	0.0873	0.0009	0.0869	0.0586	0.0436	0.0006
VAP2	0.0000	0.0000	0.0000	0.0000	**0.3904**	0.0000	0.0035	0.1285	0.3255	0.1279	0.0863	0.0022	0.1996
PHT2	0.0000	0.0000	0.0000	0.0000	0.0000	**0.4834**	0.0041	0.1514	0.3836	0.1507	0.1017	0.0026	0.2352
TRB1	0.0000	0.0000	0.0000	0.0000	0.0000	0.0000	**0.6318**	0.7849	0.0083	0.7813	0.5271	0.0133	0.0051
PMP1	0.0000	0.0000	0.0000	0.0000	0.0000	0.0000	0.0138	**0.5064**	0.0002	0.0171	0.0115	0.0086	0.0001
TRB2	0.0000	0.0000	0.0000	0.0000	0.0000	0.0000	0.0068	0.2501	**0.6337**	0.2489	0.1679	0.0042	0.0016
PMP2	0.0000	0.0000	0.0000	0.0000	0.0000	0.0000	0.0001	0.0020	0.0051	**0.4843**	0.0014	0.0000	0.0031
GEN	0.0000	0.0000	0.0000	0.0000	0.0000	0.0000	0.0037	0.1346	0.0014	0.1339	**0.0904**	0.0023	0.0009
CND1	0.0000	0.3844	0.3782	0.3785	0.0017	0.0017	0.6268	0.7797	0.0110	0.7761	0.5236	**0.3892**	0.0067
CND2	0.0000	0.0016	0.0016	0.0016	0.4881	0.4927	0.0112	0.3182	0.7979	0.3167	0.2137	0.0070	**0.4892**
ENV	1.0000	1.0000	1.0000	1.0000	1.0000	1.0000	1.0000	1.0000	1.0000	1.0000	1.0000	1.0000	1.0000
Total	1.0000	1.5052	2.0558	1.6452	1.8802	1.9779	2.6742	4.5187	3.1715	4.4974	3.0341	1.6606	1.9445

Table-29 simply explains the contributions of different components to the formation of plant exergy cost in unitary terms. For instance, Vaporizer-I produces around 19.1 MW exergy out of 21.4 MW fuel. General irreversibility within this process is nearly 2.3 MW. Ratio of irreversibility to process output provides us unit exergy cost contribution of Vaporizer-I due to its general irreversibility. By this means, sum of diagonal values at this matrix is nothing but the unit exergetic cost of plant due to irreversibilities. Since F/P equals 1 if there is no irreversibility or waste, contribution of environment (or minimum production cost) is accepted to be 1. Condenser values represent the distribution of residual costs to the components. Sum of rows in columnal direction equal to unit exergy cost of a component. Each row on the other hand represent the effect of one components irreversibility to the exergy cost contribution of other one. It is interesting to observe the interrelation between components which do work in different cycles apparently. This also explains again the working principle of a cyclic system.

Utilizing same levelized cost rates of components and fuel provided at Table-20, it is quite straightforward to associate these exergetic cost results with monetary values [42]. Table-30 provides an introduction of levelized component/fuel cost values and a monetary conversion of Table-28:

Table-30: Exergoeconomic Costs of ORC Processes

	CP($/h)	**CPe($/h)**	**CPr($/h)**	**CF($/h)**	**CR($/h)**	**Z($/h)**
GTS	2.0158	2.0158	0.0000	2.0158	0.0000	0.0000
VAP1	134.8969	23.1996	111.6973	0.9141	111.6973	22.2856
PHT1	64.8621	40.5801	24.2820	0.3024	24.2820	40.2777
TPHT	37.7968	11.8960	25.9008	0.2433	25.9008	11.6527
VAP2	72.6852	25.6152	47.0700	0.2759	47.0700	25.3392
PHT2	56.8702	11.6461	45.2242	0.2802	45.2242	11.3659
TRB1	210.4450	78.5724	131.8726	198.0310	0.0000	12.4139
PMP1	18.7576	9.9538	8.8038	17.1018	0.0000	1.6558
TRB2	108.1360	38.2344	69.9016	98.7954	0.0000	9.3406
PMP2	2.4188	1.3361	1.0827	2.1033	0.0000	0.3155

GEN	391.9564	190.1823	201.7742	318.5810	0.0000	73.3755
CND1	161.8801	123.0688	38.8113	58.2823	0.0000	103.5977
CND2	92.2942	68.8189	23.4753	33.1788	0.0000	59.1154

That table provides quite interesting information because when the levelized costs are distributed, it becomes crystal clear that cost formations in some components like VAP-I, TRB-I or PHT-2 are overwhelmingly caused by residual costs.

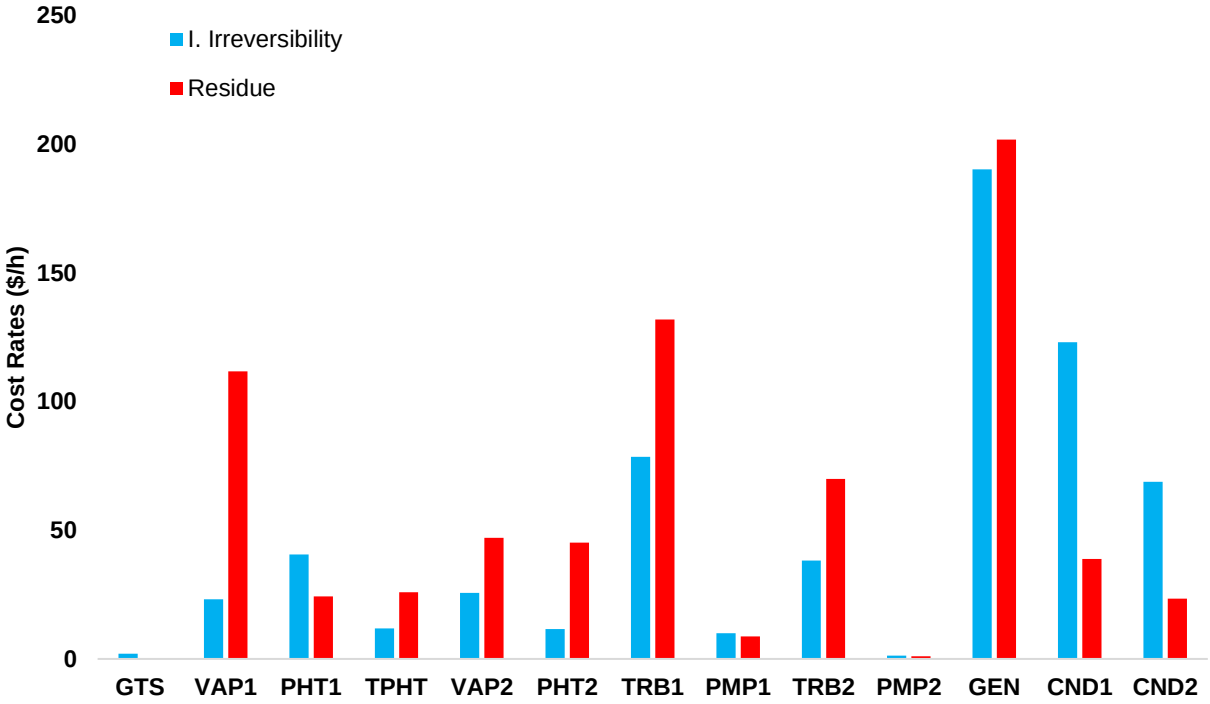

Fig.19: Decomposed Cost Rates of Components

Decomposed cost has two components, one is the cost caused by the internal irreversibility other one is the residual cost. Distinguishing between *recoverable* and *unrecoverable* losses, one should keep in mind that definition of irreversibility and entropy generation is highly related to each other. Internal irreversibility is mainly about entropy formation between different states whilst residues are mainly produced due to irreversibility of general process (i.e. external irreversibility). Once the cycle is completed it is physically impossible to recover waste heat unless there is an extra waste heat recovery system. However, investing in the technology such as working fluid alteration would lead an improvement in component performance and reduce of residues. Accordingly, residual cost would also decrease. Internal irreversibility can be reduced by

parametric or systematic optimization of the process. Figure-19 shows components which may require technology investments to reduce residual costs. Table-27 of unitary exergy costs is converted to monetary values where exergoeconomic factor *f* is also introduced:

Table-31: Unit Exergoeconomic Costs of ORC Processes

	cP($/MWh)	**cPe($/MWh)**	**cPr($/MWh)**	**cF($/MWh)**	**cR($/MWh)**	**fz**
GTS	0.0428	0.0428	0.0000	0.0428	0.0000	0.0000
VAP1	7.0640	1.2149	5.8491	0.0428	5.8491	0.1662
PHT1	15.3739	9.6185	5.7554	0.0428	5.7554	0.6227
TPHT	8.4047	2.6453	5.7595	0.0428	5.7595	0.3099
VAP2	15.6647	5.5204	10.1443	0.0428	10.1443	0.3496
PHT2	12.8782	2.6372	10.2409	0.0428	10.2409	0.2005
TRB1	15.5048	5.7889	9.7159	9.0599	0.0000	0.1419
PMP1	39.1929	20.7979	18.3950	23.9934	0.0000	0.2276
TRB2	25.8473	9.1390	16.7083	14.4784	0.0000	0.1964
PMP2	40.9008	22.5922	18.3085	23.9934	0.0000	0.3156
GEN	23.9934	11.6419	12.3515	17.9416	0.0000	0.7422
CND1	25.1639	19.1308	6.0331	9.0599	0.0000	1.0000
CND2	40.2750	30.0310	10.2441	14.4784	0.0000	1.0000

In terms of unit prices, Table-31 provides monetary analysis of the ORC system. For instance, product of generator is electricity and exergoeconomic unit price of electricity is calculated as 0.023993 $/kWh as shown in the table. A brief comparison of LEC estimation with different methodologies is provided below:

Table-32: Comparison of Unit Exergoeconomic Electric Production Prices

Methodology	**Estimation ($/kWh)**	**Deviation**
Moran	0.022772	--
SPECO	0.024030	+5.5%
ECT	0.023993	+5.4%

Assuming Moran method as a basis for comparison, SPECO and ECT varies in a 0.1% margin in terms of unit electricity price. Considering the common theoretical basis of these two methods, results indicate that conducted analyses are internally consistent.

Most important values in Table-31 are exergoeconomic factors of the devices. Condensers are out of discussion as explained before, due to the fact it is assumed that waste heat is dissipated with 100% efficiency in these devices. Figure-20 depicts the variation of exergoeconomic factors within the plant:

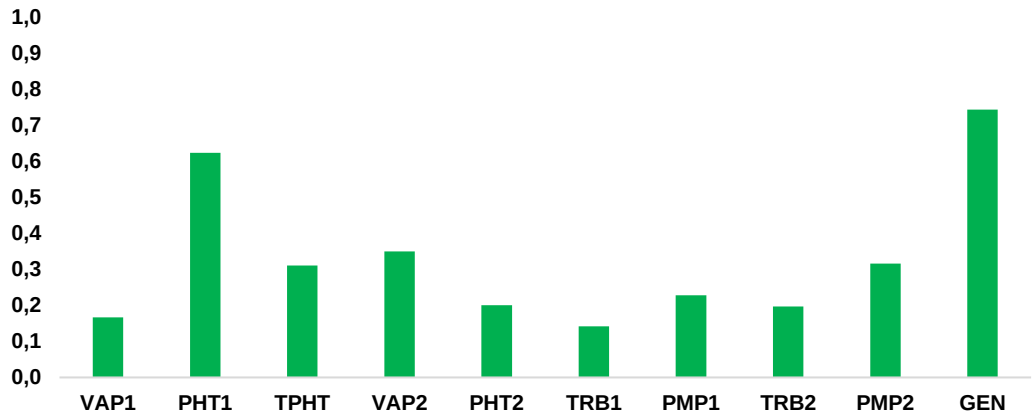

Fig.20: Exergoeconomic Factors of Plant Components

Components with an exergoeconomic factor below 0.5 are worth of further investment. This means that general irreversibility costs are overwhelming the levelized equipment costs for these devices. On the other hand, this phenomenon shows that exergetic efficiency alone is not sufficient by decision making either at plant or component level. One should always take exergoeconomic cost formations also into the consideration. For instance, Vaporizer-I has an exergetic efficiency around 90% (see F-P table) whilst its

exergoeconomic factor is around 17%. Taking solely the mathematical exergy efficiency definition into account, one could be led to a misjudgement which tells that there is a very narrow room for improvement. Oppositely, results dictate that there is much more to do in this device by economic means. Finally, Table-33 illustrates unit exergoeconomic costs of all streams in Kerem GPP:

Table-33: Unit Exergoeconomic Costs of All Streams in Kerem GPP

	B(MW)	**C($/h)**	**Ce($/h)**	**Cr($/h)**	**c($/MWh)**	**ce($/MWh)**	**cr($/MWh)**	**c*($/MWh)**
GTS	47.1366	2.0158	2.0158	0.0000	0.0428	0.0428	0.0000	0.0428
B1	60.3795	2.5822	2.5822	0.0000	0.0428	0.0428	0.0000	0.0428
B2	39.0058	1.6681	1.6681	0.0000	0.0428	0.0428	0.0000	0.0428
B3	33.3165	1.4248	1.4248	0.0000	0.0428	0.0428	0.0000	0.0428
B5	13.4324	0.5744	0.5744	0.0000	0.0428	0.0428	0.0000	0.0428
B6	6.3614	0.2721	0.2721	0.0000	0.0428	0.0428	0.0000	0.0428
B7	13.4324	0.5744	0.5744	0.0000	0.0428	0.0428	0.0000	0.0428
B8	6.8814	0.2943	0.2943	0.0000	0.0428	0.0428	0.0000	0.0428
V10	28.5002	258.2079	86.2625	171.9455	9.0599	3.0267	6.0331	5.4559
V11	6.6421	60.1769	20.1040	40.0729	9.0599	3.0267	6.0331	5.4559
V12	0.2091	1.8946	0.6329	1.2616	9.0599	3.0267	6.0331	5.4559
V13	0.6877	20.6522	10.5868	10.0654	30.0302	15.3942	14.6360	8.2284
V14	4.9067	85.5143	51.1669	34.3474	17.4281	10.4280	7.0001	7.6467
V15	9.4038	123.3111	63.0628	60.2482	13.1129	6.7061	6.4068	6.6362
V16	9.1937	133.1104	38.9296	94.1808	14.4784	4.2344	10.2441	7.4458
V17	2.3701	34.3149	10.0358	24.2792	14.4784	4.2344	10.2441	7.4458
V18	0.0785	1.1361	0.3323	0.8039	14.4784	4.2344	10.2441	7.4458
V19	0.1376	3.5549	1.6683	1.8866	25.8335	12.1237	13.7098	8.4933
V20	4.5536	60.4252	13.3144	47.1108	13.2697	2.9239	10.3458	6.6017

W23	13.5729	210.4450	78.5724	131.8726	15.5048	5.7889	9.7159	5.7979
W24	4.1837	108.1360	38.2344	69.9016	25.8473	9.1390	16.7083	8.1497
W25	0.7128	17.1018	8.2980	8.8038	23.9934	11.6419	12.3515	7.9079
W26	0.0877	2.1033	1.0205	1.0827	23.9934	11.6419	12.3515	7.9079
W27	15.5356	372.7514	180.8637	191.8877	23.9934	11.6419	12.3515	7.9079
Q28	6.4330	0.0000	123.0688	38.8113	25.1639	19.1308	6.0331	15.1539
Q29	2.2916	0.0000	68.8189	23.4753	40.2750	30.0310	10.2441	20.7121

Cost proportions of internal and external irreversibility in components are again directly reflected at this table. V10 for instance, superheated vapor of Vaporizer-I has the highest unit cost except W27 which is the electricity production. But nearly 2/3 of this cost is the residue cost. It is also interesting to see that 51.5% of the unit exergoeconomic electricity cost is directly caused by wastes of the plant. It can be stated that this fact underlines the necessity of a sort of optimization within this plant.

3.4 Off-Design Modeling of the Turbines

In this section, it will be aimed to model ORC turbine curves at off-design conditions under part-load. A thermodynamic model and statistical model will be constructed with the help of different off-design datasets. Utilizing statistical analysis tools such as maximum likelihood estimation and probability distribution, plant variables such as working fluid reduced mass flow rates or pressure ratios at turbines will be obtained for Stodola curve modelling purposes. With the help of this data, turbine characteristics (i.e. number of stages) and curves will be obtained for both cycles and results will be compared with proposed correlations from literature -namely Gabbrielli [55] and Jüdes [60]-. Outputs of this study -i.e. turbine curve modelling and validation- will be the prologue of a plant optimization.

Thermodynamic and statistical models are based on following physical assumptions:

- Steady-state conditions are assumed.

- Pipe pressure drops are neglected, thermal losses from heat exchangers or environments to the environment are not taken into the consideration.

- Geothermal brine is modelled as standard water.

- Non-condensable gases (NCG) are not taken into the account.

- Pressure drop at the turbine stages is assumed to be independent from the number of stages [54].

- Thermodynamic properties of n-pentane are calculated using the Soave-Redlich-Kwong (SRK) [98] equation of state.

- For geothermal brine, the equation provided by the International Association for the Properties of Water and Steam (IAPWS-95) [99] is utilized.

For the off-design modelling purposes of the plant different off-design datasets are utilized with different ambient temperatures throughout the different seasons of the years. After a brief explanation of the theoretical framework of turbine correlations, developed statistical model, which is vital for this study, will be examined in detail in following sections.

3.4.1 Theoretical Framework of the Turbine Correlations

Since it is steam turbines which are the subject of attention in this study, it is necessary to elaborate law of ellipse (or cone law) in detail. Stodola's cone approach proposes a methodology for prediction of outlet pressure as long as the flow is not *choked* (venturi effect) at turbine nozzles [54].

After empirical studies, Stodola described the relationship between mass flow rate, temperature and pressure as a conic surface on Cartesian system and established a relationship between design and off-design conditions utilizing these parameters. Mathematical expression of flow ratio can be expressed as follows (acc. Stodola's ellipse):

$$\frac{\dot{m}_D}{m_{off}} = \sqrt{\frac{T_{off,in}}{T_{D,in}}} \sqrt{\frac{\left(\frac{P_{D,in}}{P_{D,in,m}}\right)^2\left(1-\left(\frac{P_{C,out}}{P_{off,in}}\right)\right)^2-\left(\frac{P_{D,out}}{P_{D,out,m}}-\frac{P_{C,out}}{P_{off,in}}\frac{P_{D,in}}{P_{D,in,m}}\right)^2}{\left(\frac{P_{off,in}}{P_{off,in,m}}\right)^2\left(1-\left(\frac{P_{C,out}}{P_{off,in}}\right)\right)^2-\left(\frac{P_{off,out}}{P_{off,out,m}}-\frac{P_{C,out}}{P_{off,in}}\frac{P_{off,in}}{P_{off,in,m}}\right)^2}} \tag{69}$$

D and *off* represent design and off-design conditions in that equation while *in* and *out* refers to inlet and outlet conditions. *M* stands for maximum, *C* is the subscript of term *critical*. It is possible to simplify this equation by assuming a *condensing turbine* instead

of *backpressure turbine.* By this means, outlet critical pressure becomes negligible and the equation gets following form:

$$\frac{\dot{m}_D}{\dot{m}_{off}} = \sqrt{\frac{T_{off,in}}{T_D,in}} \sqrt{\frac{\left(\frac{P_{D,in}}{P_{D,in,m}}\right)^2 - (\frac{P_{D,out}}{P_{D,out,m}})^2}{\left(\frac{P_{off,in}}{P_{off,in,m}}\right)^2 - (\frac{P_{off,out}}{P_{off,out,m}})^2}} \tag{70}$$

If the difference between inlet and outlet temperatures are insignificant for design and off design cases, temperature related term would vanish. Maximum pressures for design and off-design conditions at inlet and outlet are also identical terms, hence these terms would also offset each other:

$$P_{off,out} = \sqrt{{p_{off,in}}^2 - \left(\frac{\dot{m}_{off}}{\dot{m}_D}\right)^2 ({p_{D,in}}^2 - {p_{D,out}}^2)} \tag{71}$$

It is possible to re-write eq. (71) using *Stodola constant (Y_D)* [54]:

$$Y_D = \frac{{P_{off,in}}^2 - {p_{D,out}}^2}{{P_{off,in}}^2 {\dot{m}_D}^2} \tag{72}$$

Off-design inlet pressure can be expressed as follows in final form:

$$P_{off,in} = \sqrt{{\dot{m}_{off}}^2 T_{in,off} Y_D - \left(\frac{\dot{m}_{off}}{\dot{m}_D}\right)^2 + {P_{off,out}}^2} \tag{73}$$

In real operating conditions, a vast majority of the turbines work under *choked flow* conditions. Choking flow is associated with *reduced mass flow rate* rather than *bulk mass flow rate* as follows:

$$\Phi = \frac{\dot{m}_{off}}{\sqrt{p_{off,in}\rho_{off,in}}} \tag{74}$$

When the flow gets choked, reduced mass flow rate reaches its maximum value. In other words, changes in pressure ratio have no effect on mass flow rate from the choking point on -i.e. Stodola curve becomes steeper-. Thus, the equations provided between 69-73 becomes useless for outlet pressure predictions at off-design conditions.

Nevertheless, turbine inlet and outlet pressures are known for different datasets in frame of this study. By a reverse engineering approach, following equation is utilized to predict turbine characteristics (number of possible stages) with the help of known pressure ratios in ORC turbines [54]:

$$Y_D = \frac{(p_r{}^{1/n})^2 - 1}{(\Phi_{in}(p_r{}^{1/n}))^2} \tag{75}$$

Where p_r represents pressure ratio while n stands for the number of possible stages. Theoretical turbine isentropic efficiency is the ratio of irreversible enthalpy transfer to the reversible (*or isentropic*) enthalpy transfer formulated as follows [41] (acc. stream numbers in Fig.2 for Turbine-1):

$$\eta_{s,T} = \frac{h_{10} - h_{11}}{h_{10} - h_{11,s}} \tag{76}$$

Thermal losses from the turbines to the environment will be estimated according to following formula:

$$W_L = \left(TLC + TLC_{Qmod} * (Q - 1)\right) * \Delta_{Tamb-Tinlet} \tag{77}$$

where TLC is the abbreviation of thermal loss coefficient, TLC_{Qmod} is the correcting factor if vapour quality drops below 1 and $\Delta_{Tamb-Tinlet}$ is the temperature difference between the environment and turbine inlet.

Gabbrielli [55] re-mentioned a former correlation in his work for direct estimation of ORC turbine isentropic efficiency in a binary geothermal plant:

$$\eta_{off,s,T} = \eta_{D,s,T} \sin\left[0.5\Pi \left(\frac{\dot{m}_{wf,off,in}}{\dot{m}_{wf,D,in}} \frac{\rho_{wf,D,in}}{\rho_{wf,off,in}}\right)^{0.1}\right] \tag{78}$$

where *wf* is the abbreviation of working fluid. This correlation simply associates off-design mass flow rate change of the working fluid with density changes at the turbine inlet conditions. Jüdes et al. [60] proposed another empirical correlation which is more sensitive to mass flow rate changes at off-design conditions:

$$\eta_{off,s,T} = \eta_{D,s,T} \left[-1.0176 \left(\frac{\dot{m_{off}}}{\dot{m_D}}\right)^4 + 2.4443 \left(\frac{\dot{m_{off}}}{\dot{m_D}}\right)^3 - 2.1812 \left(\frac{\dot{m_{off}}}{\dot{m_D}}\right)^2 + 1.0535 \left(\frac{\dot{m_{off}}}{\dot{m_D}}\right) + 0.701\right] \tag{79}$$

Outputs from thermodynamic model of the plant will be validated with the help of stated turbine efficiency and outlet pressure correlations.

3.4.2 Statistical Model

As aforementioned previously, one of the main purposes of this section is to validate the developed thermodynamic model with a special concern on the turbines.

Existing datasets are unfortunately unavailable for direct validation purposes. In fact, some vital information is missing, the most critical of which are the ORC fluid flow rates in both cycles. Despite that, such values can be derived from the existing datasets and Table-34 summarizes missing critical values and utilized methodologies to calculate them:

Table-34: Calculation Methodologies of Missing Variables

Variable	**Description**	**Methodology**
$\dot{m}_{ORC-1}$	*Flow rate of ORC cycle 1*	*Enthalpy balance in TPH-1*
$\dot{m}_{ORC-1}$	*Flow rate of ORC cycle 2*	*Enthalpy balance in PH-2*
$\dot{m}_{ratio}$	*Brine mass flow distribution rate between the cycles (i.e. in Splitter)*	*Enthalpy balance in TPH-1*
T_{19}	*PH-2 working fluid inlet temperature*	*Evaluation of thermal resistance of pipes between points 12 and 13 in Cycle-1 with existing data such as T_{12}, T_{13} and T_{amb}. Assuming that the thermal resistance of pipes in Cycle-2 is the same, T_{19} can be obtained from T_{18} and T_{amb}.*

As one can clearly extract from Figure-22, such a calculation would result in an huge uncertainty on the outputs, due to the propagation of the small uncertainties which are naturally connected with the data acquisition process. These uncertainties would make a validation process utterly useless. Therefore, a statistical method is developed to improve the accuracy of model predictions as depicted in Fig. 21:

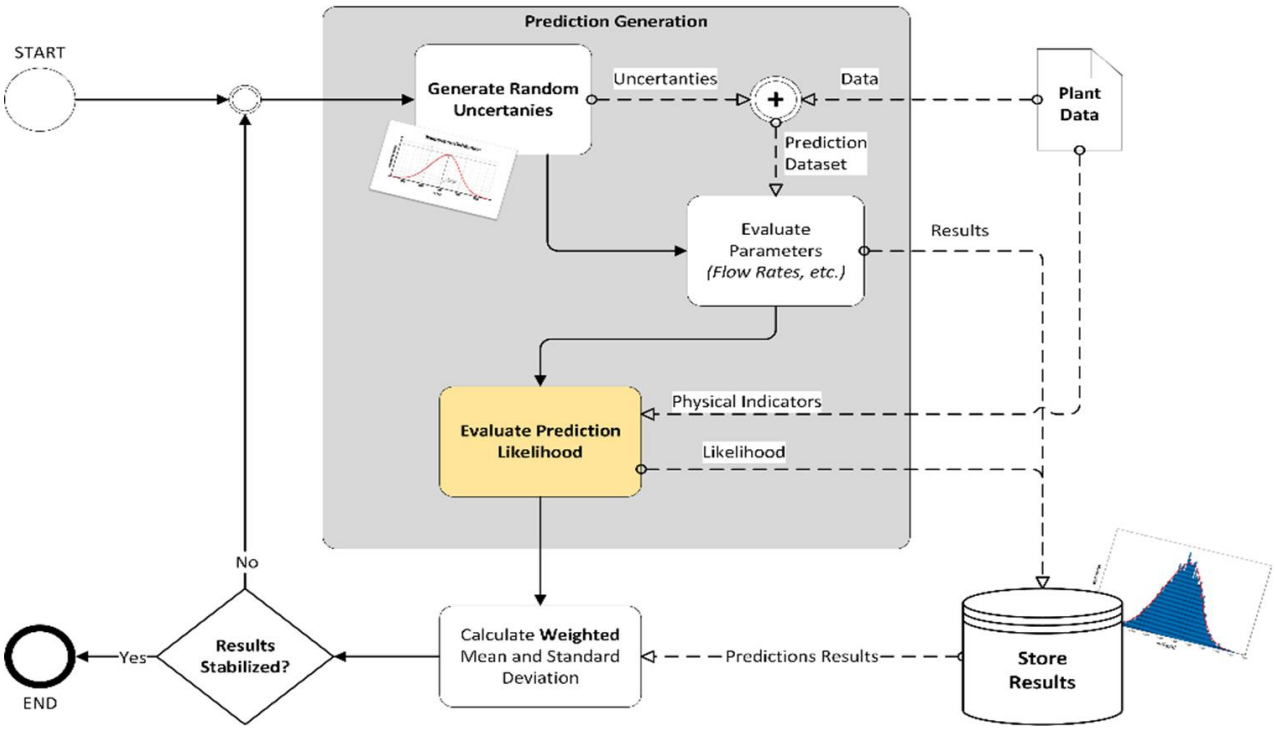

Fig. 21: Schematic Description of the Statistical Model

3.4.2.1 Maximum Likelihood Estimation

Maximum likelihood estimation (MLE) is a statistical approach for predicting the parameters of a probability distribution by maximizing a certain likelihood function, with the goal of making the observed data *most likely* under the assumed statistical model [100]. Data distribution in Figure-22 is obtained by evaluating $\dot{m}_{ORC-1}$ over different *predictions* generated by adding small random variations to the input variables.

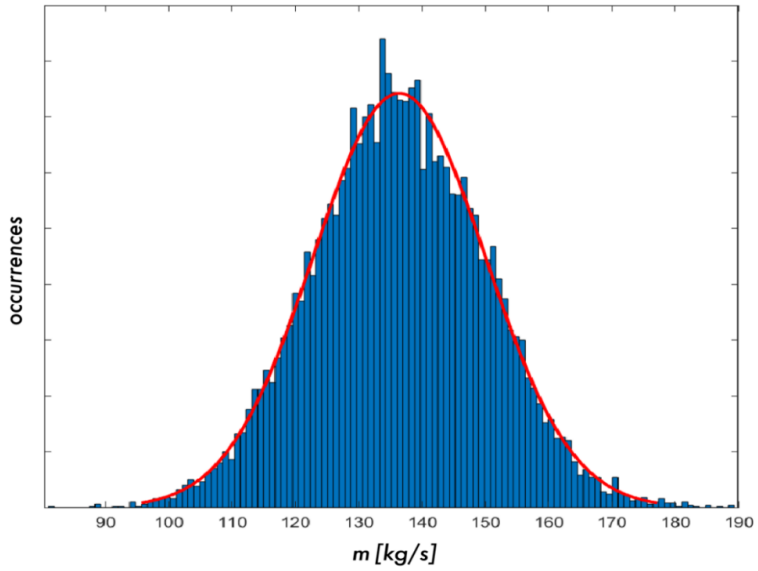

Figure 22: Probability Distribution of $\dot{m}_{ORC-1}$ for a Specific Dataset

In Fig.22, the interpolated normal distribution ($\mu = 136.39$ [kg/s]; $\sigma = 13.58$ [kg/s]) is represented in red line while the bars do represent the possible occurrences. These results have been obtained considering error levels for temperature and pressure respectively as follows err_T = 0.4 [°C] and err_P = 0.1 [bar].

A trivial outcome from the Figure-11 shall be that; different *predictions* do not have the same chance to be correct, on the contrary, some of them shall be not correct at all. Figure-23 underlines this fact from the physical point of view:

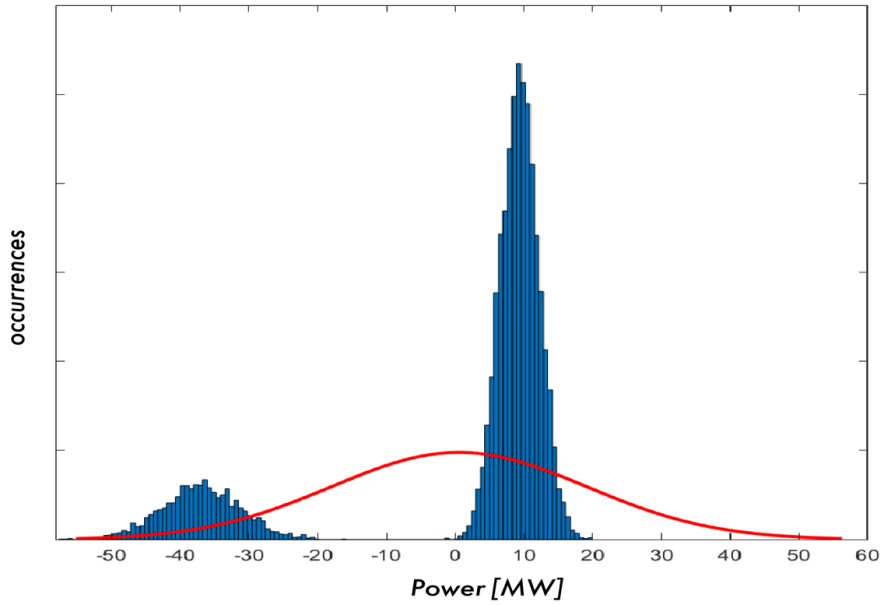

Fig. 23: Probability distribution of W_{net}

Since obtaining a negative work output from a power plant is an impossible physical phenomenon, it is mandatory to exclude such points from the probability distribution. By such an approach, it is possible to reduce the uncertainties until a certain extent. A feasible way of excluding physically unfeasible points is to consider the weighted mean and standard deviation of the *prediction* over the *likelihood* (lh_i) of that certain possibility:

$$mean = \frac{\sum value_i \, lh_i}{\sum lh_i} \tag{80}$$

To evaluate the likelihood of a specific *prediction*, some points from the datasets -like vaporizer outlet temperature- are utilized as *physical indicators* since they represent the outputs of off-design model. These indicators are employed in a manner that determines the *likelihood of the occurrence* of such a case in a physical environment under assumed conditions. Table-35 provides the physical indicators employed in the off-design model:

Table-35: Physical Indicators in the Off-Design Model

Indicator	Description	Cycle
T_{10}	*Temperature Outlet – Vaporizer*	*Cycle 1*
$\eta_{TURB\,1}$	*Turbine Isentropic Efficiency*	*Cycle 1*
Q_{12}	*Vapour Quality Outlet – Condenser*	*Cycle 1*
T_{16}	*Temperature Outlet – Vaporizer*	*Cycle 2*
$\eta_{TURB\,2}$	*Turbine Isentropic Efficiency*	*Cycle 2*
Q_{18}	*Vapour Quality Outlet – Condenser*	*Cycle 2*

The overall likelihood of the *i-th* condition is the product of the likelihoods evaluated for each (*j-th*) additional information:

$$lh_i = \prod_j lh_{ij} \tag{81}$$

Different methods are applied depending on the type of variable to be predicted:

Temperature: Knowing that temperature is calculated by the model for a specific point (T_{eval}) and the actual temperature measured in the plant in that condition (T_{mea}), maximum likelihood is expected to be occur when T_{eval} equals the T_{mea}. It is possible to evaluate such a probability like an area under the curve depicted in Fig.13.

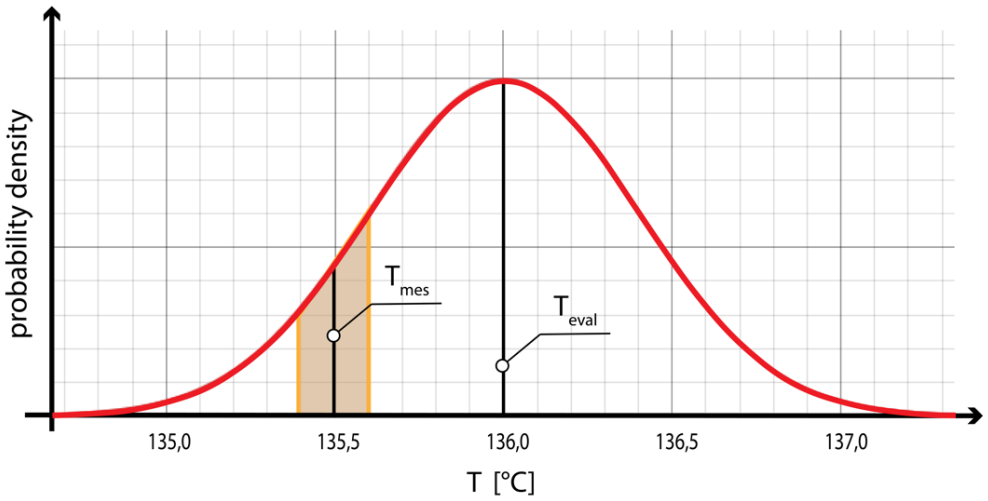

Fig. 24: Likelihood of temperature distribution (Gaussian)

If a Gaussian distribution is assumed for the measured values, the mean value would be the *actual* temperature of the fluid. Hence the likelihood can be calculated using the following formula:

$$lh_{ij} = cdf\left(T_{mes} + \frac{\Delta T_{dec}}{2}, T_{eval}, \sigma_{TC}\right) - \ cdf\left(T_{mes} - \frac{\Delta T_{dec}}{2}, T_{eval}, \sigma_{TC}\right) \quad (82)$$

Where $cdf(x, \mu, \sigma)$ is the cumulative function, i.e. the integral of a Gaussian distribution:

$$cdf(x, \mu, \sigma) = \frac{1}{2}\left(1 + \text{erf}\left(\frac{\mu - x}{\sqrt{2}\sigma}\right)\right) \ with \ \text{erf}(x) = \frac{2}{\pi}\int_0^x e^{-t^2} dt \quad (83)$$

ΔT_{dec} is the maximum interval that can be added to T_{mes} without changing the displayed number. For instance, if the temperature value is displayed with only one decimal point, temperatures like 135.34 and 135.29 will be both displayed as 135.3, hence ΔT_{dec} would be 0.1 in this case.

Efficiency: As it is expected to reach a value of the isentropic efficiency around 0.8, efficiencies much higher and lower than this value are considered to be less likely. The likelihood can be evaluated using the following equation (depicted in Fig. 14):

$$lh_{ij} = \frac{1}{1 + e^{12 - 25\eta}} \cdot \left(1 - \frac{1}{1 + e^{34 - 28\eta}}\right) \quad (84)$$

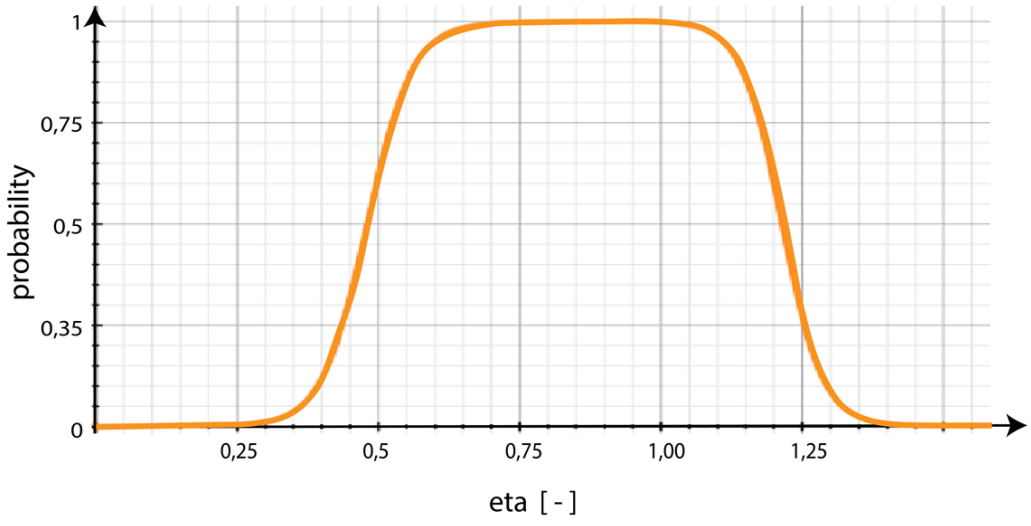

Fig. 25: Likelihood of isentropic efficiency distribution

As turbine efficiency is obtained from the enthalpy difference between turbine inlet and outlet, it is mathematically possible that the model would predict efficiencies higher than one (see Fig. 13).

By all means, this does not mean that the actual isentropic efficiency of the turbine is higher than one, it just indicates that between the two thermocouples the overall energy extracted from the fluid is higher than the work extracted *by an isentropic and therefore an adiabatic* turbine. Knowing the fact that this efficiency value also represents some thermal losses which are not yet calculated, it is logical to take these values into the account for likelihood calculations.

Vapor Quality: Since the vapor presence at condenser outlet is always avoided to protect the mechanical soundness of the pump in practical applications, likelihood of a prediction in which vapor quality at the condenser outlet takes a value other than zero is rejected:

$$lh_{ij} = \begin{cases} 1, & Q = 0 \\ 0, & Q \neq 0 \end{cases} \tag{85}$$

Likelihood of any other variable can be estimated utilizing other physical constraints.

3.4.2.2 Curve Fitting

So far described methodology aimed to reduce uncertainties in the off-design model and to focus just on the conditions which are more likely to be correct. Nevertheless, a certain amount of uncertainty would still be present in the calculated values. Due to this reason, this methodology will be extended to turbine curve fitting purposes.

Curve fitting can be simply described as fitting the best mathematical expression to a certain dataset using different techniques such as interpolation. In this case, dataset will be the off-design plant data which is previously processed by means of *likelihood of occurrence* as described in previous section.

As shown in previous sections, it is possible to estimate occurrence of datapoints in frame of the relationship between probability and likelihood. Similarly, it may also be possible to fit the *most probable* curve into these datapoints by maximizing the likelihood. In order to estimate the most probable curve, one can propose that the overall probability for the *i-th* curve (p_{c_i}) is the mean average of the *j-th* datapoints:

$$p_{c_i} = \frac{\sum_j p_{cij}}{n} \tag{86}$$

Gaussian distribution is assumed for the evaluation of $p_{c_{ij}}$ as explained previously in temperature distribution in detail:

$$p_{c_{ij}} = pdf\left(x_{c_{ij}}, x_{exp_j}, \sigma_j\right) \tag{87}$$

where x_{exp_j} is the position of the j-th experimental point, $x_{c_{ij}}$ is the position of the j-th experimental point as evaluated by the i-th curve, σ_j is the estimated standard deviation for the j-th point and $pdf(x, \mu, \sigma)$ is the probability density function for the normal (i.e. Gaussian) distribution.

Figures 26 and 27 aim to explain this interpolation methodology visually:

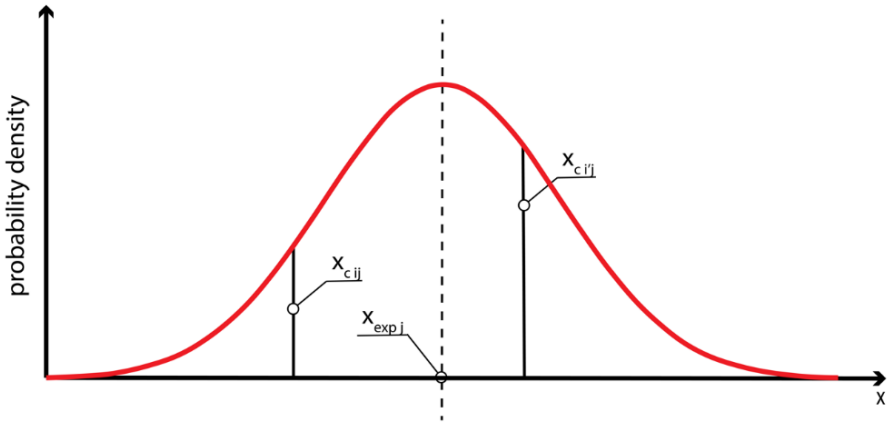

Fig. 26: Curve likelihood calculation of a single datapoint

In the Figure 26, intersections of the two curves i and i' are depicted. Notice that the curve i' is more likely to occur than i because its prediction $x_{c_{ij}}$ is closer to x_{exp_j}. Or in other words $x_{ci'_j}$ has a denser probability than $x_{c_{ij}}$.

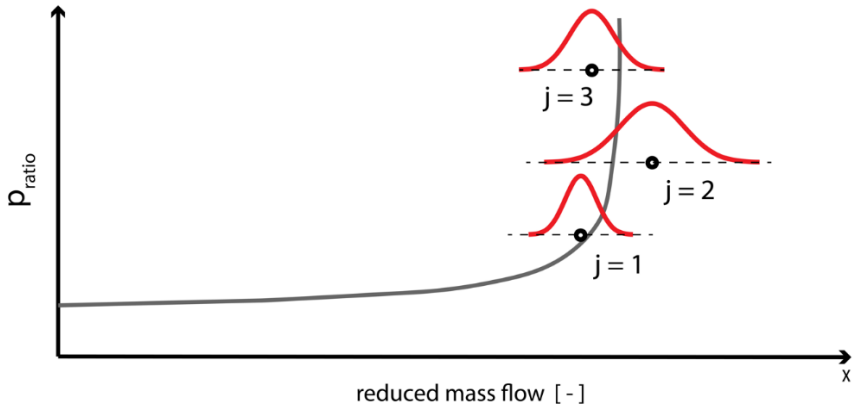

Fig. 27: An application of likelihood approach on Stodola curve

Overall probability of the Stodola curve can be estimated according to eq. (86) and (87) by taking the mean average of probability density functions of each single datapoint considering their standard deviations as shown in Fig.27. This approach can be applied to any curve fitting problem.

In order to optimize the plant variables, one should define turbine characteristics such as turbine curves, possible number of stages etc. Accordingly in this part, turbine characteristics such as the number of stages and turbine curves will be presented. Afterwards turbine isentropic efficiency calculations will be compared with Gabbrielli and Jüdes correlations for further validation purposes. The relationship between ambient temperature and thermal losses will be discussed as well.

Fig. 28 shows the probability of turbine number of stages based on Stodola equation:

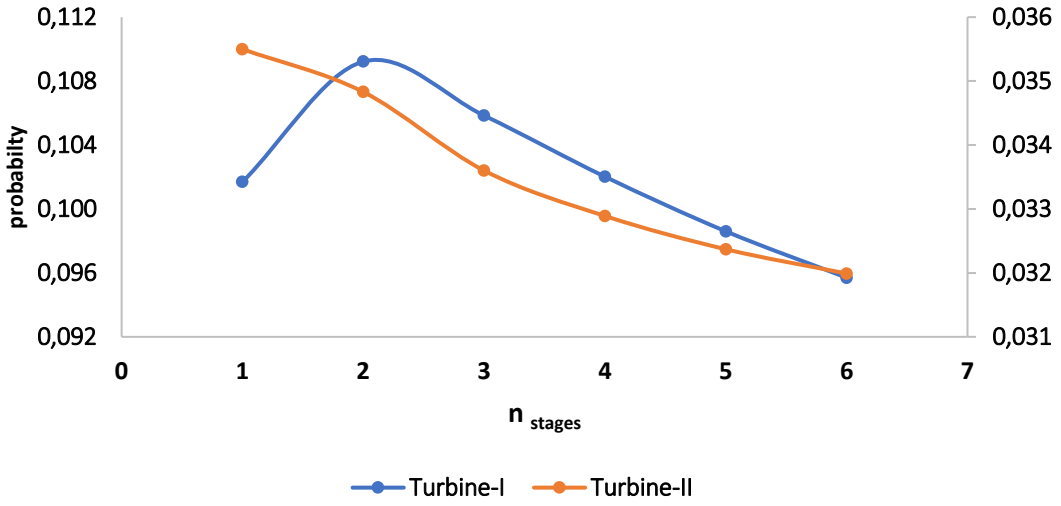

Fig. 28: Probability of Turbine Number of Stages

Fig.28 shows the probability of possible number of stages for the turbines. Both turbines are expected to be two-stage turbines [101] in real-operation conditions since they are the expanders operating with n-pentane, accordingly Fig. 28 demonstrates that the projected thermodynamic and statistical models represent valid results in terms of turbine characteristics -especially for Turbine-I-.

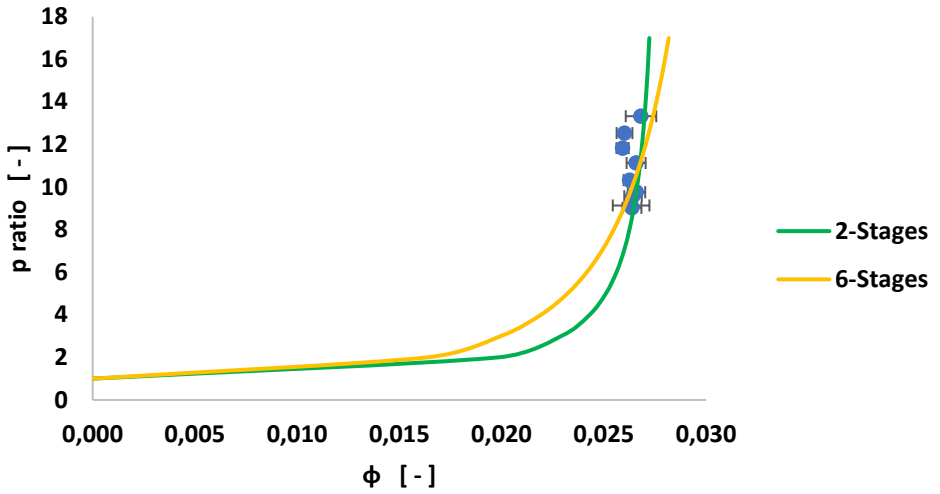

Fig. 29: Stodola Curves for Turbine-I

Fig. 29 depicts the Stodola curves for 6-Stage and 2-Stage turbine variants in terms of Φ (reduced mass flow rate) and pressure ratio (p_ratio). These two stage variants are presented due to the fact they represent the highest and lowest possibilities (see Fig. 28). As one can extract from the Fig.29 a 2-stage turbine model fits more accurately to the calculated off-design datapoints (in their standard deviations) based on existing plant datasets.

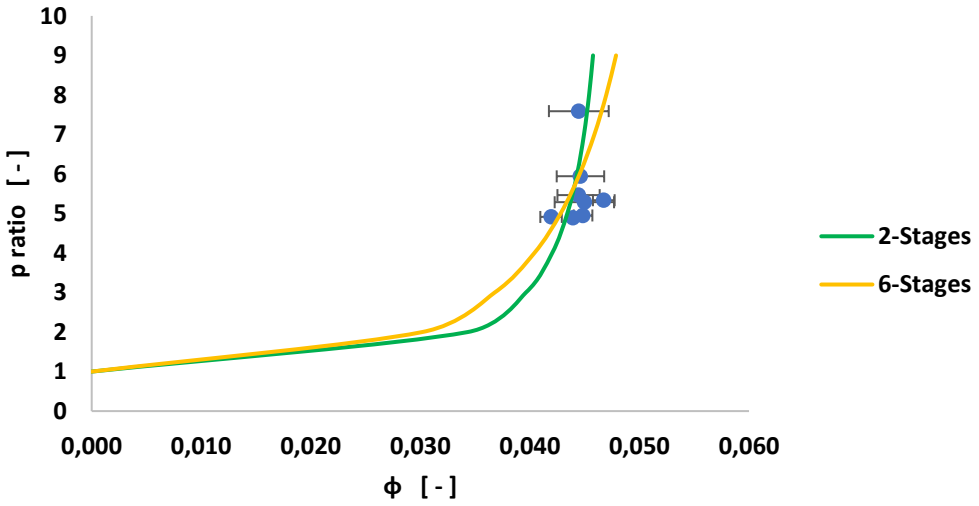

Fig. 30: Stodola Curves for Turbine-II

In Figure 30, Stodola Curves for Turbine-II are depicted. As for Turbine-I, a 2-Stage turbine model fits better to the calculated datapoints from thermodynamic and statistical models. Turbine isentropic efficiency values are also estimated with the help of constructed models.

Aside from isentropic efficiency, in real cases there are some losses from the turbines to the environment which are related with thermal losses to the environment, mechanical irreversibilities and electrical conversion inefficiencies.

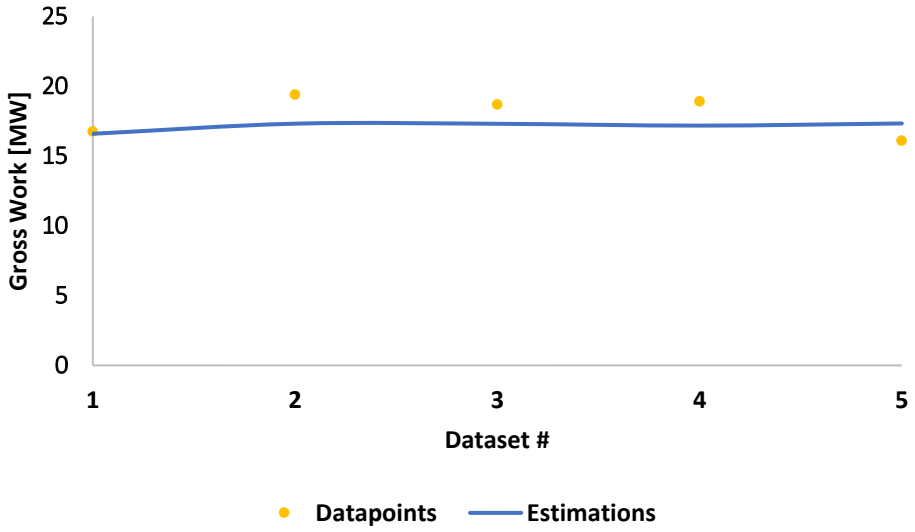

Fig. 31: Gross work output: Existing data vs. Estimations

Fig.31 shows the gross work outputs estimated with the help of constructed models - taking turbine losses (thermal losses as defined in eq. (77), mechanical losses and electrical conversion losses) into the account- against real dataset gross work outputs. Table-36 provides the parameters calculated for the estimation of thermal losses:

Table-36: Thermal losses coefficients calculated by the model

TLC	3	[kW/K]
TLC $_{Q\ mod}$	-48	[kW/K]

Taking turbine loss estimations into the account, results show a decreasing trend of overall efficiencies for both turbines with increasing reduced mass flow rates. From another point of view, one can also state that overall turbine efficiencies fluctuate around their design efficiencies. Gabbrielli and Jüdes correlations also estimate fixed efficiency values around 0.84 and 0.77 respectively for Turbine-I and II.

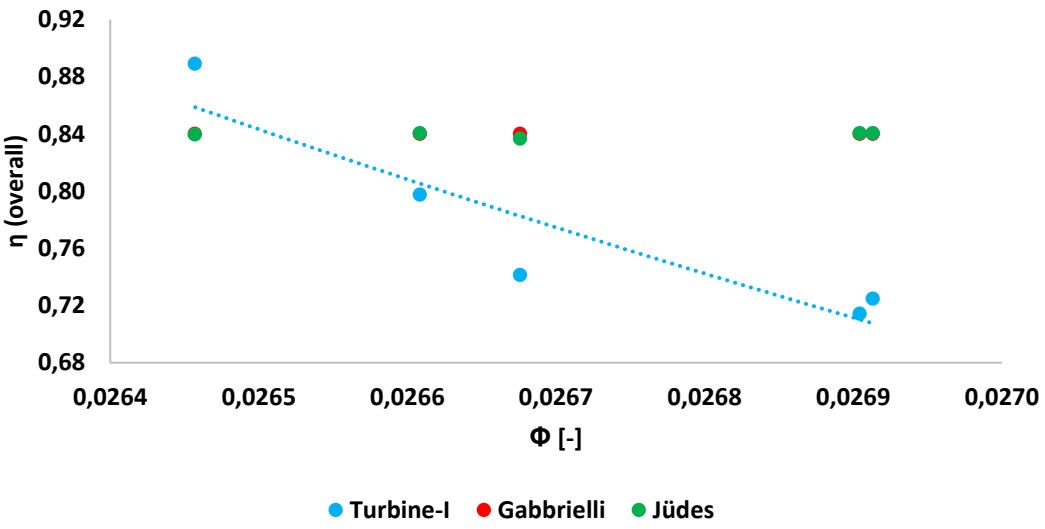

Fig. 32: Turbine-I Overall Efficiencies vs. Correlation Efficiencies

After the extraction of overall losses (thermal-mechanical-electrical), overall efficiency of Turbine-I shows a decreasing trend with increasing *reduced* mass flow rate. This may be associated with the *increased choking* of the turbine. Correlations estimate a rather fixed isentropic efficiency for off-design conditions; that is an expected outcome since these correlations are influenced mainly by the *design efficiency*, which is a constant value. On the other hand, these correlations are proposed for non-choking conditions which is invalid for off-design conditions of ORC turbines.

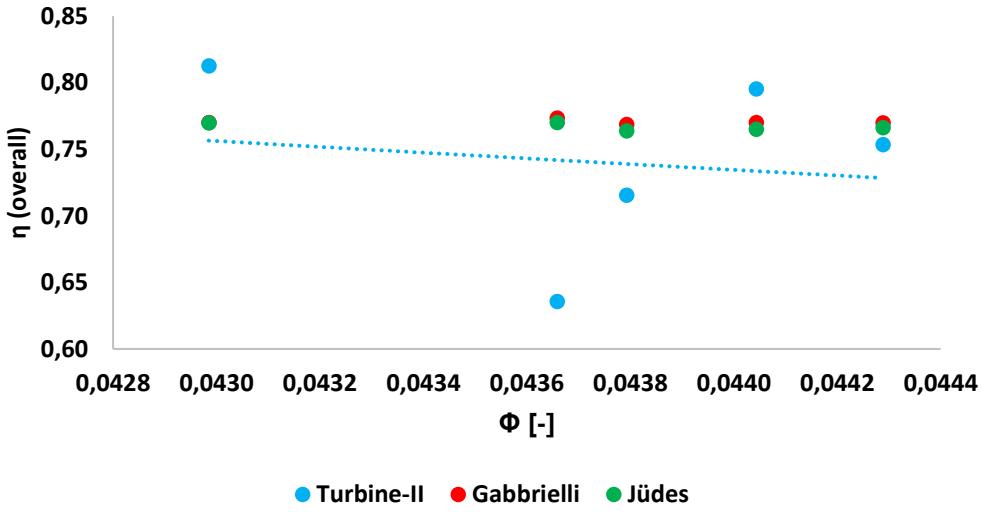

Fig. 33: Turbine-II Overall Efficiencies vs. Correlation Efficiencies

Fig.33 replicates the reverse trend between turbine efficiency and reduced mass flow rate. Value pairs are a little bit more loosely dispersed throughout the different points in Turbine-II, this may be a subject of attention for further studies.

3.5 Optimization

In Section 3.4, a methodology to obtain Stodola curves at off-design conditions under part load is presented. For the optimization purposes, obtained Stodola curves will be embedded into the off-design plant model to calculate the working fluid mass flow rates in both cycles (see Fig.2) at off-design conditions. Accordingly, first variables to be optimized become the cycling working fluid mass flow rates $\dot{m}_{ORC-1}$ and $\dot{m}_{ORC-2}$ respectively.

Working fluid mass flow rate is dependent on several thermophysical variables such as temperature, pressure and density. Therefore, an optimization of mass flow rates with a specific target such as maximizing W_{net} would also re-arrange these variables in the plant configuration.

From a fuel-product perspective, geothermal brine is the fuel of that system; hence distribution of brine between the cycles plays a decisive role in terms of energy distribution. Due to this reason, distribution rate of brine mass flow is the second variable to be optimized. By this means, it would become possible to control the W_{net} and achieve a global minimum for levelized electrical costs of the plant. Table-37 presents the input variables and cycle variables to be optimized:

Table-37: Independent and dependent variables for optimization

Parameter	Variability	Variables to be Optimized
$\dot{m}_{brine}$	Indep. / Adjustable	$\dot{m}_{ORC-1,r}$
T_{brine}	Indep. / Non-Adjustable*	$\dot{m}_{ORC-2,r}$
T_{amb}	Indep. / Non-Adjustable**	$\dot{m}_{brine,r}$

It is possible to manipulate brine inlet conditions as demonstrated in Table-37. Ambient temperature is another important variable which is non-adjustable for sure, however it is projected to demonstrate different optimal conditions throughout the different seasons of the year, therefore ambient temperature is also taken into the account. Well temperature

is another non-adjustable variable to be projected for its inevitable thermal degradation over a certain timespan.

Optimized results will be presented in two different ways. First one will be the definition of optimal conditions at given off-design datasets. In other words, from a retrospective point of view it will be examined whether the plant has been operating somewhere around "optimal" conditions. Second discussion will be about the projected optimal conditions under different physical constraints such as ambient temperature. For instance, a set of optimal operating condition suggestions will be presented between 5-30 ºC ambient temperatures throughout the year in Aydın / Germencik.

Since the plant is already operating, component optimization -such as surface area for heat exchangers or number of fans for condensers- falls out of scope for this research. A further study considering a hypothetical plant approach for the same geothermal field may also take these aspects into the account.

3.5.1 Classification of the Optimization Methods

Let $f(x)$ to be a cost function:

$$f(x) = x^2 - 1 \quad while \;\; x\; E\; Z \tag{87}$$

Objective is to minimize this function, expressed as follows:

$$\min(f(x)) \tag{88}$$

A trivial solution of this optimization problem will be x =1 (note that x=0 is not taken into the account!) however -1 is another side of the solution. This ambiguation is called as the "uniqueness of the solution" in the relevant literature. Since such problems may have more than one solution, it is vital for an optimization algorithm to prove the uniqueness of the solution and eliminate the arbitrary ones [102].

In general terms, optimization problems are divided into two sub-categories; *constrained* problems and *unconstrained* problems. A vast majority of the engineering problems are *constrained* problems because they deal with objective functions like power function or cost function which do include different variables that can vary in a definite range due to the physical restrictions.

By definition, cost function example in eq. (87) can represent an unconstrained optimization problem. In order to convert it to a constrained problem, it is necessary to impose direct or indirect constraints.

Let say the expression in eq. (87) is a function labour costs (x). Since labour costs can not be negative and shall be non-zero, now a constraint is imposed on the function:

$$\min(f(x)) \mid x > 0 \tag{89}$$

Imposing a constraint reduces the number of possible solutions as it is in this case. Taking positive labour values into the account would reduce candidate solutions by a half. On contrary, the problem shall not be "over-constrained" because an unnecessary constraint will restrain the algorithm to reach a real optimum value. For instance in eq. (87), imposing x=0 would lead the algorithm to a false optimum [102].

After a general classification of the optimization problems, it is worth of noting that there are three types of solvers -namely algorithms, iterative methods and heuristics-. Dependent on the context of the problem to be optimized, different optimization techniques are viable in the literature such as convex optimization, linear optimization, nonlinear optimization or stochastic optimization [102].

In parametric optimization of the plant, the problem is about to minimize an objective function (cost). Accordingly, an iterative convex optimization shall be appropriate for such an application.

3.5.2 A Convex Optimization Problem

Assume a continuous, differentiable and convex function -although it is generally not the case in real world-. A convex function with these properties would imply a single extreme point, which would be the *global minimum* as shown in Fig.34 (i.e. graphical description of eq. 87):

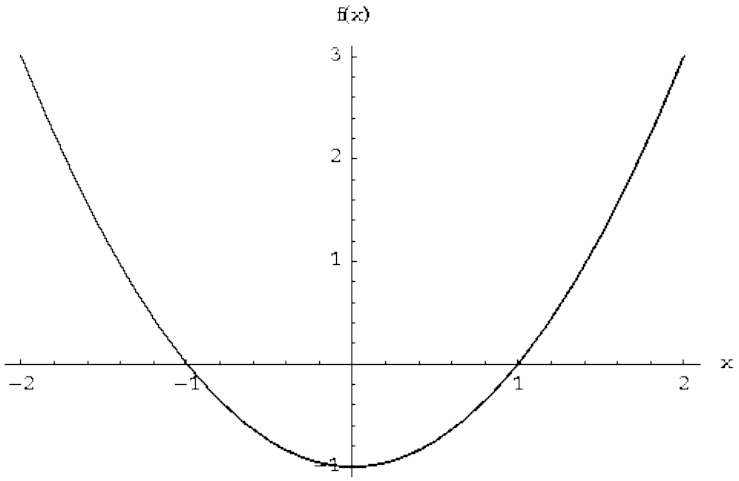

Fig. 34: A continuous convex function ($f(x) = x^2 - 1$)

Term *continuous* simply implies that there is a $f(x)$ value for every x point. The x value which equals $f'(x)$ to zero is the global minimum point which is zero for the function depicted in Fig. 17.

A second derivative test on the other hand would reveal the local minimum and maximums:

- If f'(a)=0 and f''(a)>0, then there is a local minimum at x=a.
- If f'(a)=0 and f''(a)<0, then there is a local maximum at x=a.
- If f'(c)=0 and f''(c)=0, or if f''(c) doesn't exist, then the test is inconclusive. There might be a local maximum or minimum, or there might be a point of inflection.

Another approach to determine whether the extremum points are tending to increase or not is to observe *gradient* of $f(x)$. Such approaches are called in general term gradient descent type optimization and referred to be quite efficient when a single design variable has a huge amount of possible values [102].

3.5.2.1 Gradient Descent Method (GDM)

Gradient-based methods are iterative methods. Main principle of these methods is to track the gradient of the function to determine the direction of the search and by this means to obtain an updated solution [102]:

$$x_{i+1} = x_i + sf_i p_i \tag{90}$$

where subscript i indicates number of iterations, x is the present "solution", sf_i is the utilized scaling factor and p_i is direction of the search.

Gradient Descent Method is a gradient-based method which is sometimes referred as "steepest descent" in the relevant literature. As the term implies, this method employs the "steepest" gradient in the function to determine an optimum point (maximum or minimum). Gradient of a $f(x)$ function can be expressed as follows:

$$\nabla f(x) = f'(x) \tag{91}$$

Optimum point is obtained as the slope of gradient reaches to zero. By definition, for a convex problem p_i must be towards a negative direction (for a maximization problem in a positive direction). Under this considerations eq. (90) can be rewritten as follows:

$$x_{i+1} = x_i - sf_i \nabla f(x) \mid i > 0 \tag{92}$$

sf_i can be manipulated according to the computational requirements since it is an equivalent of time-step in finite element analysis. It is worth of noting that an extremely small would result in much higher computational times while a rough selection of sf_i would cause a significant drop in accuracy.

Optimization process of the plant is executed from two different perspectives: i) retrospective point of view; which would compare the actual configuration of the plant with suggested optimal working configurations. ii) dynamic point of view; which would indicate the optimal configurations at changing environment and input conditions (ambient temperature, brine well temperature and brine mass flow rate).

Before starting the optimization process, Stodola curves presented in previous parts are embedded into the thermodynamic model in order to estimate working fluid mass flow rates under changing off-design conditions rather than a fixed isentropic efficiency assumption (see initial model). Figure 35 depicts the off-design model net work estimations against plant net work data:

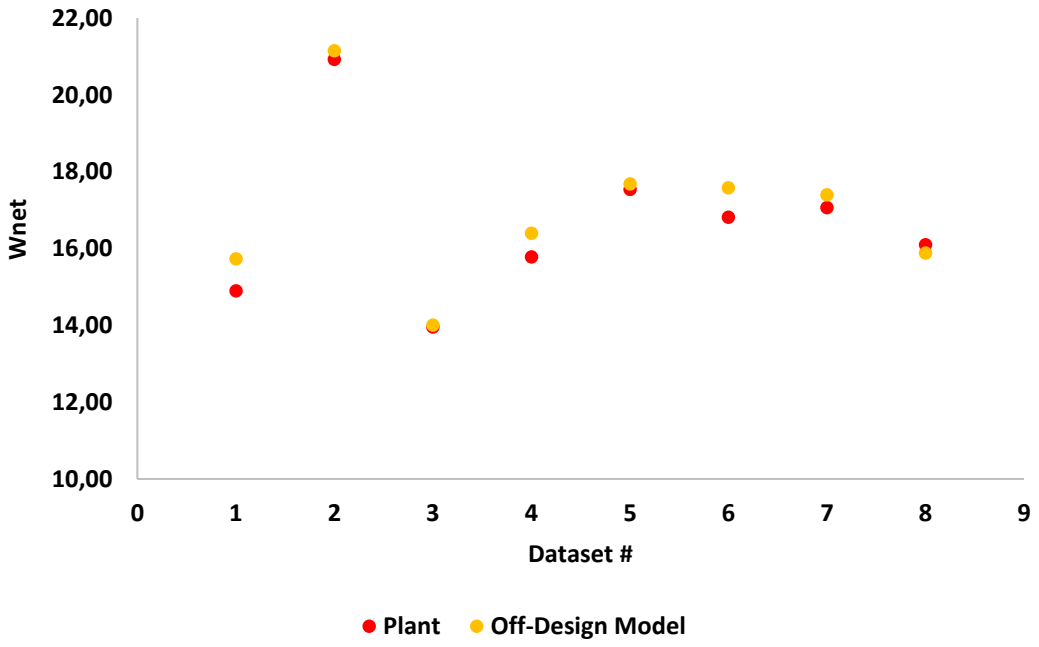

Fig. 35: Off-design model vs plant datasets (Net Work)

Data presented in Fig. 35 shows that the average difference between model net work estimations and real plant net work outputs is around 2%. An accuracy level around 98% indicates yet again that the constructed off-design model is reliable for optimization purposes.

As stated in methodology section, three parameters are subjected to an optimization. These are brine mass flow rate distribution ratio at the splitter (see Fig.2), ratio of working fluid mass flow rate to the brine mass flow rate in first cycle and same ratio in the second cycle. Since brine is the energy driver in this system, mass flow rate distribution of brine between the cycles has a direct impact on ORC configurations. On the other hand, ORC configurations such as pressure levels at heat exchanger inlets/outlets, temperatures, pressure ratios etc. are directly associated with working fluid mass flow rates. This phenomenon implies that a change in working fluid mass flow rate would have a deep impact in plant configuration and accordingly in work outputs.

Table-38 presents the plant performance under different configurations and ambient conditions for different datasets:

Table-38: Plant performance under different ambient conditions and plant configurations

Dataset No	**mbrine [t/h]**	**mbrine,r [-]**	**morc-I,r [-]**	**morc-II,r [-]**	**Tbrine [ºC]**	**Tamb [ºC]**	**II.Law eff.**	**Wnet**
1	1432	0.55	0.36	0.34	155.4	22.0	0.39	14.90
2	1674	0.54	0.36	0.36	159.4	5.3	0.45	20.92
3	1147	0.58	0.42	0.33	154.1	1.0	0.47	13.96
4	1419	0.53	0.40	0.41	163.7	26.7	0.38	15.78
5	1592	0.54	0.37	0.32	157.7	22.3	0.40	17.54
6	1363	0.59	0.42	0.31	159.7	16.0	0.44	16.82
7	1370	0.59	0.41	0.32	158.2	9.4	0.45	17.07
8	1492	0.59	0.37	0.30	156.6	22.0	0.40	16.10

Note that the value in brine distribution ratio represents the first cycle, therefore for instance for dataset-1, brine is distributed like 55% to 45% between first and second cycles. From Table-38, it can be easily extracted that majority of the brine energy is always transferred to first cycle in plant operating conditions. On the other hand, the ratio between working fluid mass flow rate and brine mass flow rate is varying between 0.36-0.42 for first cycle while 0.30 is the lowest value for second cycle.

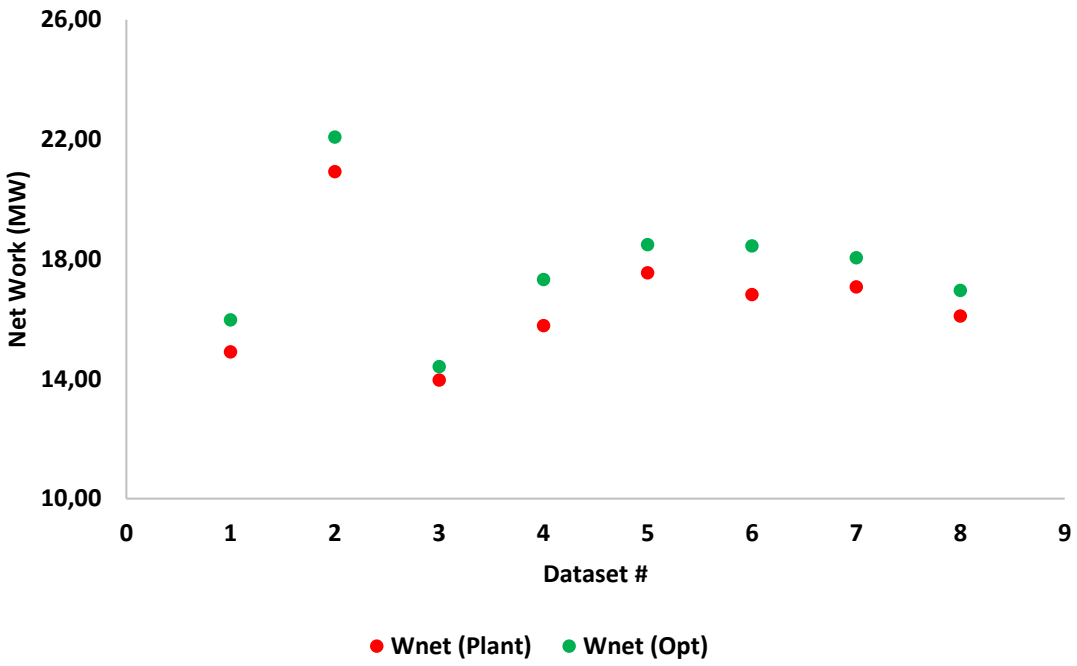

Fig. 36: Optimized configurations vs plant configurations

Fig. 36 depicts net work outputs of optimized plant configurations against plant net work outputs for the datasets presented in Table-38. Results show that it is possible to increase net work outputs for all cases even in the warmest days (point 4) or coldest days (point 3). Average of net work increase is around 730 kW, which equals 4.4% of the average plant net work output throughout the year.

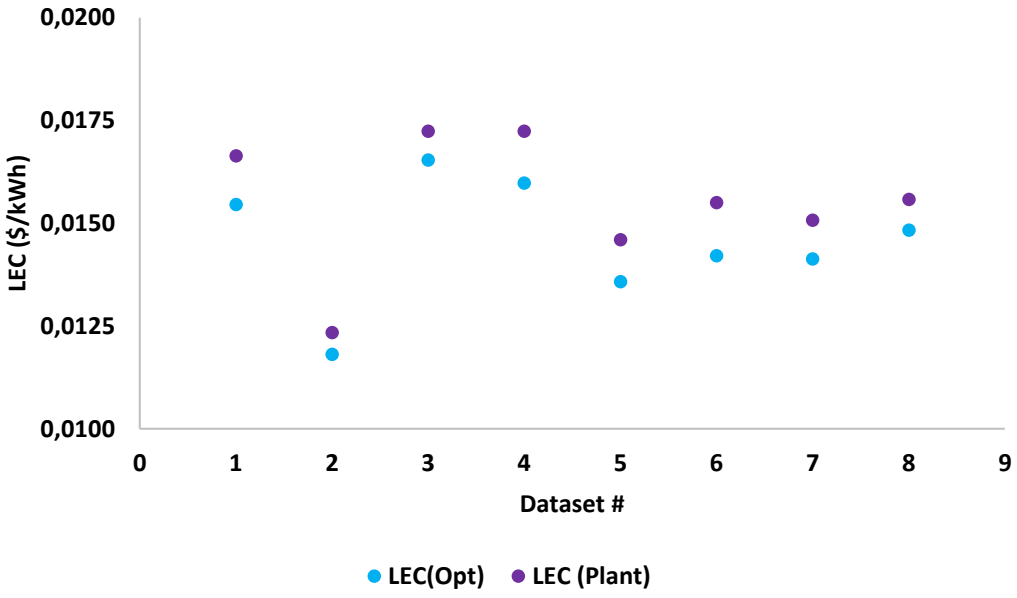

Fig. 37: Optimized LEC vs plant LEC

Figure 37 shows the levelized electrical costs which could have been achieved under optimal conditions and realized LEC values under plant working configurations for different datasets. Results show that it is possible to reduce levelized electrical cost 5.8% in average terms.

Table-39 presents the optimal configurations and their outputs in tabulated format:

Table-39: Optimal configurations and their outputs

Dataset No	**mbrine [t/h]**	**mbrine,r [-]**	**morc-I,r [-]**	**morc-II,r [-]**	**Tbrine [ºC]**	**Tamb [ºC]**	**II.Law eff.**	**Wnet**
1	1432	0.46	0.37	0.42	155.4	22.0	0.42	15.97
2	1674	0.46	0.45	0.36	159.4	5.3	0.47	22.08
3	1147	0.46	0.45	0.37	154.1	1.0	0.49	14.41
4	1419	0.46	0.47	0.38	163.7	26.7	0.41	17.32
5	1592	0.45	0.41	0.38	157.7	22.3	0.43	18.48
6	1363	0.47	0.46	0.41	159.7	16.0	0.48	18.44
7	1370	0.47	0.44	0.39	158.2	9.4	0.48	18.05
8	1492	0.46	0.40	0.42	156.6	22.0	0.42	16.96

Primary finding to be extracted from the comparison of Table-38 and 39 is that; majority of the energy shall be transferred to the second cycle rather than first cycle. In all optimum cases, an optimum brine distribution ratio is estimated around 46% and 54% for first and second cycles respectively. In design conditions, a steam line is associated with Vaporizer-II which is out of operation today, this finding may be underlining yet again the necessity of more energy transfer to second cycle to close the energy gap at Vaporizer-II for vaporization process, which is quite problematic in all off-design conditions. On the other hand, an average 10% increase of working fluid mass flow rate is suggested for cycle-1 whilst this increase suggestion is around 15% for cycle-2. Finally, by employing the optimal configurations, it may be possible to increase second law efficiency of the plant around 7% (in average) without changing inlet conditions (i.e. brine mass flow rate, temperature or pressure).

In the second part of optimization study, optimal configurations for *changing* inlet and ambient conditions will be provided for a sample dataset (i.e. dataset #6). In other words, new optimal conditions will be suggested for changing ambient temperatures, well temperatures and brine mass flow rates for a single dataset.

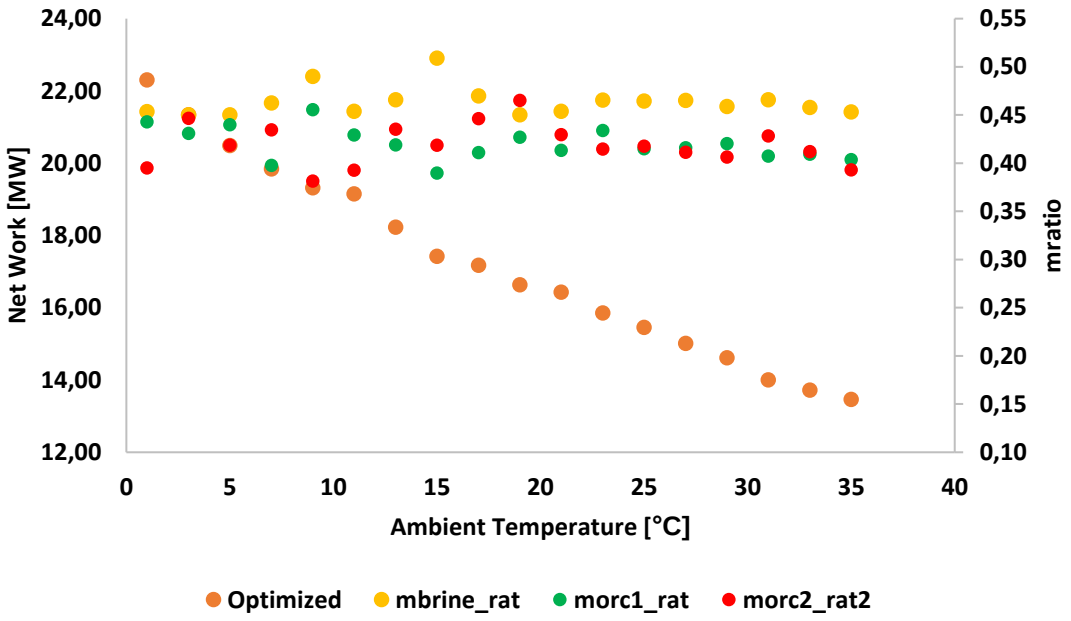

Fig. 38: Optimal plant configurations for different ambient temperatures throughout a year in Germencik (Dataset #6)

Fig. 38 demonstrates optimal plant configurations throughout different seasons of a year in Germencik [76]. As expected, plant work outputs are decreasing as the ambient temperature increases due to the challenging heat rejection processes in hot days of the year [11].

Brine mass flow distribution rate varies around an average value of 0.46 while 0.42 is the mean value for wf /brine mass flow rate for both cycles. These results shall provide a guidance to plant operators for the plant configuration in different seasons of the year to obtain the maximum net power output.

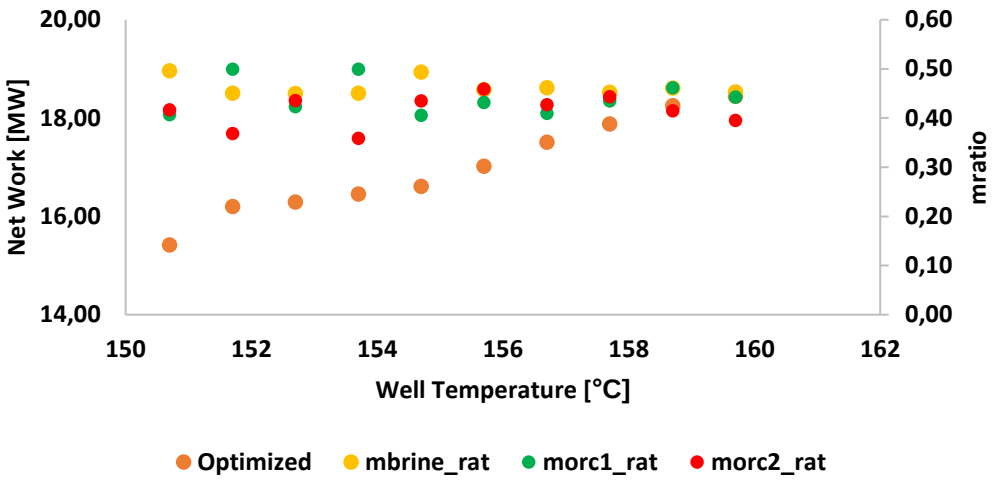

Fig. 39: Optimal plant configurations for decreasing well temperatures throughout the time (Dataset #6; Tamb: 16 ºC)

It is a known fact that the brine extracted from the wells would get cooler over a timespan due to continuous extraction and re-injection processes in power production. As one can expect, a cooler brine would transfer less energy to the system, which implies a decrease in power output as depicted in Figure 39. Optimal mass flow ratios are shown in the Figure 39 for a possible 10 ºC decrease (from actual 159.7 ºC to 149.7 ºC) of inlet temperature during plants operation period. Mean optimal brine distribution ratio is expected to be 0.46 while mean mass flow ratios in cycles are 0.44 and 0.42 respectively.

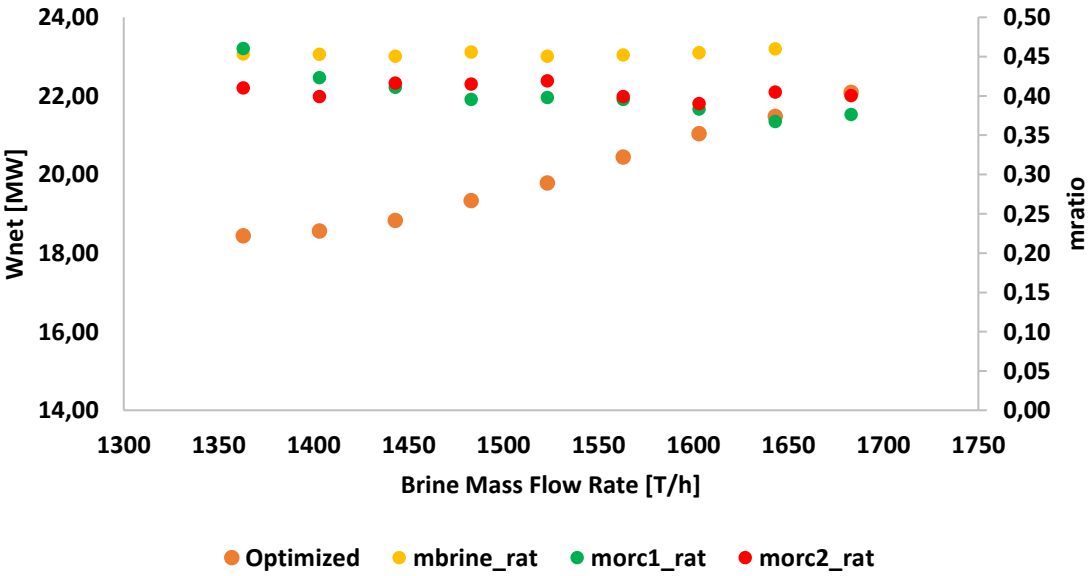

Fig. 40: Optimal plant configurations for increasing brine mass flow rates (Dataset #6; Tamb: 16 ºC)

Figure 40 depicts the effect of increasing brine mass flow rate at optimal configurations. Net work output of the plant increases as expected with the increasing brine mass flow rate. Mean value for optimal brine distribution rate is 0.46, for ORC-I mass flow ratio 0.41 and for ORC-II 0.40 respectively.

Major drawback of an optimization with gradient tracking is the possibility of stalling at local extremes instead of reaching a global extreme. Figure 41 shows a clear global extreme in terms of net work for a random off-design dataset optimization according to different working fluid mass flow ratios at Cycle-1 and Cycle-2 respectively. In all optimization studies, results are obtained at global extremes instead of stalling at local ones as provided between Figures 36-40.

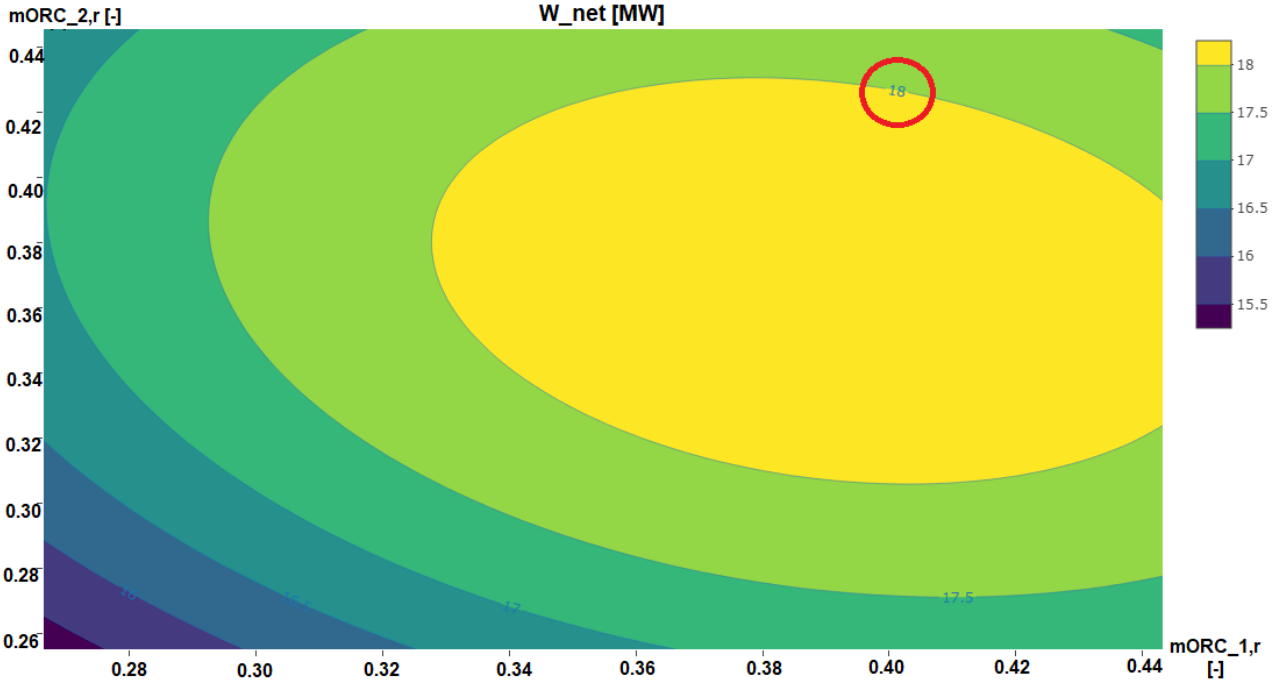

Fig. 41: A global maximum for Wnet at a random off-design dataset

4. CONCLUSIONS

In this thesis, a thermoeconomic optimization of an existing binary geothermal plant was aimed after a comprehensive thermodynamic investigation. In order to achieve this goal, design and off-design plant data are collected at the first step. A thermodynamic model of the plant is built on this data with the help of different simulation software. Initial thermodynamic model is validated with similar plant data in the relevant literature. Afterwards, a novel approach for working fluid selection is proposed by the employment of factorial cost estimation techniques. To complement the thermodynamic analysis, an exergoeconomic analysis of the plant is conducted by employment of different techniques. All of these studies are carried out with a single dataset around plant design conditions with a fixed isentropic turbine efficiency assumption. However, to perform an optimization, a working off-design model of the plant is required. Accordingly, turbine curves (i.e. Stodola curves) are modelled with the help of off-design plant data. A statistical model is proposed in MATLAB environment in order to increase accuracy of the off-design thermodynamic model. These curve models are validated by empirical correlations proposed in the relevant literature. Validated curve models are embedded into off-design model for optimization purposes. At the final stage, a convex optimization with a gradient-based methodology is performed in MATLAB environment to find optimal plant configurations with the aim of net work maximization and LEC minimization.

Conclusions of this thesis can be summarized as follows:

- Initial exergy analysis suggests that the first law efficiency of the plant based on brine's energy input is 4.82% whilst the second law efficiency is around 25.7% based on brine's exergy input. Majority of the exergy destruction occurs during brine re-injection (21.9%).
- According to initial thermodynamic model, the first and second law efficiencies of ORC system (by extracting the reinjection losses) are 9.3% and 32.95%, respectively. In ORCs, major sources of exergy losses are turbines and pumps (25.44%), heat exchangers (21.78%) and condensers (10.8%).
- Based on the proposed approach for working fluid selection, R113 is determined as the novel working fluid of the plant instead of n-pentane. By this means, it is

possible to increase the first and second law efficiencies of the plant, 0.59% and 3.18%, respectively.

- Waste heat recovery options by brine re-injection are investigated. Based on the novel working fluid selection approach, R115 is determined to be the candidate working fluid for WHR cycle. It is shown that, with this, it may be possible to further reduce the LEC, by 1% and to increase the overall efficiencies (I. Law; +0.1%, II. Law; +0.26%).
- It is necessary to emphasize that heat exchanger initial investment costs are roughly 30% of the total capital investment according to applied factorial cost estimations, meaning an optimization of heat exchanger surface areas may have an important impact on the total capital investments in addition to improvements such as defining a more compatible working fluid with heat source as exemplified in this study.
- There is a direct relationship between vapor expansion ratio (VER) and net work output for dry working fluids, isentropic fluids behave differently from dry fluids in terms of VER and net work output.
- Results also demonstrate that the expression used for LEC estimation is highly sensitive to the second law efficiency.
- LEC based on exergoeconomic analysis is determined to be around 0.028 $/kWh by Moran's Method under initial assumptions (i.e. fixed isentropic efficiency, relatively low mechanical and electrical conversion efficiency). On the other hand, SPECO and ECT predicts LEC around 0.024 $/kWh which indicates a 5.5% deviation from Moran.
- 51.5% of electric cost formation is inflicted by waste heat/residue costs at initial plant model.
- Exergoeconomic factors of different plant components beneath 0.5 such as Vaporizer-I or Top-Preheater indicate that despite their high exergetic efficiencies (%90 and %80 respectively) they are worth of any investment to reduce general irreversibility. This also shows that exergetic efficiency solely shall not be a design parameter unless it is accompanied by exergoeconomic factor as a representative of cost relationships.
- Among the utilized methodologies, Moran method is the less comprehensive one since it evaluates system only by single input (fuel) and output (electricity) level.

SPECO gives a better and quick overview of the system by cost-stream associations however the most comprehensive analysis can be obtained with an application of ECT as shown.

- In off-design plant model, Stodola curves and probability calculations demonstrate that both turbines are most likely to have 2 stages.
- Average losses are 2.3 MW and 1.2 MW from Turbine-I and Turbine-II respectively throughout the different seasons.
- After the extraction of losses, overall turbine efficiencies demonstrate a reverse trend with increasing reduced mass flow rate. This may be associated with the increased choking of the turbine.
- Correlations estimate rather fixed efficiency values at off-design conditions (84% for Turbine-I and 77% for Turbine-II); that is an expected outcome since these correlations are influenced by the design isentropic efficiency, which is a constant value.
- On the other hand, these correlations are most likely to be proposed for non-choking conditions which are invalid for off-design conditions of existing ORC turbines.
- Datapoint dispersion in Turbine-II does not demonstrate a strong correlation with physical constraints such as -pressure ratio and reduced mass flow rate- as it does for Turbine-I; this phenomenon may need further attention for future work.
- Average difference between off-design model net work estimations and real plant net work outputs is around 2%.
- Results show that it is possible to increase net work outputs for all cases even in the warmest days or coldest days. Average of net work increase is around 730 kW, which equals 4.4% of the average plant net work output throughout the year.
- By this means, it is possible to reduce levelized electrical cost 5.8% in average terms for off-design conditions.
- In all optimum cases, an optimum brine distribution ratio is estimated around 46% and 54% for first and second cycles respectively. In design conditions, a steam line is associated with Vaporizer-II which is out of operation today, this finding may be underlining yet again the necessity of more energy transfer to second cycle to close the energy gap at Vaporizer-II for vaporization process, which is quite problematic in all off-design conditions.

- On the other hand, an average 10% increase of working fluid mass flow rate is suggested for cycle-1 whilst this increase suggestion is around 15% for cycle-2 at off-design conditions.
- By employing the optimal configurations, it may be possible to increase second law efficiency of the plant around 7% (in average) without changing inlet conditions (i.e. brine mass flow rate, temperature or pressure).
- Optimal configurations are presented at different ambient temperatures throughout a year. Brine mass flow distribution rate varies around an average value of 0.46 while 0.42 is the mean value for wf /brine mass flow rate for both cycles. These results shall provide a guidance to plant operators for the plant configuration in different seasons of the year to obtain the maximum net power output.
- Impact of increasing brine mass flow rate and decreasing well temperatures on optimal configurations are also discussed.

4.1 Future Work

Above all, a future work may include further off-design stabilization of the Turbine-II outputs. Advanced off-design modelling of heat exchangers is another topic to be expanded. Last topic -but not least for sure-; would be an implementation of different optimization algorithms for comparison purposes. GDM is one of the oldest techniques in this particular field for non-linear optimization and it contains some drawbacks -like stalling at local minimums as discussed-. In frame of this research, it was aimed to present the initial optimization results based on existing and off-design plant data, however a more comprehensive research would be a good complementation without any doubt. On the other hand, a multi-objective optimization study of a hypothetical plant configuration in a similar geothermal field can be equally interesting.

5. REFERENCES

[1] Kose R., Research on the generation of electricity from the geothermal resources in Simav region. Renew. Energy 2005; 30: 67-79.

[2] Cerci Y., Performance evaluation of a single flash geothermal power plant in Denizli, Turkey. Energy 2003; 28: 27-35.

[3] https://www.enerji.gov.tr/en-US/Pages/Geothermal

[4] Bhatia S.C., Advanced renewable energy systems, Woodhead Publishing India, 2014, ISBN: 978-1-78242-269-3.

[5] Kalina A.I. New Binary Geothermal Power System. International Geothermal Workshop 2003, Geothermal Energy Society.

[6] Macchi E., Astolfi M., Organic Rankine Cycle (ORC) Power Systems: Technologies and Applications, 1st Edition, Woodhead Publishing, 2016, ISBN (e-book) : 978-0-08100-511-8.

[7] Satanphol K, Pridasawas W, Suphanit B. A study on optimal composition of zeotropic working fluid in an Organic Rankine Cycle (ORC) for low grade heat recovery. Energy 2017; 123: 326-39.

[8] Kanoglu M., Exergy analysis of a dual-level binary geothermal power plant. Geothermics 2002; 31: 709-724.

[9] DiPippo R. Second law assessment of binary plants generating power from low-temperature geothermal fluids. Geothermics 2004 ;33: 565-86.

[10] Yıldırım D., Özgener L., Thermodynamics and exergoeconomic analysis of geothermal power plants, Renewable Sustainable Energy Reviews 2012;16: 6438-6454.

[11] Kahraman M., Sorgüven E., Olcay A.B., Thermodynamic and thermoeconomic analysis of a 21 MW binary type air cooled geothermal powerplant and determination of the effect of ambient temperature variation on the plant performance. Energy Conversion and Management 2019; 192: 308-320.

[12] Yari M., Exergetic analysis of various types of geothermal power plants. Renewable Energy 2010; 35: 112–121.

[13] Unverdi, M., Cerci, Y., Performance analysis of Germencik Geothermal Power Plant. Energy 2013; 52: 192-200.

[14] Unverdi M., Investigation of waste heat recovery of binary geothermal plants using single component refrigerants. International Conference on Green Energy Technology 2017; 83.

[15] Gökgedik H.,Yürüsoy M., Keçebaş A., Thermodynamic evaluation of a geothermal power plant for advanced exergy analysis. Energy 2015; 88: 746-755.

[16] Yılmaz C., Thermoeconomic cost analysis and comparison of methodologies for Dora II binary geothermal power plant. Geothermics, 2018; 75: 48-57.

[17] Leveni, M., Giampaolo M., Cozzolino R., Mendecka, B.. Energy and exergy analysis of cold and power production from the geothermal reservoir of Torre Alfina, Energy 2019; 180: 807-818.

[18] Li J., Pei G, Li Y., Wang D., Ji J., Energetic and exergetic investigation of an organic Rankine cycle at different heat source temperatures. Energy 2012; 38: 85-95.

[19] Rodríguez C.E.C., Palacio J.C.E, Venturini O.J., Lora E.E.S., Cobas V.M., dos Santos D.M., et al., Exergetic and economic comparison of ORC and Kalina cycle for low temperature enhanced geothermal system in Brazil. Applied Thermal Engineering 2013; 52:109–119.

[20] Vetter C, Wiemer H, Kuhn D. Comparison of sub- and supercritical Organic Rankine Cycles for power generation from low-temperature low-enthalpy geothermal wells, considering specific net power output and efficiency. Applied Thermal Engineering 2013; 51:871–9.

[21] Zare V., A comparative thermodynamic analysis of two tri-generation systems utilizing low-grade geothermal energy. Energy Conversion and Management 2016; 118: 264–274.

[22] Walraven D, Laenen B, D'haeseleer W. Comparison of thermodynamic cycles for power production from low-temperature geothermal heat sources. Energy Convers. Manag. 2013; 66 :220–33.

[23] Dincer I., El-Emam R.S., Exergy and exergoeconomic analyses and optimization of geothermal organic Rankine cycle. Applied Thermal Engineering 2013; 59: 435-444.

[24] Yang L., Gong M., Guo H., Dong X., Shen J., Wu J., Effects of critical and boiling temperatures on system performance and fluid selection indicator for low temperature organic Rankine cycles, Energy 2016; 109: 830-844.

[25] Zhai H., An Q., Shi L., Analysis of the quantitative correlation between the heat source temperature and the critical temperature of the optimal pure working fluid for subcritical organic Rankine cycles, Applied Thermal Engineering 2016; 99: 383–391.

[26] He C., Liu C., Gao H., Xie H., Li Y., Wu S., Xu J., The optimal evaporation temperature and working fluids for subcritical organic Rankine cycle, Energy 2012; 28: 136-143.

[27] Astolfi M., Romano M.C., Bombarda P., Machhi E., Binary ORC (Organic Rankine Cycles) power plants for the exploitation of medium - low temperature geothermal sources - Part B: Techno-economic optimization, Energy 2014; 66: 435-446.

[28] Aghahosseini S, Dincer I. Comparative performance analysis of low temperature Organic

Rankine Cycle (ORC) using pure and zeotropic working fluids, Applied Thermal Engineering 2013; 54(1): 35-42.

[29] Basaran A., Ozgener L., Investigation of the effect of different refrigerants on performances of binary geothermal power plants. Energy Conversion and Management 2013; 76: 483–498.

[30] Thurairaja K., Wijewardane A., Jayasekara S., Ranasinghe C., Working fluid selection and performance evaluation of ORC, Energy Procedia 2019; 156: 244-248.

[31] Wang X., Levy E.K., Pan C., Romero C.E., Banerjee A., Rubio-Maya C., Pan L., Working fluid selection for organic Rankine cycle power generation using hot produced supercritical CO2 from a geothermal reservoir, Applied Thermal Engineering 2019; 149: 1287-1304.

[32] Zeyghami M., Performance analysis and binary working fluid selection of combined flash-binary geothermal cycle, Energy 2015; 88: 765-774.

[33] Heberle F., Preißinger M., Brüggemann D., Zeotropic mixtures as working fluids in organic Rankine cycles for low-enthalpy geothermal resources. Renewable Energy 2012; 37: 364-370.

[34] Longo G.A., Mancin S., Righetti G., Zilio C., Brown J.S., Assessment of the low-GWP refrigerants R600a, R1234ze(Z) and R1233zd (E) for heat pump and organic Rankine cycle applications. Applied Thermal Engineering 2020; 167: 114804.

[35] Ye Z., Yang J., Shi J., Chen, J. Thermo-economic and environmental analysis of various low-GWP refrigerants in Organic Rankine cycle system. Energy 2020; 199: 117344.

[36] Yang J., Ye Z., Yu B., Ouyang H., Chen, J. Simultaneous experimental comparison of low-GWP refrigerants as drop-in replacements to R245fa for Organic Rankine cycle application: R1234ze(Z), R1233zd(E), and R1336mzz(E). Energy 2019; 173: 721-731.

[37] Papadopoulos A.I., Stijepovic M., Linke P., On the systematic design and selection of optimal working fluids for organic Rankine cycles. Applied Thermal Engineering 2010; 30: 760-769.

[38] Zhao Y., Biao F., Haiyun M., Lei Z., Chenjun D., Bing L., Yong Z., Siyi C., Zongyu Y., Analysis of Lower GWP and Flammable Alternative Refrigerants, International Journal of Refrigeration 2021; doi: https://doi.org/10.1016/j.ijrefrig.2021.01.022.

[39] Gomez J.M., Lamas J.P., Martin M., Ortega J.M.P., A multi-objective optimization approach for the selection of working fluids of geothermal facilities: Economic, environmental and social aspects, Journal of Environmental Management 2017; 203: 962-972.

[40] Bekiloğlu H.E., Bedir H., Anlaş G., Multi-objective optimization of ORC parameters and selection of working fluid using preliminary radial inflow turbine design, Energy Conversion and Management 2019; 183: 833–847.

[41] Dincer I., Rosen M.A., *Exergy*, Energy, Environment and Sustainable Development, Elsevier Science, 2012.

[42] Valero A., Lozano M.A, 1993. Theory of exergetic cost, Energy 18 (9), 939-960.

[43] Moran, M. J., Availability analysis: A guide to efficient energy use. Englewood Cliffs, NJ: Prentice-Hall, 1982.

[44] Lazzaretto, A., Tsatsaronis, G., 2006. SPECO: a systematic and general methodology for calculating efficiencies and costs in thermal systems. Energy 31 (8–9), 1257–1289.

[45] Kwak H.Y., Kim, D.J., Jeon, J.S., 2003. Exergetic and thermoeconomic analyses of power plants. Energy 28 (4), 343–360.

[46] Pan M., Lu F., Zhu Y., Huang G., Yin J., Huang F., Chen G., Chen Z., 2020. Thermodynamic, exergoeconomic and multi-objective optimization analysis of new ORC and heat pump system for waste heat recovery in waste-to energy combined heat and power, Energy Conversion and Management 222, 113200.

[47] Fiaschi D., Manfrida G., Rogai E., Talluri L., 2017. Exergoeconomic analysis and comparison between ORC and Kalina cycles to exploit low and medium-high temperature heat from two different geothermal sites, Energy Conversion and Management 154, 503-516.

[48] Zhao Y., Wang J., 2016. Exergoeconomic analysis and optimization of a flash-binary geothermal power system, Applied Energy 179, 159-170.

[49] Abdolalipouradl M., Mohammadkhani F., Khalilarya S., 2020. A comparative analysis of novel combined flash-binary cycles for Sabalan geothermal wells: Thermodynamic and exergoeconomic viewpoints, Energy 209, 118235.

[50] Samadi F., Kazemi N., 2020. Exergoeconomic analysis of zeotropic mixture on the new proposed organic Rankine cycle for energy production from geothermal resources, Renewable Energy, 152, 1250-1265.

[51] Zare V., 2015. A comparative exergoeconomic analysis of different ORC configurations for binary geothermal power plants, Energy Conversion and Management, 105, 127-138.

[52] Nasruddin N., Saputra I.D., Mentari T., Bardow A., Marcelina O., Berlin S., 2020. Exergy, exergoeconomic, and exergoenvironmental optimization of the geothermal binary cycle power plant at Ampallas, West Sulawesi, Indonesia, Thermal Science and Engineering Progress, 19, 100625.

[53] Shokati N., Ranjbar F., Yari M., 2015. Comparative and parametric study of double flash and single flash/ORC combined cycles based on exergoeconomic criteria, Applied Thermal Engineering, 91, 479-495.

[54] Cooke D.H. On Prediction of Off-Design Multistage Turbine Pressures by Stodola's Ellipse, J. Eng. Gas Turbines Power; 1985, 107(3): 596-606.

[55] Gabbrielli R., 2012. A novel design approach for small scale low enthalpy binary geothermal power plants, Energy Conversion and Management; 64: 263–272.

[56] Calise F, Capuano D, Vanoli L., 2015. Dynamic simulation and exergo-economic optimization of a hybrid solar-geothermal cogeneration plant. Energies (8):2606-46.

[57] Wang J, Wang J, Dai Y, Zhao P., 2017. Assessment of off-design performance of a Kalina cycle driven by low-grade heat source. Energy; 138: 459-72.

[58] Yoon SY, Kim MJ, Kim IS, Kim TS., 2017. Comparison of micro gas turbine heat recovery systems using ORC and trans-critical CO2 cycle focusing in off-design performance. Energy Procedia ; 129: 987-94.

[59] Keeley KR., A theoretical investigation of the part-load characteristics of LP steam turbine stages. CEGB memorandum RD/L/ES0817/M88. 1988, Central Electrical Generating Board, UK.

[60] Jüdes M, Vigerske S, Tsatsaronis G., 2009. Optimization of the design and partial-load operation of power plants using mixed-integer nonlinear programming. In: Pardalos PM, Kallrath J, Rebennack S, Scheidt M, editors. Optimization in the energy industry. first ed. Springer-Verlag; p. 193-220.

[61] Fiaschi D., Manfrida G., Maraschiello F., 2015. Design and performance prediction of radial ORC turboexpanders, Applied Energy,138: 517-532.

[62] Dawo F., Wieland C., Spliethoff H., 2019. Kalina power plant part load modeling: Comparison of different approaches to model part load behavior and validation on real operating data, Energy; 174: 625-637,

[63] Yılmaz C., Koyuncu I., Alcin M., Tuna M., 2019. Artificial Neural Networks based thermodynamic and economic analysis of a hydrogen production system assisted by geothermal energy on Field Programmable Gate Array, International Journal of Hydrogen Energy**;** 44 (33): 17443-17459.

[64] Özkaraca O., Keçebaş A., 2019. Performance analysis and optimization for maximum exergy efficiency of a geothermal power plant using gravitational search algorithm, Energy Conversion and Management; 185: 155-168.

[65] Clarke J., McLeskey J.T., 2015. Multi-objective particle swarm optimization of binary geothermal power plants, Applied Energy, 138: 302-314.

[66] Pollet M., Gosselin L., Dallaire J., Mathieu-Potvin F., 2018. Optimization of geothermal power plant design for evolving operating conditions. Applied Thermal Engineering, 134: 118-

129.

[67] https://www.thermopedia.com/content/1016/

[68] Pieve M., Salvadori G., 2011. Performance of an air-cooled steam condenser for a waste-to-energy plant over its whole operating range. Energy Conversion and Management; 52: 1908-1913.

[69] Morozyuk, T., Tsatsaronis G. 2018. Splitting physical exergy: Theory and application. Energy; 167: 698-707.

[70] Winterbone D.E., Turan A., Advanced Thermodynamics for Engineers, Butterworth-Heinemann, 2015.

[71] Brodyansky, V.M., Sorin, M.V., Le Goff, P., The Efficiency of Industrial Processes: Energy Analysis and Optimization, Elsevier Science, 1994.

[72] Kotas, T. J., The exergy method of thermal plant analysis, Malabar, 1985.

[73] Tsatsaronis G., Thermoeconomic analysis and optimization of energy systems, Prog. Energy Combust. Sci. 1993; 19: 227-257.

[74] Pal R., On the Gouy–Stodola theorem of thermodynamics for open systems, International Journal of Mechanical Engineering Education, 2017; 45(2): 194-206.

[75] https://www.nist.gov/srd/refprop

[76] https://mgm.gov.tr/tahmin/il-ve-ilceler.aspx?il=AYDIN&ilce=GERMENCIK

[77] Chen, H.; Goswami, D.Y.; Stefanakos, E.K. 2010. A review of thermodynamic cycles and working fluids for the conversion of low grade heat. Renew. Sustain. Energy Rev.; 14: 3059–3067.

[78] Zhang X., Zhang Y., Cao M., Wang J., Wu Y., Ma C., 2019. Working Fluid Selection for Organic Rankine Cycle Using Single-Screw Expander, Energies; 12: 3197.

[79] Györke G., Groniewsky A., Imre A.R., A Simple Method of Finding New Dry and Isentropic Working Fluids for Organic Rankine Cycle, Energies 2019; 12: 480.

[80] Durmuş T., Salavatlı jeotermal santralinin ekserji analizi, İTÜ Enerji Enstitüsü Yüksek Lisans Tezi, 2006.

[81] https://www.chemengonline.com/2019-chemical-engineering-plant-cost-index-annual-average/.

[82] Bejan, A., Tsatsaronis, G., Thermal Design and Optimization. John Wiley & Sons, 1996.

[83] Gorji-Bandpy, M., Goodarzian, H., Exergoeconomic optimization of gas turbine power

plants operating parameters using genetic algorithms: A case study, Thermal Science, 2011; 15: 43–54.

[84] Kim, S., Oh, S., Kwon, Y., Kwak, H. Exergoeconomic analysis of thermal systems. Energy 1998; 23: 393–406.

[85] Dhillon, B.S., Life Cycle Costing for Engineers, CRC Press, 2009.

[86] Lemmens S., Cost Engineering Techniques and Their Applicability for Cost Estimation of Organic Rankine Cycle Systems, Energies, 2016; 9: 485.

[87] Turton R., Bailie R.C., Whiting W.B., Shaeiwitz J.A., Analysis Synthesis and Design of Chemical Processes Third Edition, Prentice Hall, 2009.

[88] Smith, R. Chemical Process Design and Integration, Wiley & Sons, West Sussex, UK, 2005.

[89] Toffolo, A., Lazzaretto, A., Manente, G., Paci, M. A multi-criteria approach for the optimal selection of working fluid and design parameters in Organic Rankine Cycle systems. Appl. Energy 2014; 121: 219–232.

[90] Oyopedo S.O, Fagbenle R.O., Adefila S.S., Mahbub A., Exergy costing analysis and performance evaluation of selected gas turbine power plants, Cogent Engineering 2015; 2: 1101048.

[91] Gorji-Bandpy, M., Goodarzian, H., Biglari, M., The cost-effective analysis of a gas turbine power plant. Energy Sources, Part B: Economics, Planning and Policy 2010; 5: 348–358.

[92] IRENA, 2017. Geothermal Power: Technology Brief, International Renewable Energy Agency, Abu Dhabi.

[93] Kenneth Jr W, Advanced Thermodynamics for Engineers, International addition. New York: McGraw-Hill, Inc.; 1995.

[94] A Lazzaretto, G. Tsatsaronis, "On the Calculation of Efficiencies and Costs in Thermal Systems". In: Proceedings of the ASME Advanced Energy Systems Division, AES-Vol.39. 1999.

[95] Torres C., Valero A., 2018. A New Methodology to compute the exergy cost. Part I: The Flow Process Table, Proceedings of ECOS 2018.

[96] Torres C., Valero A., 2018. A New Methodology to compute the exergy cost. Part II: The generalized irreversibility cost formula, Proceedings of ECOS 2018.

[97] Leontief, W. Input-Output Economics. 2nd. edition. Oxford University Press, 1986.

[98] Murdock, J. W. Fundamental fluid mechanics for the practicing engineer, CRC Press, 1993 ISBN 978-0-8247-8808-7.

[99] Pruss A, Wagner W., 2002. The IAPWS Formulation 1995 for the Thermodynamic

Properties of Ordinary Water Substance for General and Scientific Use, Journal of Physical and Chemical Reference Data 31; 387.

[100] Rossi, R. J. , 2018. Mathematical Statistics: An Introduction to Likelihood Based Inference. New York: John Wiley & Sons. ISBN 978-1-118-77104-4.

[101] Meroni A., Andreasen J.G., Persico G., Haglind F. (2018), Optimization of organic Rankine cycle power systems considering multistage axial turbine design, Applied Energy; 209: 339-354.

[102] Christensen J., Bastien C., 2016. Nonlinear Optimization of Vehicle Safety Structures Modeling of Structures Subjected to Large Deformations, Butterworth-Heinemann, ISBN: 978-0-12-804424-7.

APPENDIX

APP. 1 – Matlab Code of Convex Optimization in UNISIM

hycell.m

```
function CellObject = hycell(SpreadsheetObject, CellNameString)
% HYCELL Returns the column cell array of activeX objects of cells in
Hysys.
%    hycell(SpreadsheetObject, CellNameString) returns the object for
the
%    cell name given by CellNameString. CellNameString may be a cell
array.
%
%    Copyright (C) 1999 Olaf Trygve Berglihn <olafb@pvv.org>
%    Please read the files license.txt and lgpl.txt

%% $Id: hycell.m,v 1.5 1999/04/20 08:52:52 olafb Exp $
%% -----------
%% Change log:
%%
%% $Log: hycell.m,v $
%% Revision 1.5  1999/04/20 08:52:52  olafb
%% The library is now under LGPL license.
%%
%% Revision 1.4  1999/04/18 13:54:11  olafb
%% hysyslib/
%%
%% Revision 1.3  1999/04/16 08:38:16  olafb
%% Added support for cell arrays of aciveX objects
%%
%% Revision 1.2  1999/04/07 11:56:43  olafb
%% *** empty log message ***
%%

CellObject = {};

if isa(CellNameString, 'cell')
  for n1 = 1:size(CellNameString,1)
    for n2 = 1:size(CellNameString,2)
    CellObject{n1,n2} = get (SpreadsheetObject, 'Cell',
CellNameString{n1,n2});
    end
  end
else
  CellObject{1} = get (SpreadsheetObject, 'Cell', CellNameString);
end
```

hyconnect.m

```
function hyapp = hyconnect(FileNameString, VisibleBoolean)
% HYCONNECT Connecting Matlab as a controller for Hysys via
ActiveX/COM
%    hyconnect(FileNameString, VisibleBoolean) connects to the Hysys
%    case-file specified by FileNameString. If given no arguments, the
%    current and open Hysys-case will be used. The optional boolean
variable
```

```
%    VisibleBoolean controls wether the application window will be
shown
%    (takes values 0 and 1, 1 by default). Returns the activeX
application
%    server object.
%
%    Copyright (C) 1999 Olaf Trygve Berglihn <olafb@pvv.org>
%    Please read the files license.txt and lgpl.txt

%% $Id: hyconnect.m,v 1.4 1999/04/20 09:04:39 olafb Exp $
%% ----------
%% Changelog:
%%
%% $Log: hyconnect.m,v $
%% Revision 1.4  1999/04/20 09:04:39  olafb
%% *** empty log message ***
%%
%% Revision 1.3  1999/04/16 08:38:16  olafb
%% Added support for cell arrays of aciveX objects
%%
%% Revision 1.2  1999/04/07 11:58:14  olafb
%% *** empty log message ***
%%
%% Revision 1.1  1999/03/27 17:24:31  olafb
%% Initial revision
%%


% Connect to Hysys via Matlab activeX library function in Windows
version.
% Since the activeX-library is not included in Matlab at compilation,
a
% feval or eval syntax must be used.

hy  = feval('actxserver', 'UnisimDesign.Application');

if nargin <= 1
   hy.Visible = 1;
else
   hy.Visible = VisibleBoolean;
end


% This try/catch clause does not work yet. Only a dispatch warning is
% issued.
%
try
 if nargin > 0
  invoke (hy.SimulationCases, 'Open', FileNameString);
 end
catch
  lasterr;
  disp('Check the path of the filename. If file is not in');
  disp('local directory, include full path to file');
end

hyapp = hy;
```

hyintegtoggle.m

```
function hyintegtoggle(ApplicationObject)
% HYSOLVERTOGGLE Toggle integrator active/inactive in Hysys
%    hysolvertoggle(ApplicationObject) toggles the solver in Hysys.
%
%    Copyright (C) 2008 Olaf Trygve Berglihn <olafb@pvv.org>
%    Please read the files license.txt and lgpl.txt


h = actxserver('WScript.Shell');
h.AppActivate(regexprep(ApplicationObject.Caption, '.*- ', ''));
h.SendKeys('{F9}');
release(h);
```

hyisintegrating.m

```
function isintegrating = hyisintegrating(ApplicationObject)
% HYSOLVERTOGGLE Toggle solver active/inactive in Hysys
%    hysolvertoggle(ApplicationObject) toggles the solver in Hysys.
%
%    Copyright (C) 2008 Olaf Trygve Berglihn <olafb@pvv.org>
%    Please read the files license.txt and lgpl.txt


isintegrating =
ApplicationObject.ActiveDocument.Solver.Integrator.IsRunning;
```

hyset.m

```
function hyset(CellObjects, Value)
% HYSET Function to change a value of a spreadsheet cell in Hysys
%    hyset(CellObjects, Value) changes the value of CellObjects to
Value.
%    CellObjects and Value must be matrises of the same dimension.
%    CellObjects can contains a single object or a cell array of
objects.
%
%    Copyright (C) 1999 Olaf Trygve Berglihn <olafb@pvv.org>
%    Please read the files license.txt and lgpl.txt

%% $Id: hyset.m,v 1.5 1999/04/20 08:52:53 olafb Exp $
%% ----------
%% Changelog:
%%
%% $Log: hyset.m,v $
%% Revision 1.5  1999/04/20 08:52:53  olafb
%% The library is now under LGPL license.
%%
%% Revision 1.4  1999/04/18 14:04:43  olafb
%% Added support for cell matrises of activeX-objects.
%%
%% Revision 1.3  1999/04/18 13:54:12  olafb
%% hysyslib/
%%
%% Revision 1.2  1999/04/16 08:38:16  olafb
%% Added support for cell arrays of aciveX objects
%%
```

```
%% Revision 1.1  1999/04/07 12:00:29  olafb
%% Initial revision
%%

if isa(CellObjects, 'cell')
  for n1 = 1:size(CellObjects,1)
    for n2 = 1:size(CellObjects,2)
   %   if isa(CellObject{n1,n2}, 'activex')
    CellObjects{n1,n2}.CellValue = Value(n1,n2);
   %  end
    end
  end
else
  CellObjects.CellValue = Value;
end
```

hysolvertoggle.m

```
function hysolvertoggle(ApplicationObject)
% HYSOLVERTOGGLE Toggle solver active/inactive in Hysys
%    hysolvertoggle(ApplicationObject) toggles the solver in Hysys.
%
%    Copyright (C) 2008 Olaf Trygve Berglihn <olafb@pvv.org>
%    Please read the files license.txt and lgpl.txt


h = actxserver('WScript.Shell');
h.AppActivate(regexprep(ApplicationObject.Caption, '.*- ', ''));
h.SendKeys('{F8}');
release(h);
```

hyspread.m

```
function SpreadsheetObject = hyspread(ApplicationObject,
SpreadsheetNameString)
% HYSPREAD Returns the activeX object for a spreadsheet in Hysys
%     hyspread(ApplicationObject, SpreadsheetNameString)
%
%    Copyright (C) 1999 Olaf Trygve Berglihn <olafb@pvv.org>
%    Please read the files license.txt and lgpl.txt

%% $Id: hyspread.m,v 1.2 1999/04/20 08:52:53 olafb Exp $
%% ----------
%% Changelog:
%%
%% $Log: hyspread.m,v $
%% Revision 1.2  1999/04/20 08:52:53  olafb
%% The library is now under LGPL license.
%%
%% Revision 1.1  1999/04/07 12:01:39  olafb
%% Initial revision
%%
%%
```

```
SpreadsheetObject = get ...

(ApplicationObject.ActiveDocument.Flowsheet.Operations,...
                     'Item', SpreadsheetNameString);
```

hyvalue.m

```
function CellValue = hyvalue(CellObject)
% HYVALUE Returns the value of a Hysys spreadsheet cell.
%    hyvalue(CellObject) - CellObject can be a single object or a cell
%    array of objects.
%
%    Copyright (C) 1999 Olaf Trygve Berglihn <olafb@pvv.org>
%    Please read the files license.txt and lgpl.txt

%% $Id: hyvalue.m,v 1.5 1999/04/20 08:52:54 olafb Exp $
%% ----------
%% Changelog:
%%
%% $Log: hyvalue.m,v $
%% Revision 1.5  1999/04/20 08:52:54  olafb
%% The library is now under LGPL license.
%%
%% Revision 1.4  1999/04/18 14:04:44  olafb
%% Added support for cell matrises of activeX-objects.
%%
%% Revision 1.3  1999/04/18 13:54:12  olafb
%% hysyslib/
%%
%% Revision 1.2  1999/04/16 08:38:16  olafb
%% Added support for cell arrays of aciveX objects
%%
%% Revision 1.1  1999/04/07 12:03:37  olafb
%% Initial revision
%%

if isa(CellObject, 'cell')
  for n1 = 1:size(CellObject,1)
    for n2 = 1:size(CellObject,2)
%      if isa(CellObject{n1,n2}, 'activex')
    CellValue(n1,n2) = CellObject{n1,n2}.CellValue;
%      end
    end
  end
else
  CellValue = CellObject.CellValue;
end
```

UNISIMOptimizer.m

```
classdef UNISIMOptimizer

    properties

        UNISIM
        inputs
        opt_target
```

```
        maximize
        result

    end

    methods

        function this = UNISIMOptimizer()

            this.UNISIM = hyconnect();
            sprd = hyspread(this.UNISIM, 'INPUT-OUTPUT');
            this.inputs = hycell(sprd,{'F4', 'F5', 'F6'});

            this.opt_target = hycell(sprd,{'F17'});             %F17 -
> net power, F18 -> efficiency
            this.maximize = 1;                                  %1 ->
Maximixe, 0 -> Minimixe

            this.result = this.optimize();

        end

        function result = optimize(this)

            x_0 = this.read_initial_point();
            [A, b] = this.constraints;
            options = optimoptions('fmincon','StepTolerance',1e-
20,'Display','iter');
            result = fmincon(@this.opt_function, x_0, A,
b,[],[],[],[],[],options);

        end

        function [A, b] = constraints(this)

            A = [-1, 0, 0;
                  1, 0, 0;
                  0,-1, 0;
                  0, 1, 0;
                  0, 0,-1;
                  0, 0, 1];

             b = [-0.45, 0.65, ...
                  -0.2,  0.5, ...
                  -0.2,  0.5];

        end

        function first_points = read_initial_point(this)

            first_points = zeros(length(this.inputs), 1);

            for i = 1:length(this.inputs)

                first_points(i) = hyvalue(this.inputs{i});

            end
```

```
    end
    function opt_param = opt_function(this,x)
        for i = 1:length(x)
            hyset(this.inputs{i}, x(i));
        end
        this.wait_solution()
        if this.maximize
            opt_param = -hyvalue(this.opt_target{1});
        else
            opt_param = hyvalue(this.opt_target{1});
        end
    end
    function wait_solution(this)
        while this.UNISIM.ActiveDocument.solver.isSolving
        end
    end
end
```

APP. 2 – Publications Produced From This Thesis

Özcan Z., Ekici Ö., A novel working fluid selection and waste heat recovery by an exergoeconomic approach for a geothermally sourced ORC system, Geothermics, 2021; 95: 102151. https://doi.org/10.1016/j.geothermics.2021.102151

Özcan Z., Ekici Ö., Thermodynamic analysis of a binary geothermal plant, International Journal of Exergy, 2021; in press., DOI: 10.1504/IJEX.2021.10039372.